Effects of Pyrolysis Conditions on Coal Char Properties

A Thesis

Presented to the

Department of Mechanical Engineering

Brigham Young University

In Partial Fulfillment

of the Requirements for the Degree

Master of Science

by

Thomas K. Gale

August 1994

Effects of Pyrolysis Conditions on Coal Char Properties

Thomas K. Gale

Department of Mechanical Engineering

M.S. Degree, August 1994

ABSTRACT

Concern about comparability and validity of different methods for producing coal chars for research has motivated this investigation of the effect of devolatilization conditions on the physical, chemical and reactivity properties of coal chars. It is evident from the findings of this study that care must be taken to prepare chars under conditions similar to those of full scale coal combustion boilers prior to performing char oxidation studies. Two different entrained flow reactors were used to prepare chars under a variety of different pyrolysis conditions at maximum particle temperatures and heating rates between 840 to 1627 K and 10^4 to $2x10^5$ K/s respectively. The following are a few of the specific findings: (1) The presence of steam in the post flame gases of methane/air flat flame burners is a significant factor in increasing meso-pore surface area of chars prepared in such burners. (2) The high moisture content of low rank coals may explain why low rank coals form chars with higher meso-pore surface areas than bituminous coals, i.e., Zap lignite with high moisture content yields chars with significantly higher N_2 surface areas than lower moisture content Zap lignite. However, coal moisture content has less effect on micro-pore surface area. (3) The heating rate at which the transition from increasing swelling to decreasing swelling occurs is approximately $5x10^3$ K/s for plastic coals. (4) Following devolatilization, intrinsic coal char reactivity is a function of its ash free true density regardless of the pyrolysis conditions.

Acknowledgments

This work was sponsored by the Advanced Combustion Engineering Research Center at Brigham Young University. Funds for this center are received from the National Science Foundation, the State of Utah, 28 industrial participants, and the U.S., Department of Energy. I would also like to thank Mathew Watt for helping conduct the HPCP experiments and Todd Brady for performing CHN analysis. I would especially like to thank Dr. Bartholomew for the many hours and sincere effort he gave to help me. I would also like to thank Dr. Fletcher for the genuine help he provided in helping me understand the whole coal combustion picture. Finally, I would like to thank Dean Smoot and all those associated with the establishment of ACERC, without which this work and my thesis would not have been possible.

Table of Contents

List of Tables

List of Figures

Chapter 1

Introduction

Background

Understanding the coal combustion process is essential to the development of cleaner and more efficient coal utilization processes. There are essentially two steps involved in coal combustion: The pyrolysis and oxidation of the liquid and volatile mater, followed by the oxidation of the residual porous char matrix. Char oxidation takes 5-10 times longer than devolatilization to bring to completion. However, the pyrolysis process significantly affects the resulting char structure and hence char oxidation. A porous char particle with a large internal surface area may be more accessible to reactant molecules at certain gasification temperatures. Not only are the porosity and internal surface area of the char affected by the pyrolysis process, but also the chemical composition, i.e., the hydrogen to carbon ratio of the char may be correlated with the reactivity of the char.

Swelling, surface area, porosity, mass release, true density and chemical composition affect char reactivity; thus, understanding the effects of pyrolysis conditions on such properties is important in order to model coal combustion. In addition to predicting full scale boiler conditions for complete char burnout, an understanding of how different pyrolysis conditions affect char reactivity and other char properties is essential for further development of combustion techniques to reduce NO_x, SO_x and to control ash deposit formation.

A number of different experimental methods and reactor types are currently used to produce chars for laboratory study in the coal science community. These different reactors operate under controlled conditions that are typically very reproducible from one run to another. However, the variation of the pyrolysis conditions from one method to another and from one type of apparatus to another may be large. Comparisons of data obtained in different laboratories are justified by matching experimental conditions thought to be most critical, such as temperature and residence time, or temperature and mass release.

However, due to the diverse nature of the different reactors that are used, it has been difficult to match all of the parameters necessary to make a valid comparison.

Accordingly, it is important to determine the effects of varying pyrolysis conditions on the physical and chemical structure of the resulting char and how the magnitude of each effect compares with another.

Questions to be Answered

This investigation was a very comprehensive study of the effects of pulverized coal pyrolysis conditions on char properties in two laboratory scale reactors. A list of questions answered from this study are as follows:

(1) What are the differences in reaction conditions between methane/air flat flame burners and nitrogen gas drop tube reactors that account for differences in coal char properties such as internal surface areas, swelling ratio, intrinsic reactivity, porosity, true density and element release?

(2) Is swelling of plastic coals more affected by temperature, heating rate or residence time?

(3) Assuming that a pyrolysis heating rate exists at which swelling decreases for plastic coals, what is the heating rate at which maximum particle swelling occurs, and what is the range of heating rates in which swelling decreases?

(4) How is internal char surface area affected by the presence of steam, carbon dioxide or oxygen in the pyrolysis atmosphere at high heating rates and temperatures and low residence times?

(5) What effect does parent coal moisture content have on internal surface areas?

(6) What physical or chemical char properties correlate best with intrinsic reactity?

(7) What are the mechanisms involved in production of char internal micro- and meso-pore surface area, total porosity, swelling, and mechanisms affecting intrinsic char reactivity?

(8) What is the effect of coal type and rank on the above questions?

This list of questions is answered in the present research. Only one particle size

was examined, and a limited range of particle temperatures, heating rates and residence times was used.

Objectives of This Work

The major objective of this research is to determine how pyrolysis conditions affect char properties such as particle diameter, porosity, internal surface area, and intrinsic reactivity. Char prepared in methane/air flat flame burners have much different properties than chars prepared in electrically heated drop tube reactors in inert gas. Differences between flat flame burners and drop tubes include, heating rate, temperature, residence time, and differences in the flow gas composition, i.e., flat flame burners contain significant quantities of oxygen, steam and carbon dioxide in their post flame. Each of these variables will be varied independently in the drop tube reactor to determine the effects on char properties.

Relevance of this Work

Data obtained from laboratory scale, high temperature char oxidation studies are often used to model the coal combustion process in full-scale boilers. Char prepared for such oxidation studies is typically devolatilized without much consideration of the temperature, heating rate, residence time or gas atmosphere which exists in the actual industrial scale boiler during the initial stage of coal combustion when devolatilization occurs. The present work shows the importance of preparing chars at conditions similar to those of full scale industrial boilers before char oxidation studies are performed to provide data for modeling the char oxidation process in these same industrial boilers. In addition, the present work provides information about the early stages of the coal combustion process that may be combined with information about char oxidation. This combined information can be used to effectively model the total coal combustion process for improved control and operation of industrial boilers. This improved control will provide cleaner and more efficient use of coal as an energy source.

Approach

Physical structure, ultimate analysis, and low-temperature reactivity are compared for chars prepared in two different reactors at Brigham Young University, a flat flame methane burner and a high temperature drop tube furnace. Each reactor typically operates at different conditions, although it is possible to find conditions for the drop tube that approach those of the flat flame. The main conditions tested in these experiments were: maximum particle temperature, heating rate, residence time, and gas atmosphere.

Three coals were selected for the study to provide a comparison of rank and swelling properties. Chars were prepared from these coals in the High Pressure Controlled Profile (HPCP) reactor under a variety of different pyrolysis conditions. Chars were also prepared in a Flat Flame Burner (FFB) at one condition for comparison. Chars previously prepared in the HPCP had a much smaller internal surface area than chars previously prepared in the flat flame burner. By adjusting conditions in the HPCP independently, it was possible to determine how each of the pyrolysis conditions contributes to resulting char properties. Where possible, properties of completely devolatilized HPCP and FFB chars were compared.

Chapter 2

Review and Analysis of Previous Work

Internal Surface Area and Graphitization

Structural Development During Carbonization. Early insight into the influence of pyrolysis conditions and feed stock properties were provided by Franklin [1]. In a study of the variation of structure with preparation temperatures between 1000 and 3000 °C, she identified two well defined but markedly different carbon precursor types, non-graphitizing and graphitizing. Carbonization of these precursor carbons took place in a packed bed at a heating rate of 5 °C/min and a residence time of 2 hours. Graphitization, she observed, takes place when layered planes or groups of layered planes rearrange to favor crystallite growth. Pre-orientation of these layered planes existing in graphitizing carbons facilitates this process. Furthermore, graphitizing carbons are prepared, in general, from weak crosslinking substances containing large amounts of hydrogen. Non-graphitizing carbons are formed, in general, from strong crosslinking substances containing very little hydrogen and/or a significant quantity of oxygen. On heating at low temperatures, non-graphitizing carbons develop a strong system of crosslinking which immobilizes the structure and unites the crystallites in a rigid mass of char with a hard and highly porous fine-structure. Such structures are preserved at high temperatures.

Franklin [1] also found that at temperatures below 2000 °C, anthracites form strongly cross-linked, highly porous chars which greatly resemble non-graphitizing carbons. However, at higher temperatures (above 2000 °C) cross-linking breaks down, and crystallite growth causes highly graphitic carbons to be formed. Franklin [2] also observed that true (skeletal) densities of carbonaceous solids, prepared at similar heating rates and residence times as in the above study [1], increases with increasing carbonization temperatures between 600 and 1200 °C, reaching a maximum of 2.1 g/cc and maintaining this same density value between 1200 °C and 1650 °C.

Surface Area Measurement Techniques. In early adsorption studies, Walker et al. [3,4] and Anderson et al. [5,6] observed that coals are unique adsorbents with micro-pores having openings of about 0.5 nm which are accessible to CO_2 at > 195 K but inaccessible to nitrogen, argon or methane at 78 K because of diffusional restrictions. This work led to the development of adsorption techniques for measuring internal surface areas of coals [3-7] and later chars [e.g., 7,8]. Meso-pore surface areas are determined by N_2 gas adsorption at 77 K using the Brunauer, Emmett and Teller (BET) equation [9]. Total surface areas, containing mainly micro-pores, are determined by CO_2 adsorption at 298 or 273 K, also using the BET equation. Micro-pore surface area may be determined from CO_2 adsorption at 298 or 273 K by using the Dubinin Polanyi (DP) equation [10]. In the following literature review, CO_2 surface area will refer to that calculated by the Dubinin Polanyi equation. Micro-pore surface area is a measure of surface area within pores having a diameter of 2 nm or less. Meso-pore surface area is a measure of surface area within pores having diameters greater than 2 nm but less than 50 nm. Macro-pores have pore diameters greater than 50 nm.

Effects of Temperature, Heating Rate, Carbon Conversion, and Oxidation. In the past two decades a number of studies have examined effects of pyrolysis conditions, i.e. temperature, heating rate, residence time, etc., on internal surface areas, densities, and porosities of the resultant chars [3-20]. Most of these studies involved low pyrolysis temperatures, low heating rates, and long residence times relative to typical conditions for pulverized coal combustion. For example, Nandi et al. [11] prepared Pennsylvania anthracite chars at heating rates of 5 °C/min, residence times of about 2 h, and temperatures between 500 and 1000 °C in a packed bed. Under these conditions, meso-pore (N_2) and micro-pore (CO_2) surface areas were observed to increase at temperatures up to 600 or 700 °C and then decline there after. However, when St. Nicholas anthracite was pyrolyzed at temperatures of 900 °C with no soak-time

(significantly lower residence time), the surface area was higher than for any other char prepared.

Because excess oxygen is often used in flat flame burners to consume volatiles during coal char preparation, it is important to understand the effects of partial oxidation on char surface area. Effects of low temperature (350 to 600 °C), long residence time (4 hours), oxidation (5% O_2, 95%N_2) of bituminous coals and semi-anthracite on internal char surface area were examined by Ludvig et al. [12]. Oxidation significantly increased char N_2 surface area, e.g. from <1 to 72 m^2/g for hvA-bituminous coal; however it sometimes slightly increased and sometimes slightly decreased CO_2 surface area.

N_2 surface areas of bituminous coal chars were observed to increase by Sahu et al. [13] from 50 to 450 m^2/g with increasing carbon conversion up to 50% during combustion in oxygen at 500 °C. Char was prepared at 1600 K for 2 seconds in an inert atmosphere in an electrically heated drop tube. Above 50% combustion conversion, the N_2 surface area remained constant or declined slightly with further conversion.

Since steam and carbon dioxide are gases that exist in the post flame of methane/air flat flame burners and therefore some char gasification may occur, it is important to examine the effects of partial char gasification on surface area. Kojima et al. [14] performed pyrolysis experiments in an inert environment for a number of different coal types at 1273 K and heating rates between 5 and 700 K/min. He found that increasing the pyrolysis heating rate, prior to CO_2 gasification, significantly increased surface area and porosity of char macro- and micro-pores following subsequent gasification. In other words, the chars prepared at the higher heating rate had a higher BET surface area after partial CO_2 gasification.

White et al. [8], who did extensive surface area and porosity measurements of chars prepared in a flat flame burner with 0% post flame oxygen from a number of U.S. coals of varying rank, found that the internal surface area (CO_2 and N_2) and porosity of the chars

increased significantly during pyrolysis at 1475 K. The preparation heating rate observed was approximately 10^4 K/s. The post flame gases of the flat flame burner contained significant amounts of steam and carbon dioxide.

Specific Investigation of a Swelling Coal. From work on Illinois No. 6 coal, a high swelling coal, Zygourakis [15] states that the conditions that most strongly influence the pyrolysis process are heating rate, particle size and pressure. Preparation temperature was not specified. High pressures may increase char swelling by preventing volatiles from leaving the char particles until significant swelling has taken place due to the entrapped volatile mater. For Illinois No. 6 coal char, macro-porosity and N_2 surface area increased with increasing preparation heating rate from 0.1 to 1000 K/s by factors of 2.5 and 6.7, respectively. The same trends were found for lignite chars, except the macro-porosity and N_2 surface area increased by only a factor of 1.4. The effects of heating rate are associated with the effects of residence or bake time. The effect of particle size (125 μm to 710 μm) was also studied. It was found that the particle size had no effect on the resulting porosity of the char. Zygourakis presents this as evidence that the internal heating rate of the particle was not affected by particle size. However, internal surface area decreased as particle size increased.

N_2 Surface Areas of Low Rank Coal Chars Following Combustion or Preparation in an Inert Environment. Nsakala et al. [16] found that increasing pyrolysis residence time beyond complete devolatilization increased CO_2 and N_2 surface areas, true densities, and porosities of North Dakota lignite (Beulah Zap) chars prepared in nitrogen at 1073 K. The increase in surface area reached a maximum at about 600 ms. N_2 surface areas of greater than 100 m^2/g were observed. He also reported higher surface areas for chars prepared with a heating rate of 10 K/min relative to 8000 K/s. This result was also, unavoidably, an effect of residence time since it took nearly an hour and a half to reach the maximum particle temperature at the lower heating rate.

Fletcher et al. [17] also observed an increase in N_2 surface area for a similar North Dakota lignite to that of Nsakala's when pyrolyzed in 100% nitrogen. Both the lignite and a sub-bituminous coal (New Mexico) experienced a significant increase in N_2 surface area during pyrolysis in an inert atmosphere, while a hv-bituminous coal (Pittsburgh No. 8) experienced very little increase in surface area during pyrolysis. Chars were prepared from the New Mexico sub-bituminous coal at two different temperatures. Char prepared at 1050 K experienced very little increase in N_2 surface area, while the N_2 surface area of a char prepared at 1250 K increased to above 300 m^2/g. The increase in N_2 surface areas of low rank coals during pyrolysis was ascribed to light gas evolution from their rigid char matrix, which tends to fracture the coal structure to create escape paths for trapped gases. Another interesting point to consider is the difference in parent coal moisture content. The moisture of the size-classified lignite and sub-bituminous coals was 18.04 and 9.31% respectively, while that for the hv-bituminous coal was only 1.5%.

In contrast to the high (>100 m^2/g) N_2 surface areas reported by Nsakala et. al. [16] and by Fletcher et al. [17], McDonald et al. [18] observed an N_2 surface area of only 6.5 m^2/g for a North Dakota (32.2% moisture in parent coal) char produced in a drop tube furnace in an inert atmosphere at 1300 K, a heating rate of 10^4 to 10^5 K/s and a residence time of 200 ms. However, in the case of Dietz (23.7% moisture in parent coal) chars, increasing residence time from 200 ms to 9 minutes (heating rate decrease from 10^4 to 10 K/s) increased N_2 surface area from 7 to 42 m^2/g. Moreover, McDonald et al. found that it was possible to produce Zap and Dietz chars having N_2 surface areas of 140 and 217 m^2/g respectively in a reactive methane flame at 1473 K, a heating rate of 10^5 K/s and a residence time of 100 ms.

Effect of Residence Time. Hecker et al. [19] showed that Dietz chars prepared in a reactive methane flame at a maximum particle temperature of 1700 K and

heating rate of 10^4 to 10^5 K/s increase in CO_2 and N_2 surface area with increasing residence time. The pyrolysis process was complete within 50 ms for most chars prepared. Hence, the increases in residence times were essentially increases in post pyrolysis residence times. At a residence time of 25 ms, the N_2 surface area is only slightly higher than zero, and the CO_2 surface area is about 150 m^2/g; at 125 ms, N_2 and CO_2 surface areas are >200 and >400 m^2/g respectively.

Mitchell et al. [20] showed an increase in CO_2 and N_2 surface area for Lower Kittanning and Hiawatha (Utah sub-bituminous) coal chars with combustion conversion in 6 or 12% oxygen at particle temperatures between 1600 and 1800 K at short residence times. A maximum in these surface areas was observed between 35 and 60% conversion, after which a significant decline in surface areas was observed. The maximum N_2 surface area observed for Hiawatha coal char prepared in 6% oxygen was above 100 m^2/g, but Lower Kittanning coal char N_2 surface area did not increase significantly in 6% oxygen and only increased to about 50 m^2/g in 12% oxygen.

Carbon Activation Studies. Since many laboratories utilize methane/air flames to prepare char from coal, the effects of CO_2, H_2O and O_2 gasification are of interest. Accordingly, studies on the activation of carbons by such reactant gases are considered. Rodriguez [21] discussed the process of carbon activation during gasification in CO_2, H_2O and O_2. Graphite is composed of layered planes formed by carbon atoms ordered in regular hexagons. Each carbon atom within a plane is bonded to three adjacent carbon atoms by sigma bonds. The fourth electron is part of a pie bond. The layered planes are parallel and are held together by van der Waals forces. The spacing between layers is only 0.335 nm. Non-graphitic carbons or coal chars are formed during pyrolysis. During pyrolysis, the non-carbon material is volatilized and released from the char particle, and crosslinking sets in to form a rigid structure. Except for swelling coals, the carbon matrix

normally retains the same structure; the difference being pores and gaps are left where the volatiles were released and some particle shrinkage may occur. These non-graphitic carbons consist of aromatic sheets and strips, often bent and resembling a mixture of wood shavings and crumpled paper [21]. These structures contain molecular size gaps between them called micro-pores. Consequently, the larger the disorientation of the carbon matrix, the more micro-porous it will be. After devolatilization (carbonization), much of the micro-porosity may be blocked by decomposition of tars and restructuring of the char matrix. Partial gasification (physical activation) of these chars will remove some of the carbonized material and make more of the micro-pores available to adsorptive gases. Generally, activation of carbons is performed at long residence times. Much of the following work considered was performed utilizing residence times of from 2 to 10 hours. Surface areas obtained from these long residence time experiments are several thousand m^2/g, and prepared from large particles or slabs.

In general, progressive gasification causes micro-pore enlargement and therefore a shift from micro- to meso- and macro-porosity. According to Marsh and Rand [22], most meso- and macro-pore increase during gasification occurs due to (1) widening of existing pores and (2) opening of previously inaccessible pores. Rodriguez [1] found that increasing temperature from 1098 to 1223 K for CO_2 gasification of peach stones created wider pores. Furthermore, increasing the gasification temperature slightly increased micro-porosity but increased meso-porosity to a much larger extent.

Tomkov et al. [23] reported that increasing the carbonization temperature of brown-coals from 773 to 1173 K produced a char, after CO_2 activation, with a larger micro-pore volume and more uniform micro-pore structure (pore diameters were of similar size). Rodriguez [21] reported similar results for carbonization and gasification of peach stones.

In addition to carbonization and gasification temperature, inorganic impurities catalyze the conversion of small pores to large pores. A number of different investigators

[22,24-26] have shown that for char prepared with a catalyzed reaction experiencing the same mass release as char prepared in a non-catalyzed reaction, the micro-porosity is smaller and the meso- and macro-porosity is higher than for the non-catalyzed char. Precursor carbons included: coal, polyfurfuryl alcohol carbon, peat char, and almond shells, and the inorganic catalysts used included: Cr, Fe, Ni, Mo, Na, and Ca. Reaction and carbon loss, during catalyzed gasification, takes place mainly in the vicinity of catalyst particles especially if pore diffusion limitations exist. This selectivity during gasification is what causes larger pores to develop.

Finally, it is important to compare effects of gasification in the three different reactant gases of interest, CO_2, H_2O and O_2. Rodriguez [21] concluded from a gasification investigation of carbonized olive stones at temperatures between 1073 and 1098 K that micro-porosity is similar for chars prepared in steam and carbon dioxide. However, meso- and macro-porosity are larger for chars prepared in steam. These results are substantiated by Wigmans [27] who did his research on peat semicoke in a bench scale kiln. Tomkov et al. [28] reported that activation of brown-coal with oxygen at 673 K produces greater micro-porosity at burnoffs of 25% than activation in steam, but oxygen becomes an ineffective agent for increasing internal surface area at burnoffs as high as 50 or 75%, whereas steam is still effective. The micro-porosity of chars activated in steam decreases at high burnoff, although the meso-porosity continues to increase, whereas in the case of oxygen the volume of meso-pores remains almost constant. Tomkov and coworkers concluded that activation (an increase in meso- and/or micro-pore surface area) by oxygen occurs during the initial stages of gasification; at this point the oxygen surface groups chemisorb at the entrances of the micro-pores, thus isolating them from further reaction, which proceeds only in larger pores. However, pore diffusional restrictions for oxygen could cause the same results as chemisorbed oxygen surface groups. Nevertheless, at 673 K, diffusion limitations probably do not occur.

Intrinsic Rates

Correlations with Parent Coal Rank, Char Properties and Preparation Conditions. Hyde et al. [29] showed that intrinsic char reactivity correlates with parent coal rank, lower rank coals having the highest reactivity. Jenkins et al. [30] reported a decrease in reactivity (773 K, in air) with increasing pyrolysis temperature for a wide variety of coal chars of differing rank prepared at a heating rate of 10 K/min. This decrease in reactivity was attributed to a decrease in concentration of feeder pores and a simultaneous degradation of reactive chemical structures involving hydrogen. However, the effect of hydrogen release or mass release was not distinguished from any possible effects of meso-porosity or N_2 surface area. Other research groups have reported a decrease in reactivity, especially intrinsic reactivity, with increasing preparation temperature [31-33].

Kothandaraman et al. [34] performed pyrolysis experiments on PSOC 140 lignite coal in helium at temperatures between 800 and 2000 K in which evolution of pore structure was examined. They found that increasing preparation heating rate from 1.0 K/s to 2000 K/s increased both total porosity and the relative number of large pores. However, apparent reactivity decreased with increasing pyrolysis temperature due to changes in reaction kinetics of the char, even though total porosity increased.

A number of investigators [31,32,37] have shown that intrinsic reactivity of char prepared from a given coal type decreases with increasing residence time or soak time at the heat treatment temperature. Both heat treatment temperature and residence time influence intrinsic reactivity by promoting an ordered carbon matrix; the ordering process is often accompanied by an increased mass release during devolatilization. Hydrogen content decreases with increasing mass release [17,38-39], and intrinsic reactivity of pyrolyzed char is sometimes correlated with its hydrogen content [29,37,40]. It has been suggested [29,41] that the correlation between intrinsic char reactivity and hydrogen content is related more to the release of aromatic hydrogen than aliphatic hydrogen. This is consistent with densification or progress towards graphitization being the cause of decreasing reactivity.

However, coal chars do not generally become genuinely graphitic during devolatilization in a typical combustion process.

Charpenay et al. [40] developed a char reaction rate model based on the prediction of intrinsic rates, and the extrapolation of those predicted intrinsic rates to higher temperatures using the Thiele modulus [42] to account for pore diffusion. Intrinsic reactivity was determined from a weighted formula which includes (1) the number of active carbon sites and catalytic sites available, (2) hydrogen content of the char characterizing the degree of pyrolysis, and (3) oxygen content of the parent coal characterizing coal rank. The contribution of active carbon sites is determined by coal type, extent of devolatilization and, for swelling coals, plasticity. Catalytic sites are determined by the dispersed mineral content, especially calcium. The degree of disorder, for plastic coals, is considered as a function of pyrolysis heating rate. At higher temperatures, a random pore model is used to model pore diffusion in high rank coals, and a volumetric model was used for low rank coals. High temperature rates determined for the pore-diffusion-restricted regime using this method have a factor of 2 uncertainty.

Rybak [33] observed that apparent and intrinsic char reactivity increases with increasing pyrolysis heating rate from 14 K/min to 10^4 K/s for chars prepared from a lignite and two different bituminous coals. However, different heating rates were obtained in his study by using two very different types of reactors, an entrained flow reactor and a fixed bed reactor with 0.1 and greater than 600 sec residence times respectively. Consequently, his results showing H/C ratio and intrinsic reactivity to be much lower for chars prepared in the fixed bed reactor address effects of residence time and mass release more than heating rate. Ashu et al. [43] also reported an increase in intrinsic reactivity with an increase in preparation heating rate from 10 K/min to 8×10^3 K/s for chars prepared from North Dakota lignite, which was also probably more a function of residence time and differences in mass release. Ashu et al. [43] also studied effects of rapid heat treatment in nitrogen gas of chars previously pyrolyzed. He found that subjecting chars to rapid heat

treatment slightly increased their intrinsic reactivity (by factors of 1.1 to 1.3), due to production of active carbon sites.

In contrast to the results of Rybak [33] and Ashu et al. [43], Solomon et al. [37] found that intrinsic reactivity of hv-bituminous coal char prepared at 30 K/min is higher than that prepared at 10^4 K/s. Furthermore, pyrolysis heating rates between 30 K/min and 2×10^4 K/s were found [37] to have little effect on lignite char reactivity. Solomon's data however, also have uncertainties associated with preparing chars in different reactors (of different residence times, particle number densities, heat transfer rates, and temperatures) in order to obtain different maximum particle pyrolysis heating rates. In another study of lignite char, Solomon et al. [43] reported that mineral matter in lignite increases crosslinking reactions that decrease both tar yield and hydrogen release, thereby increasing intrinsic char reactivity. For demineralized Zap lignite, tar evolution extent was higher while the extent of CO and CO_2 evolution was lower. High heating rates increased the amount of tar evolution for chars prepared from both untreated and demineralized Zap lignites, in both cases reducing the H/C ratio of the chars and hence their intrinsic reactivity.

Chitsora et al. [32] observed that TGA steam gasification rates of German bituminous coal char are higher when prepared at 4000 K/min in a fluidized bed than when pyrolyzed at 10 or 100 K/min in a fixed bed reactor. Preparation temperature and residence time ranged from 773 to 1173 K and 0.2 to 14400 sec respectively. Besides formation of more carbon active sites during rapid heating, lower intrinsic char reactivities at very low heating rates were attributed to carbon deposition [45] from the cracking of methane into pores during pyrolysis. However, at high heating rates (~1000 K/s), there is not sufficient time for cracking and carbon deposition to take place. Steam gasification rates were also observed to decrease with increasing pyrolysis temperature or pressure. Contraction of the char particles as a result of the high pressure, leading to the sealing up of the pores, is one explanation for the decrease in rate. For a swelling coal, it is more likely that the decrease

in reactivity is due to the creation of unbroken cenospheres with an initial physical structure that has very little available surface area and an orderly chemical structure of low reactivity. At high preparation temperatures, however, the effect of pyrolysis pressure on char reactivity was undetectable. No influence of the type of gas atmosphere used during pyrolysis was found for these different conditions, even in steam or hydrogen atmospheres. A possible explanation could be that the pressure during pyrolysis for these experiments was too low to cause deep penetration of the respective gases into the char structure.

Relationship Between Reactivity and Internal Char Surface Area and Porosity. It has been an ongoing problem in the coal science community to determine what surface should be used to normalize the intrinsic rate data. It is also of great interest to determine the role of char pore structure and surface area at elevated temperatures where diffusion resistance occurs. Accordingly, the following studies on the relationship between char structure and reactivity is presented.

The so-called intrinsic reactivity of coal chars may be independent of very small micro-pores. For example, Hurt et al. [46] studied the effects of pore structure and internal surface area on non-catalytic carbon reactions using spherocarb and sucrose carbons. Intrinsic rates were determined at temperatures between 400 and 600 ^{o}C in oxygen and carbon dioxide. Spherocarb is highly macro-, meso- and micro-porous, but sucrose is essentially non-macro or meso-porous and consists mainly of very small micro-pores. Therefore, micro-pore diffusion lengths for sucrose carbon are as long as the particle radius. Spherocarb micro-pore diffusion lengths, on the other hand, are limited to half the length of microporous material between macro- or possibly meso-pore surfaces. Micro-pore diffusional restrictions scale to L^2/D, where L is the micropore length and D is the micro-pore diameter. Consequently, as observed by Hurt et al. [46], TGA low temperature reactivity rates of sucrose carbon are significantly lowered by micro-pore diffusion restrictions, whereas the TGA low temperature reactivity for Spherocarb is not

affected by micro-pore diffusion. The reactivities for sucrose carbon are considered "intrinsic" for all practical purposes even though diffusion limitations exist, since they are lowered by restricted rather than Knudsen diffusion. Restricted diffussion involves forces directly associated with pore walls rather than by gas mass transport. Gasification causes micro-pore widening in sucrose carbon, which decreases diffusional restrictions by increasing meso-porosity [46]. Hippo et al. [47] confirmed the existence of a relationship between feeder pores and micro-porous diffusion restrictions for non-catalytic reactions of carbon. Pore diffusional restrictions are important for chars with little or no meso- or macro-porosity and very small micro-pores. As shown by Gopalakrishnan et al. [48], coal chars may have pore volumes larger than for Spherocarb for large pores, especially macro-pores, even though the parent coal generally has a very small porosity. However, as in the present work, some coal chars may have meso-porosities as low as the parent coal, even though they have very high micro- and macro-porosities. Thus, most of the increased porosity for these coal chars relative to coals resides in micro- and macro-pores.

Catalytic effects during low temperature oxidation of coal char can be very important, especially from chars prepared from low-rank coals. Gasification of coal chars often occurs in the immediate vicinity of catalytic mineral matter [49]. Sintering of catalytic minerals during heat treatment of carbons has been observed by Wigmans et al. [50], with formation of particles too large to re-enter the micro-porous network. This process causes a migration of catalytic material out of the micro-pores and on to the surfaces of larger pores [50,51]. Consequently, catalyzed gasification or oxidation may not occur in micro-pores of coal chars even under intrinsic reaction conditions.

The relationship between coal char pore structure and reactivity is not well defined from previous work. While Jenkins et al. [30] suggest that pore structure affects apparent oxidation rates of chars in air at 500 °C, this hypothesis has not been satisfactorily substantiated with data correlating reactivity with char porosity or surface area. Hurt et al. [52], found that the intrinsic rate of CO_2 gasification of a sub-bituminous coal is insensitive

to large changes in total surface area occurring during heat treatment or reaction. Rather, char gasification rate was thought to be a function of active site concentration and catalytic mineral matter which lie preferentially on large pore surfaces. Consistent with Hurt et al. [52], Serio et al. [41] reported that intrinsic reactivity (400-500 °C) of chars prepared from five coals of various rank was not significantly influenced by variations in either N_2 or CO_2 surface areas.

Effects of Tar/Char Separation and Char Chemical Structure. The effects of collection conditions on char reactivity are also open to question. McDonald et al. [18] have suggested that, due to tar condensation in pores following a rapid quench, pyrolysis experiments in an inert environment may be less representative of char produced in a conventional boiler than char produced in a flame. They hypothesized that tar condensation increases reactivity, and decreases N_2 surface area while having little effect on CO_2 surface area. However, this hypothesis may be questioned because of complications due to large differences in residence time and heating rate in the three different reactors used in their study to prepare chars.

Fletcher et al. (1992) studied the chemical structure of chars prepared from a number of different parent coals using NMR. It was found that chemical structural features obtained from NMR analysis of fully devolatilized chars are very similar, even though there was a wide diversity in the parent coal structures. It was concluded that differences in measured heterogeneous char intrinsic and global reactivities were caused by differences in the physical structure of the char.

Swelling

Sinnatt et al. [53] studied swelling during pyrolysis in atmospheres of nitrogen, coal gas, hydrogen, steam, and at reduced pressure in coal gas. Pyrolysis in nitrogen, coal gas and hydrogen caused swelling of the char and formation of nearly identical cenospheres. However, the char prepared in an atmosphere of steam consisted of fewer cenospheres.

Brookes [54] pyrolyzed Silkstone coal at different heating rates by exposing 150 to 850 μm coal particles to instantaneous or gradually increasing radiation intensity. Although not specified, his reported particle temperature of 1470 K indicates fairly high heating rates. Char swelled the most when exposed to gradually increasing intensity of radiation. The idea that swelling decreases with increasing heating rate was also noted by Kallend and Nettleton [55] .

Street et al. [56] studied pyrolysis of low, medium and high rank coals in air and in nitrogen. Chars prepared in nitrogen had much larger swelling ratios, more open structures, and smaller internal surface areas than chars prepared in air. Street and coworkers suggested that differences in the swelling ratio are due to crosslinking reactions brought about by oxidation. Swelling was also influenced by the duration and temperature of pyrolysis. While maximum particle heating rate was not reported, the relatively low maximum particle temperatures (573 to 923 K) used indicate a low heating rate.

Shibaoka [57] studied effects of both heating rate (5 to 1800 K/s) and particle size on the swelling of sub-millimeter size hv-bituminous, mv-bituminous, and sub-bituminous coal particles during devolatilization in air. It was found that char particles expand with increasing heating rate and form distinctly cellular structures. The finer the particle size, the greater was the relative degree of expansion.

From their experiments on swelling of bituminous coal during pyrolysis in air and pure nitrogen, Tsai and Scaroni [58] reported swelling ratios that conflicted with the findings of Street, et al. [56]. However, the maximum particle temperature and maximum particle heating rate attained by Tsai and Scaroni were much higher, i.e., 1200 K and 10^4 K/s respectively, than those of Street and coworkers. Pyrolysis of coal in nitrogen caused particle diameter increases of up to 20% with subsequent decreases in diameter of up to 10%. On the other hand, combustion of the coal in air produced diameter increases of up to 30% with subsequent shrinkage of the char particles influenced by burning. Another significant result was that the internal surface areas of particles treated in air and in nitrogen

were identical until the onset of oxidation in the combustion experiment.

Fletcher [59] recently studied the pyrolysis of coal for five different ranks in two different reactors. The maximum particle temperature and heating rate for his experiments were 1200 to 1500 K and 10^4 to 10^5K/s respectively. Chars were produced in a flat flame burner with 0, 6, and 12% post flame oxygen or in an electrically-heated drop tube, enabling percentages of oxygen and nitrogen to be varied. Particle diameters increased as much as 50% in the drop tube and by more than 20% in the FFB. Special care was taken to avoid any oxidation of the char after pyrolysis and during char collection. Oxygen in the post flame gases of the flat flame burner and in the drop tube reactor did not influence char particle swelling. Fletcher attributed the differences in the swelling ratio and surface properties of the chars created in the two reactors to differences in the heating rate between reactors and/or the presence of post flame gases in the flat flame burner other than oxygen, such as CO_2 or H_2O.

Hamilton [60,61] performed pyrolysis experiments on vitrinite from coals of different ranks between heating rates of 0.1 K/s to 10^4 K/s. His experiments were performed in an electrically heated grid reactor and concentrated on the effects of parent coal rank, and maximum particle heating rate and temperature on coal char plasticity. Bituminous vitrinites developed the greatest plasticity during pyrolysis. The farther removed in rank a vitrinite was from bituminous, the less plastic it became. Plasticity for all coal ranks began with the formation of cenospheres at heating rates of 1 K/s to 100 K/s and a consistent maximum particle temperature of 1273 K. Only small additional changes in char morphology were observed for heating rates of 100 K/s to 10^4 K/s. Char particles flattened out on the grid when high plasticity was achieved. In addition to a correlation with heating rate, Hamilton found plasticity to increase with increasing particle temperatures between 683 K to 1273 K at a constant heating rate of 10^3 K/s.

Zygourakis [62] demonstrated that the macro-porosity of 250-300 μm char particles

prepared from Illinois No. 6 coal increases with maximum particle heating rate for relatively low heating rates i.e. 0.1, 1.0, 10, 100 and 1000 K/s. Macro-porosity of char particles was determined by scanning electron microscopy (SEM). Char particle swelling also increased with increasing heating rate.

Attempts have been made to describe the various paths which swelling may take during pyrolysis, dependent on heating rate. One such model, developed by Solomon et al. [63], proposed that coal melts and gas bubbles form due to gas evolution into internal micro-pores during the initial stages of pyrolysis. Gas bubble size then increases by expansion and coalescence in molten particles. Whether the coal particles swell, fracture or form ruptures in the particle surface due to escaping volatiles is dependent upon the heating rate. A rough estimate of the heating rate at which swelling begins to decline was determined [63] from electron micrographs to be about 10^4 K/s.

Pre-Oxidation Effects

Depending upon the experimental methods used, such as low heating rates and long residence times or drying prior to pyrolysis, coal may experience pre-oxidation prior to devolatilization. In light of this fact, a section has been devoted to briefly lay out some of the known effects of coal pre-oxidation on char properties following pyrolysis.

Mahajan et al. [7] performed a weathering studying on caking coals from which they made the following observations: 1) pre-oxidation of caking coals in the temperature range of 120-250 ^oC increases the CO_2 surface area of the chars following pyrolysis. 2) pyrolysis in H_2 increases weight loss and decreases reactivity of chars compared with those prepared in N_2. 3) oxygen in the pre-oxidized coal acts to crosslink the aromatic and hydro-aromatic building blocks during the early stages of pyrolysis. 4) pre-oxidation temperature has no effect on the weight loss during pyrolysis or the time it took to obtain 50% conversion; only the level of pre-oxidation (i.e., amount of chemisorbed oxygen) and not the oxidation conditions has an effect on the resulting reactivity. 5) water vapor contained

in air during pre-oxidation may have an effect on char reactivity. 6) smaller particles are pre-oxidized to a higher level. Also, for the same pre-oxidation level, weight loss above 450 °C is generally larger for the smaller size fraction during pyrolysis. 7) pyrolysis in H_2 removes some of the oxygen in the parent coal.

Furimsky et al. [64] described the mechanisms involved in the pyrolysis of pre-oxidized coal. Pre-oxidation of coal causes the formation of O bridges. These O bridges may contribute somewhat to the loss of fluidity of the coal matrix. More significantly, when heated in the early stages of pyrolysis, the O bridges can rearrange to form much more rigid structures. During pre-oxidation, various unstable functional groups containing O are formed, which subsequently decompose on heating and are precursors for reactions that cause decreased fluidity. Furthermore, oxidation of the coal decelerates pyrolysis reactions that yield volatile products. This is because of the O-containing functional groups that cause crosslinking in the coal matrix and form a rigid structure.

Maloney et al. [65] studied the influence of pre-oxidation on gasification of PSOC-1099 and PSOC-1133 coal at temperatures between 1073 and 1273 K. Pre-oxidation of coals took place by means of air oxidation in a fluidized-bed at 448 K. They found that chars prepared during rapid heating (10^4 K/s) form balloon like cenospheres. Rapid heating of coal during pyrolysis negates any effect of pre-oxidation on the resulting char structure, i.e., the heating rate is so high that bonds are broken and fluidity occurs before significant crosslinking due to an increased oxygen content can occur. However, chars prepared from pre-oxidized coals under a slow heating rate (0.2 K/s) have more than twice the CO_2 surface area than that from the fresh coal. Nevertheless, there is little difference between the CO_2 or N_2 surface areas or swelling ratios of chars prepared from pre-oxidized and non-pre-oxidized parent coals at the high heating rate.

A study by Chitsora et al. [32] was performed on the influence of pyrolysis conditions on the TGA reactivity of char in H_2O. The range of preparation pressures was between 1.0 and 66 bar. Pre-oxidation of coal did not have any influence on H_2O

reactivity of chars produced at low heating rates up to 100 K/min. However, in the case of chars prepared at higher heating rates (i.e. 4000 K/s), it was found that chars prepared from non-oxidized coals were more reactive than those from pre-oxidized coals.

Summary of Previous Work

From the previous studies discussed in the internal surface area and graphitization section [1-28], two somewhat general trends regarding the effects of pyrolysis conditions on char surface areas are evident: (1) Under preparation conditions that form chars with significantly higher surface areas than for their parent coal, N_2 and CO_2 surface areas increase with increasing pyrolysis temperature and increasing residence time and (2) N_2 surface areas are affected by pyrolysis in the presence of a reactive atmosphere (containing O_2, CO_2 and/or H_2O). Nevertheless, there are some discrepancies among the different studies. N_2 surface areas for North Dakota lignite chars prepared in inert atmosphere at apparently comparable temperatures and heating rates were vastly different among the studies of Nsakala et al. [16] and Fletcher et al. [17] and McDonald et al. [18]. Only the studies of White et al. [8], McDonald et al. [18], Hecker et al. [19] , Flether et al. [17] and Mitchell et al. [20] were carried out at high heating rates, high temperatures, and low residence-time conditions, i.e. conditions more representative of large pulverized coal boilers. Of these, only the work of Hecker et al. [19] provides a definitive correlation of N_2 and CO_2 surface areas with residence time. None of the other previous studies provide definitive, independent correlations of N_2 and/or CO_2 surface areas with pyrolysis temperature, residence time, heating rate, oxygen concentration, and/or steam concentration for pulverized coal combustion.

From the previous studies on coal char reactivity it is clear that intrinsic reactivity of coal chars decreases with increasing pyrolysis temperature and increasing residence time at a given temperature. This can be explained by ordering of layered planes in the carbon matrix accompanied by greater total mass release, oxygen and/or hydrogen release at higher temperatures and residence times. However, there are contradictory conclusions and a lack

of consensus regarding the effects of particle pyrolysis heating rate and pyrolysis atmosphere on char reactivity, or the relationship of intrinsic and global reactivity to char properties such as char particle porosity and surface area.

From the information on coal char swelling, it is apparent that pyrolysis heating rate significantly influences the magnitude of swelling. It appears that there is a particle heating rate at which coal char diameters increase most. There is also evidence to suggest that oxygen in the pyrolysis gas atmosphere does not affect coal char swelling unless char oxidation occurs. However, it is unclear what effect slight char oxidation or gasification has on swelling.

Chapter 3

Experimental and Analytical Methods

Coal Types and Classification

Two hv-bituminous coals, Utah Blind Canyon and Pittsburgh No. 8 and a lignite, North Dakota (Zap), were selected to provide a comparison among coals of different rank. The three coals studied are listed in Table 3.1 along with their rank and origin. A rough

Table 3.1
Rank and Source of Coals Studied

Coal Name	Rank	Location	Source
Beulah-Zap	Lignite A	Mercer Co., ND	Particle Reduction Services
Utah Blind Canyon	H.V. Bituminous C	Emery Co., Utah	Huntington Power Plant
Pittsburgh No. 8	H.V. Bituminous A	Greene Co., PA	PETC

pulverized grind of Utah Blind Canyon hvC- bituminous coal was obtained from the Huntington Power Plant. A size- classified Pittsburgh No. 8 hvA-bituminous coal was obtained from the PETC Direct Utilization/AR&TD suite of coals (PSOC-1451D), and is the same coal used by other researchers [17, 59, 66, 67]. A highly weathered (during ten years storage at BYU) North Dakota (Zap) lignite-A with a high moisture content, used by other researchers [68], was obtained originally from Particle Reduction Services. Analyses of these coals are given in Table 3.2. The Utah Blind Canyon (UBC) and North Dakota (Zap) coal used in this study were classified in a Vortec cyclone separator and then sieved

Table 3.2
Coal analysis

Coal Type	% of daf coal C	H	N	S	O	dry % Ash	as received % Moisture
Pittsburgh No. 8	83.5	5.69	1.78	0.96	8.1	4.08	1.49
Utah Blind Canyon	79.6	5.81	1.70	---	12.9[a]	9.59	2.36
North Dakota (Zap)	67.2	4.30	1.00	1.06	26.5	6.00	23.3
[b]North Dakota (Zap)	70.8	4.54	1.34	1.06	22.2	9.40	7.04

a. S+O
b. Similar Zap coal used for preparing char from coal with a lower moisture content.

twice using standard US mesh sieves to obtain the 63 - 74 μm size fraction. Coal samples were refrigerated at 5 °C to reduce low temperature oxidation. In addition to the 23% moisture content Zap lignite used to prepare the majority of the Zap chars in this research, one char sample was prepared from a different but similar Zap lignite (also listed in Table 3.2) containing 7% moisture in order to examine effects of parent coal moisture content. This 7% moisture content Zap lignite was obtained from the tailings of the Argon Premium Samples, and was sized and classified under the same conditions as the 23% moisture content Zap lignite. In order to reduce the number of variables considered in this research, only one pulverized coal size fraction was used. The 63-74 μm size fraction is small enough that particle temperature gradients should be insignificant for most of the experiments. In addition, it is a size fraction that is similar to those used in industrial coal fired boilers, and many other investigators have used this same size fraction.

Char Preparation

Chars were prepared from these coals in a flat flame methane burner (FFB) at several different residence times and also in a high pressure controlled profile (HPCP) drop tube reactor under a variety of different pyrolysis conditions at comparable residence times and heating rates. Characteristics of these reactors are described below. Experiments were performed in the HPCP in helium, nitrogen or air to achieve maximum particle temperatures in the range of 950 K to 1627 K, heating rates of 10^4 to $2x10^5$ K/s, and residence times of 135 to 1000 ms. Helium was used to increase the heating rate in the HPCP, since helium has a higher thermal conductivity, diffusivity and heat capacity than nitrogen or oxygen. Experiments were performed in the HPCP in both inert and reactive (O_2 or H_2O-containing) environments. Chars were prepared in the FFB at 1470 K, a heating rate of $7x10^4$ K/s, and a residence time of 50 ms.

High Pressure Controlled Profile Drop Tube Reactor (HPCP). The High Pressure Controlled Profile Reactor (HPCP) is an electrically-heated, laminar flow,

drop tube reactor which has the capability of independently varying temperature, pressure, gas atmosphere, particle velocity, and residence time [69]. Figure 3.1 contains a schematic of the HPCP [69]. The height of the water cooled coal injection probe and the gas flow rate are adjusted independently to change residence time. Coal is injected with a small amount of inert gas at a feed rate of approximately 1 g/h. A water-cooled, nitrogen quenched collection probe is used to collect the char and tar. A virtual impactor followed by a cyclone separates the char from the tar. Tar is collected on glass fiber filters.

The HPCP, which injects particles downward, has a small cool gas region along the centerline in the wake of the injection probe. The particle heating rate in the HPCP depends on the gas atmosphere used, the gas and wall temperatures, the gas velocity, and the injection probe position in the HPCP.

Flat Flame Burner (FFB). The flat flame burner (FFB) [70] produces a laminar methane/air flame, with post flame gases consisting of 4% O_2, 7.5% CO_2, 18% H_2O, and 70.5% N_2. Four percent oxygen in the post flame gases of the flat flame burner was determined by measurement with a Thermox Oxygen analyzer [68]. Using axial and radial gas temperature measurements, feed flow conditions of methane, air and nitrogen, and 4% oxygen in the post flame gases as feed parameters, the Edwards combustion equilibrium program [71] was used to determine the remaining post flame gas composition. Coal particles are injected upward through the base of the methane/air flame along its centerline. A small amount of inert gas is used to entrain the coal particles which are fed to the reactor at a rate of 1-2 g/h. Residence time is adjusted by moving the position of the collection probe, which is water-cooled and nitrogen-quenched to prevent further reaction after collection. Char is separated from unburned tars and aerosols by a glass cyclone. The FFB is designed to have a constant radial gas temperature profile, such that particles injected up through the flame front reach their maximum temperature within a centimeter after leaving the injection probe. In actual operation, there was a blue cone in the flame directly above the injection probe that extended beyond the initial flat flame. This cone

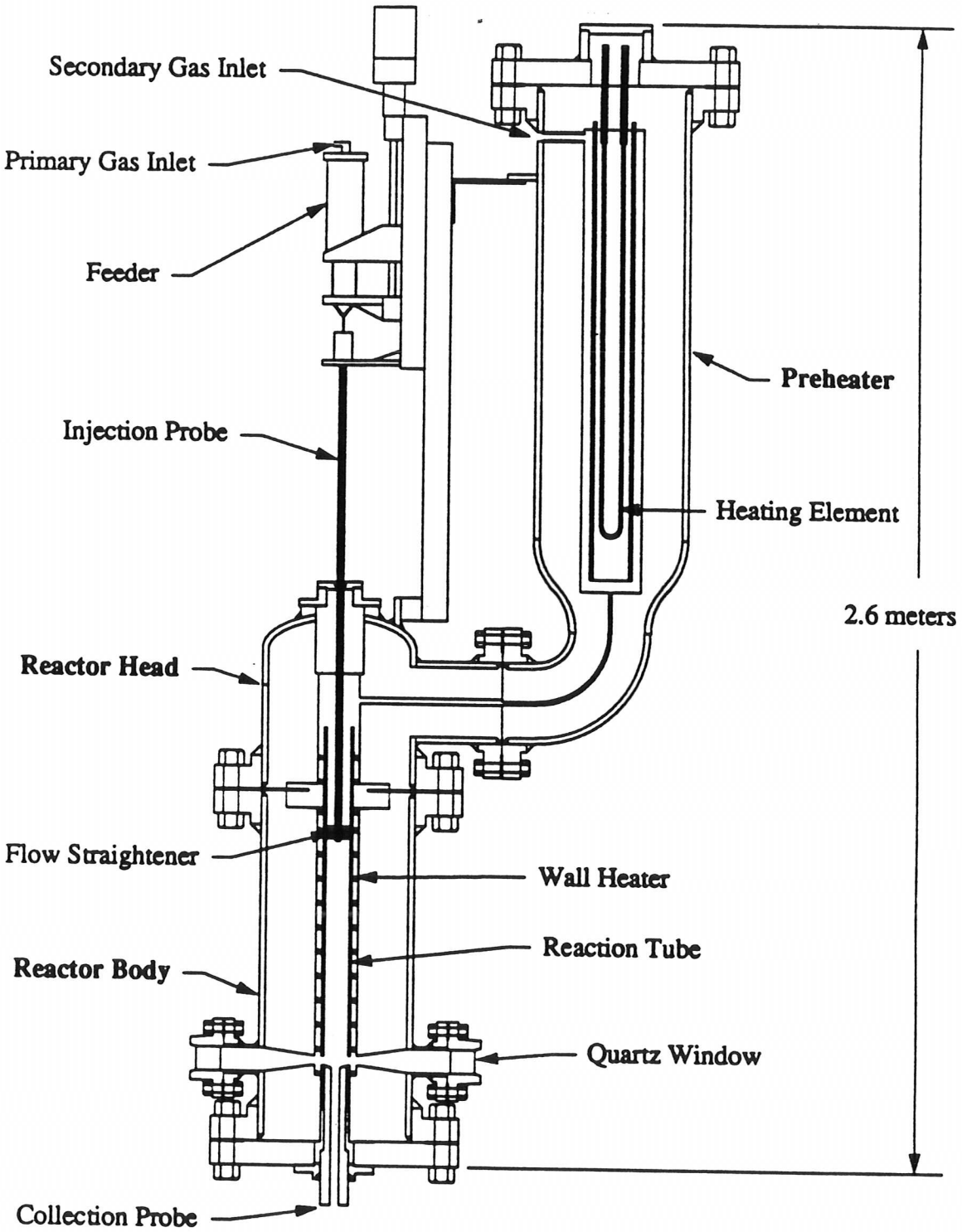

Figure 3.1. Cross section of HPCP drop tube reactor. (With Permission [69])

decreased the heating rate of the particles passing through it.

Modeling Heating Rate & Particle Temperature

Heating rate, temperature, and total volatile yield of char particles in the HPCP and the FFB were calculated using a single-particle transient mass and energy balance [67]. The energy conservation equation [67] used in the CPD model to describe the particle temperature history in the HPCP and FFB is contained in the following equation:

$$m_p c_p \frac{dT_p}{dt} = hA_p(T_g - T_p)B/(e^B - 1) - \sigma\epsilon_p A_p(T_p^4 - T_w^4) - \frac{dm_p}{dt}\Delta H, \qquad (3.1)$$

where $h = \mathrm{Nu}k_g/d_p$. This equation expresses thermal inertia in terms of convective heat transfer from the surrounding gas, radiative heat transfer, and the global heat of reaction during devolatilization. The convective term is corrected for high rates of mass transfer with a blowing parameter [73], represented by $B/(e^B - 1)$, where

$$B = c_{pg}\left(\frac{-dm_p}{dt}\right)/2\pi d_p k_g. \qquad (3.2)$$

The heat of reaction ΔH is set to -100 cal/g, according to the recommendations of Freihaut [39], although these calculations were found [67] to be relatively insensitive to the value used for ΔH. The CPD devolatilization model [72] was used to calculate the devolatilization rate. NMR data for the parent coals were used as input parameters. While NMR data for the specific Pitt.8 coal used in this research was available, NMR data for the specific Zap and Utah coal used in this research were not available. Therefore, when modeling the Zap and UBC experiments, NMR data were varied to obtain model predictions that fit the entire data set for each coal. Particle temperature histories were calculated based on measured gas and wall temperatures. Calculated mass release agreed with measured values (See Fig. 3.2). Calculated heating rates may deviate up to a factor of

two due to uncertainties in heat capacities and particle sizes [67]; however, such errors do not affect the trends between different experiments.

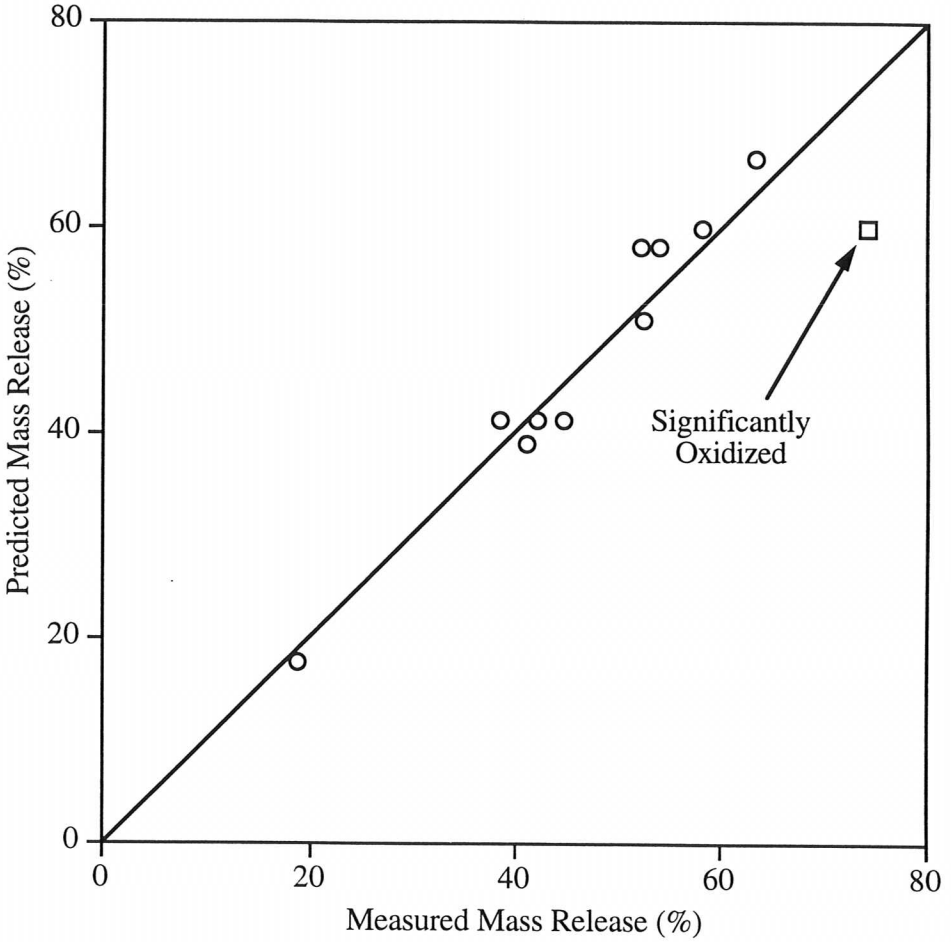

Figure 3.2. Predicted mass release from CPD model versus measured mass release from titanium tracer analysis for Pittsburgh No. 8 coal chars.

Particle temperature and heating rate versus residence time curves generated by the CPD model are illustrated in Figure 3.3 (a and b). The maximum particle heating rates and temperatures for each test condition were used to define char preparation conditions in this study. Although dependent upon temperature, pyrolysis generally occurred between residence times of 50 and 150 ms for chars prepared in helium and between 25 and 300 ms for chars prepared in nitrogen. The corresponding particle temperatures during pyrolysis were generally between 800 and 1000 K. The particle and gas temperatures in helium are

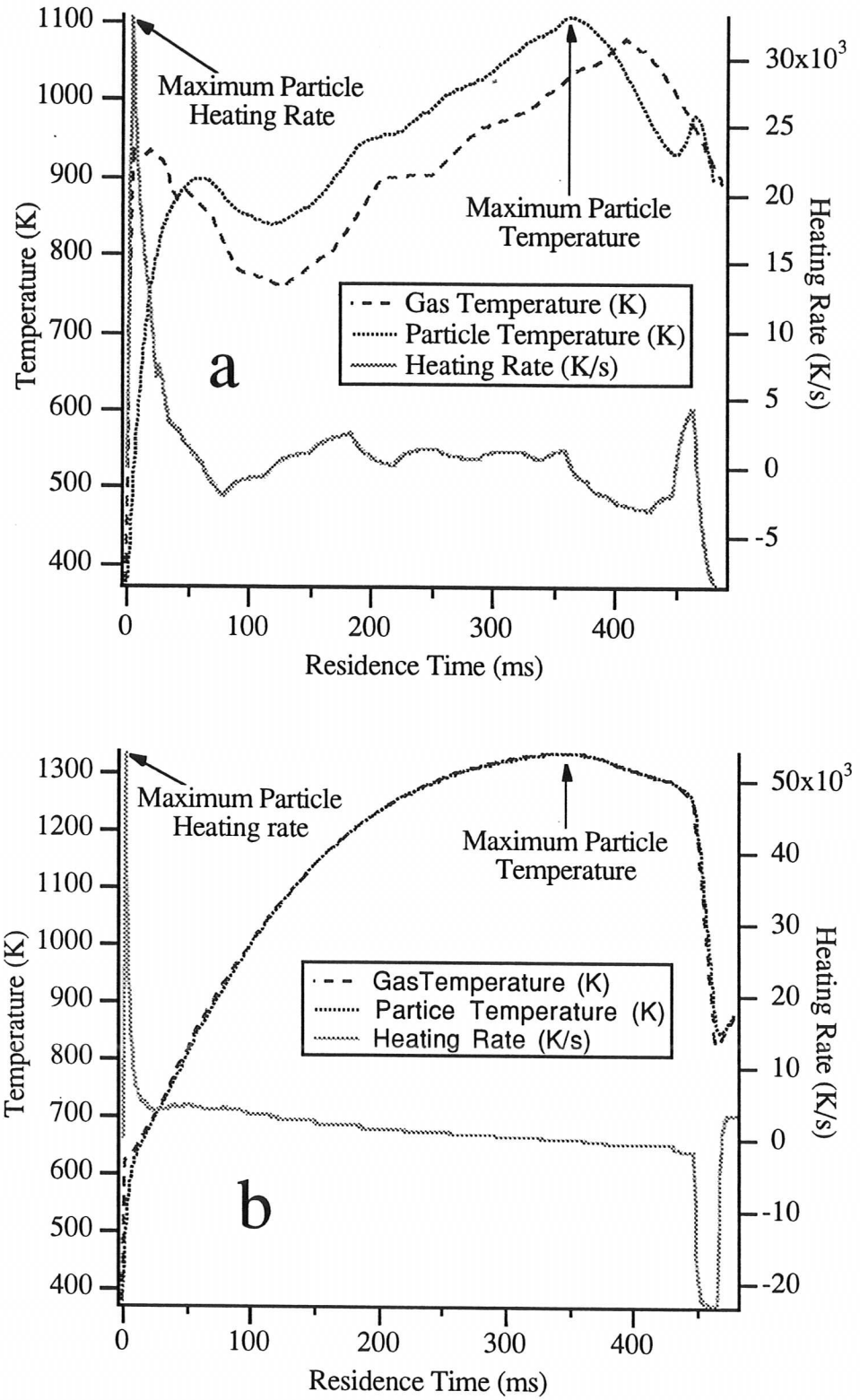

Figure 3.3a,b. Gas and particle temperatures and particle heating rates versus residence time generated by the CPD model using measured gas and wall temperature profiles and a gas velocity profile for Pittsburgh No. 8 coal char preparation. Figure a is for pyrolysis in nitrogen, and Figure b is for pyrolysis in helium.

quite similar due to the high thermal conductivity and diffusivity of helium. On the other hand, there is quite a difference between gas and particle temperatures for the nitrogen experiments because of the lower thermal conductivity and diffusivity of nitrogen. In fact, the particle temperatures in nitrogen are at times higher than the surrounding gas temperature due to radiative heat transfer from the hot reactor walls.

Characterization of Residual Char

Physical and Chemical Properties. Meso-pore (N_2) and micro-pore (CO_2) surface areas were obtained from adsorption isotherms at 77 K and 296 K respectively. The Brunauer, Emmett and Teller (BET) and Dubinin Polanyi (DP) equations [3-10] were used to determine N_2 and CO_2 surface areas respectively. True (skeletal) densities were determined by helium pycnometry [8]. Apparent densities were calculated from tap density measurements assuming a packing factor of 0.45 [8]. Porosities were calculated from the ratio of apparent to true density ($1 - \rho_a/\rho_t$). Mass release data on dry ash free (daf) basis were obtained using Ti as a tracer, as measured by Inductively Coupled Plasma (ICP) analysis. Carbon, hydrogen and nitrogen contents were obtained from CHN analysis of the chars, and oxygen was determined by difference. Ultimate analysis of parent coals however, was obtained from Commercial Testing & Engineering in Denver Colorado. Swelling ratios (d_p/d_{po}) were calculated from measured values of total mass release ($1-m/m_o$) on a daf basis and apparent density (ρ/ρ_o) [58,74] as follows:

$$d_p/d_{po} = (1-m/m_o)(\rho_o/\rho)^{1/3} \qquad (3.4)$$

Rate Measurements. Intrinsic oxidation rates of 1.0 mg char samples were measured isothermally in 10% oxygen at a heating rate of 80 °C/min up to temperatures in the range of 350-525 °C using a standard thermogravimetric system. Oxidation rates, i.e., the slope of the mass vs. time curve, were obtained at 10, 25, 50, 75, and 90% (daf) burnout. Apparent activation energies for a given char were determined from an Arrhenius plot of oxidation rates at each specified burnout level. Due to the higher reactivity of Zap

char, it was necessary to obtain its kinetic parameters at a lower temperature than for the less reactive hv-bituminous chars. Consequently, in order to compare data for different coal ranks, intrinsic reactivities for Zap char at 500 °C were calculated from activation energies and pre-exponential factors obtained from reactivities measured at 400 °C assuming a reaction order of 0.6. All rates were normalized to the residual char mass (daf).

Error Analysis. Uncertainties and standard deviations for each char property measurement along with limited char preparation repeatability measurements are contained in Tables A2.1 and A2.2 in Appendix A2. Appendix A2 also contains a detailed explanation of the error analysis.

Complete Devolatilization. Most of the samples analyzed in this study were collected after complete devolatilization. In this study, a completely devolatilized char particle is defined as one that has reached a plateau along the Total Volatile Yield versus Residence Time curve. In other words, it is a particle that is collected just following the rapid volatile release period, although relatively slow volatile release may still be occurring.

The CPD model [72] was used to determine the theoretical total volatile yield as a function of residence time for a given coal, size fraction, temperature profile, and velocity profile. Figure 3.4 contains plots of theoretical mass release versus time curves created by the CPD model from two different temperature profiles. The two temperature profiles were obtained from essentially the same reactor operating conditions and two different gases, helium and nitrogen. The CPD model is normally used to predict pyrolysis in nitrogen but was modified to account for the different thermal conductivity, heat capacity, and molecular weight of helium. There are two plateaus in the figure that would be defined as complete devolatilization if the char particle represented by the corresponding curve were collected at the residence time where the plateau occurs. The two plateaus are labelled A & B in the figure. There is one for the nitrogen curve and one for the helium curve. If a char sample was collected at a residence time corresponding to positions C, D or E in the figure, the char particles would be defined as partially devolatilized.

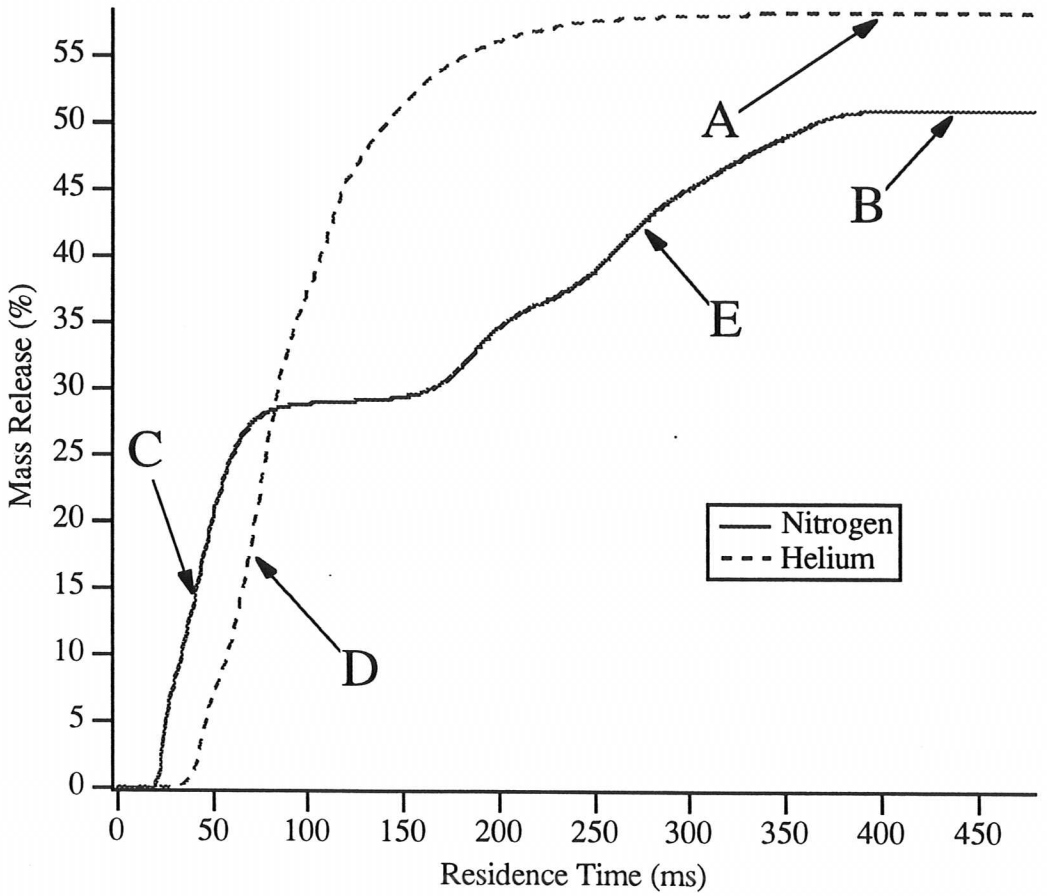

Figure 3.4. Total mass release versus residence time as predicted by the CPD model [72] using measured temperature and velocity profiles from HPCP experiments for Pittsburgh No. 8 coal devolatilization in helium and in nitrogen gas.

Chapter 4*

Effects of Pyrolysis Conditions on Internal Surface Areas, Densities and Porosities of Coal Chars

Introduction

The production of high surface area porous carbons during high temperature pyrolysis of organic materials is an important general phenomenon. It is a key step in combustion and gasification of coals. It is also a route to producing (1) high surface area carbons used as adsorbents and catalyst supports (meso- and macro-porosity becoming increasingly more important for new processes involving adsorption in the liquid stage [21]), (2) carbon molecular sieves used in the separation and purification of gases such as oxygen and nitrogen from air, and (3) graphitized carbons used as electrodes in electrochemical processes.

In coal combustion, the oxidation rate of porous char formed during the initial rapid pyrolysis of coal depends on process conditions and char physical/chemical properties including (1) the diffusion of reactant gases to the surface and into the pores of char particles, (2) the concentration of active sites, (3) the crystallinity and structure (extent of graphitization), and (4) the nature of organic impurities contained. In consideration of (1) above, char pore structure and internal surface area, which in turn partially determine access to the internal surfaces and active sites by oxygen or other reactive gases, are important. Coal chars are high internal surface area materials which generally contain a network of micro-, meso-, and macro-pores, the structure and distribution of which depends upon coal rank and pyrolysis conditions; moreover, the pore structure and surface area of coal chars change greatly in the course of their burnout. Any attempt to completely understand and model coal combustion requires a knowledge of how coal rank and pyrolysis conditions influence the initial char structure and internal surface area.

* The main body of the results from this research is separated into three sections comprising chapters 4-6. Each Chapter has its own mini-introduction, results section, discussion, and conclusions. A general summary is given in Chapter 7.

Ultimately, an understanding of the char formation mechanism is desirable.

This research focuses on (1) the effects of maximum particle temperature, heating rate and residence time on the physical properties, i.e. N_2 and CO_2 surface areas and porosities, of chars prepared from three coals of different rank in an inert environment at high temperatures, high heating rates, and low residence times, (2) the effects of different reactive gas atmospheres on internal surface areas, true (skeletal) densities and porosities of these same coal chars, and (3) the effects of total mass release on densification or graphitization, as indicated by the true density of these chars.

Results

Tables A1.1-A1.3 (see Appendix A1) list the pyrolysis conditions at which the chars in this research were prepared. Table A1.4 (see Appendix A1) contains physical properties and total percentage mass release of these chars. Figure 4.1 shows the internal surface area versus total mass release of chars from all three coals following pyrolysis in the HPCP in an inert atmosphere. The micro-pore (CO_2) surface area of all three coal chars begins to increase at 40% mass release and continues to increase with increasing total (daf) mass release to about 60%. At 60% mass release, maximum CO_2 surface areas for Pittsburgh No. 8 (Pitt. 8) and Utah Blind Canyon (UBC) chars are about the same (300 m^2/g) and very large relative to maximum N_2 surface areas (about 20 m^2/g). Both CO_2 and N_2 surface areas of North Dakota (Zap) char are much higher than for the UBC and Pitt. 8 chars prepared under the same conditions. The maximum error in the CO_2 surface area measurements was $\pm$ 6.2%. Except for short residence time Pitt. 8 char, CO_2 surface areas are generally significantly larger for chars relative to coals as reported in previous studies [7,8,11,19,20]. The CO_2 surface area of the Pitt. 8 char, however, initially decreases with mass release while those of the other coal chars do not. This decrease in CO_2 surface area can be explained due to the fact that Pitt. 8 is a plastic coal. Upon heating, a plastic coal initially melts, the coal matrix assumes a liquid state, and micro-pores may be covered. After the initial coal melt, crosslinking reactions cause a rigid char structure to be

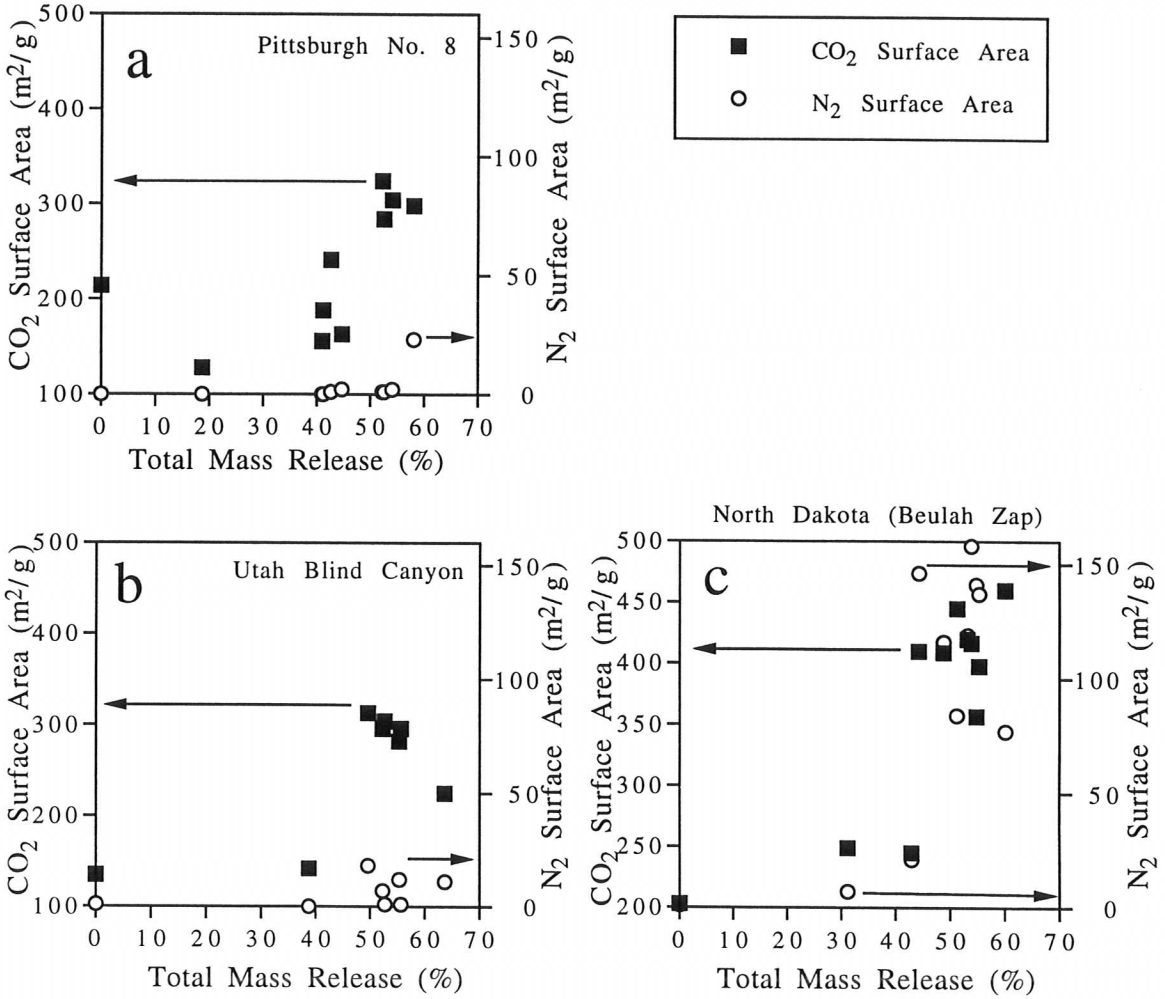

Figure 4.1a,b,c. Internal surface areas versus total mass release for chars prepared in an inert environment in the HPCP at temperatures between 950 to 1627 K, heating rates between 10^4 to 7.5×10^4 K/s, and residence times between 135 and 980 ms.

formed. As pyrolysis continues, closed micro-pores are reopened along with new micro-pores as mass is released.

As shown in Figure 4.2, internal surface areas generally increase with residence time when prepared in an inert atmosphere in the HPCP at pyrolysis temperatures between 840 and 1106 K. Much of the data represented in Figure 4.1 and in Figure 4.2 is from the same set of char samples, as is the case with many of the figures and tables throughout this section and the entire work. All data in Figure 4.2 are for fully devolatilized chars; therefore, while the residence times include the devolatilization time, the effect of varying residence time is related to baking of chars rather than increasing mass release. Generally, CO_2 surface areas increase with increasing residence time except for the initial decrease exhibited by the Pitt. 8 char. For Zap chars prepared between 840 and 1106 K, N_2 surface area trends mimic those for CO_2 surface area, i.e. N_2 surface area increases from 0 to 130 m^2/g while CO_2 surface area increases from 200 to 450 m^2/g. This is not true for the chars formed from the other coals, whose N_2 surface areas stayed near zero.

Figure 4.3 contains plots of the internal surface areas versus maximum particle temperature and heating rate for all three coals. CO_2 surface area data for Pittsburgh No. 8 and UBC chars are limited to chars prepared in a narrow range of residence time because the effects of residence time on the CO_2 surface area of these chars dominate over temperature and heating rate effects in this range. However, both CO_2 and N_2 surface area data for Zap char are presented for chars prepared with a wider range of residence times, because Zap char surface areas are less affected by changes in residence time. CO_2 surface areas of Pitt. 8 chars increase 100 m^2/g and of Zap chars increase 50 m^2/g with increasing maximum particle temperature and heating rate, while those for the UBC char do not change in the range of temperatures and heating rates considered. In contrast, N_2 surface areas of Zap chars actually decrease from 20 to 50 m^2/g for these temperatures and heating rates. The CO_2 surface areas of all three coal chars are larger than those of the parent coals.

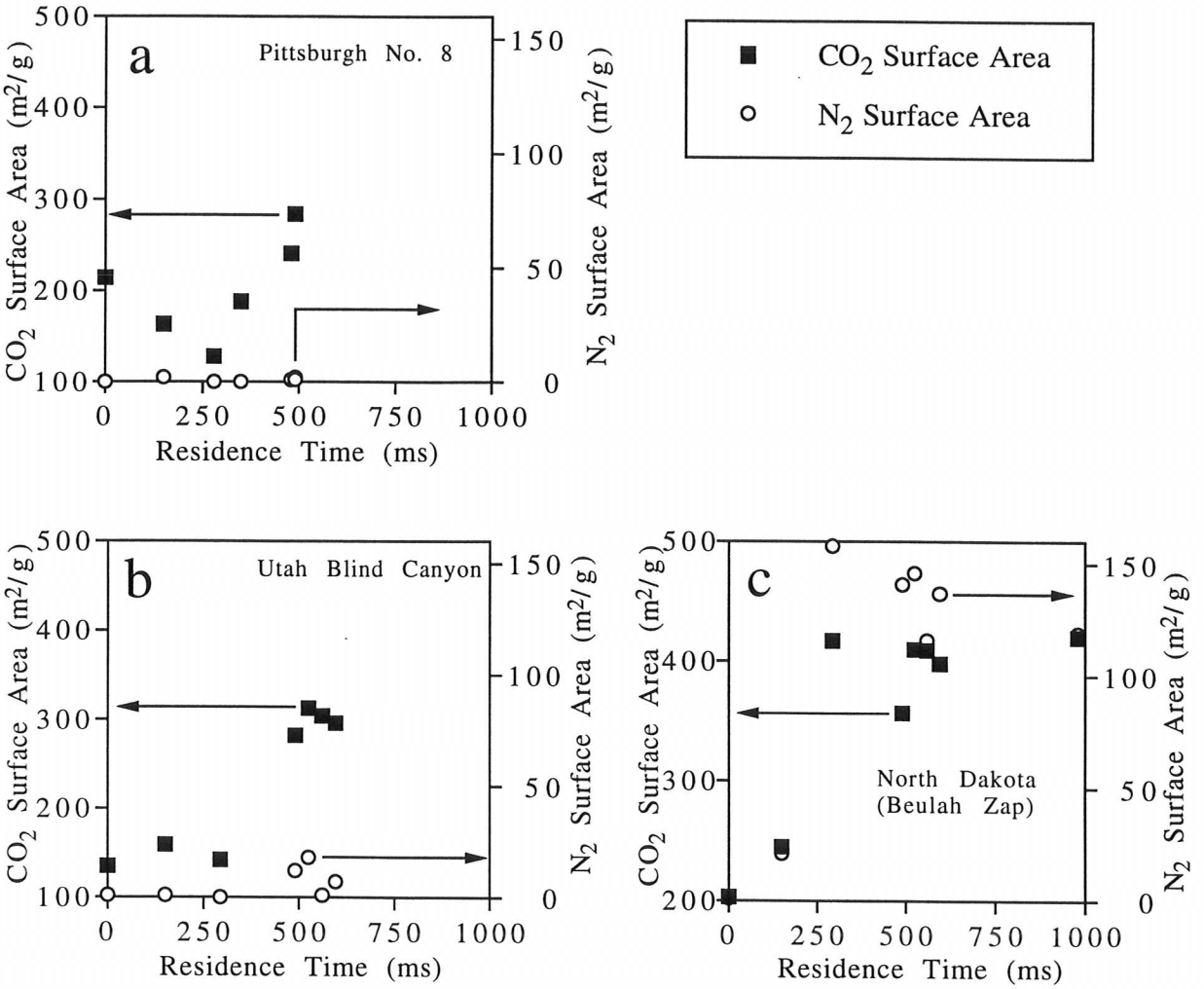

Figure 4.2a,b,c. Internal surface area versus residence time for chars prepared in an inert environment in the HPCP at temperatures between 840 and 1106 K, and heating rates between 10^4 and $4x10^4$ K/s.

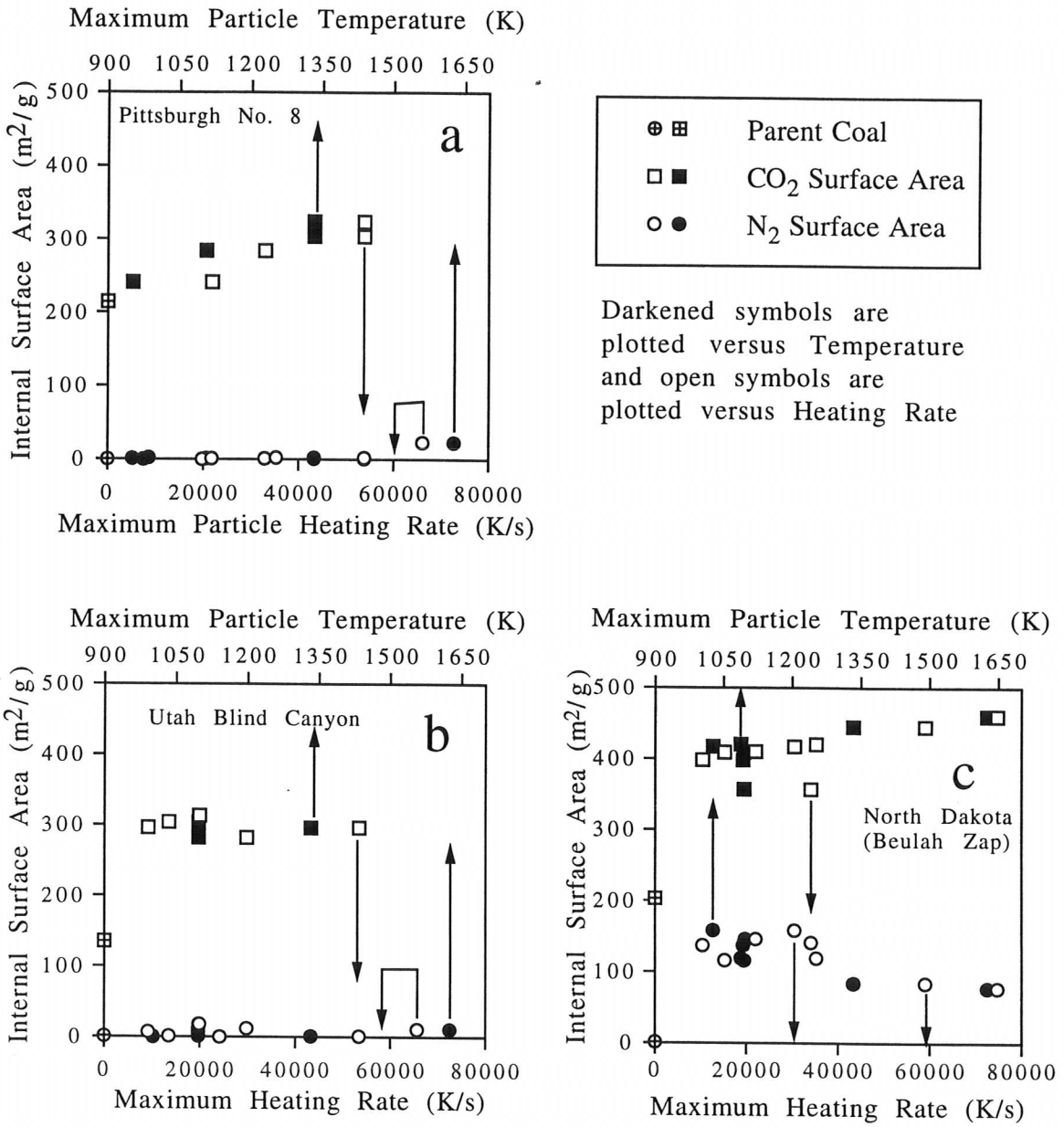

Figure 4.3a,b,c. Internal surface area versus maximum particle temperature and heating rate for chars prepared in an inert environment in the HPCP. N_2 surface area data represent chars prepared with a wide range of residence times. However, CO_2 surface area data represents chars prepared between 480 and 490 ms for Figure a, and 490 and 595 ms for Figure b. The North Dakota CO_2 surface area data represents chars prepared with a wide range of residence times from 135 to 980 ms.

However, while most UBC and Zap char CO_2 surface areas are at least two times larger than that of their parent coal, Pitt. 8 chars are at most 100 m^2/g larger than that of the 214 m^2/g Pitt. 8 coal CO_2 surface area. The plasticity of the Pitt. 8 coal causes some of the micro-pores to be covered or destroyed during pyrolysis, and hence the CO_2 surface area does not increase as much as with the other coal chars.

Surface areas of Pitt. 8 chars prepared in different pyrolysis atmospheres are compared in Figure 4.4. For chars prepared in the HPCP at 986 K and 150 ms, the addition of oxygen or steam to the pyrolysis atmosphere has little effect on CO_2 surface area, considering that the repeatability for CO_2 surface areas of approximately 300 m^2/g chars prepared at the same conditions is $\pm$ 20 m^2/g ($\pm$ 6.2%). However, a pyrolysis atmosphere of 4% O_2 and 96% N_2 increases the N_2 surface area from 2 (N_2 atmosphere) to 23 m^2/g with a repeatability of $\pm$ 1.0 m^2/g, or $\pm$ 4%. Steam has no effect on N_2 surface area at this low residence time (compare Samples 1 and 3). Addition of 4% O_2 to the pyrolysis gas at 1627 K and 135 ms has no effect on CO_2 surface area and slightly decreases N_2 surface area. Because this char was prepared at a much higher temperature (1627 vs 986 K) and heating rate than the 150 ms char, it had experienced much more severe pyrolysis conditions. The char prepared in the FFB at 1470 K and 50 ms (Sample 6) has a 42 m^2/g (21%) larger CO_2 surface area and a 14 m^2/g (78%) larger N_2 surface area than the char prepared in 4% O_2 in the HPCP (Sample 5) under a somewhat similar temperature and heating rate to the FFB. Even though the maximum particle temperatures in the FFB were lower than for the 135 ms HPCP char, the particle heating rates were about the same. This indicates that the presence of steam in the FFB experiments at high heating rates may facilitate more significant gasification at lower residence times than the lower heating rate HPCP experiments at longer residence times.

The presence of oxygen in the pyrolysis gas atmosphere has only a small positive

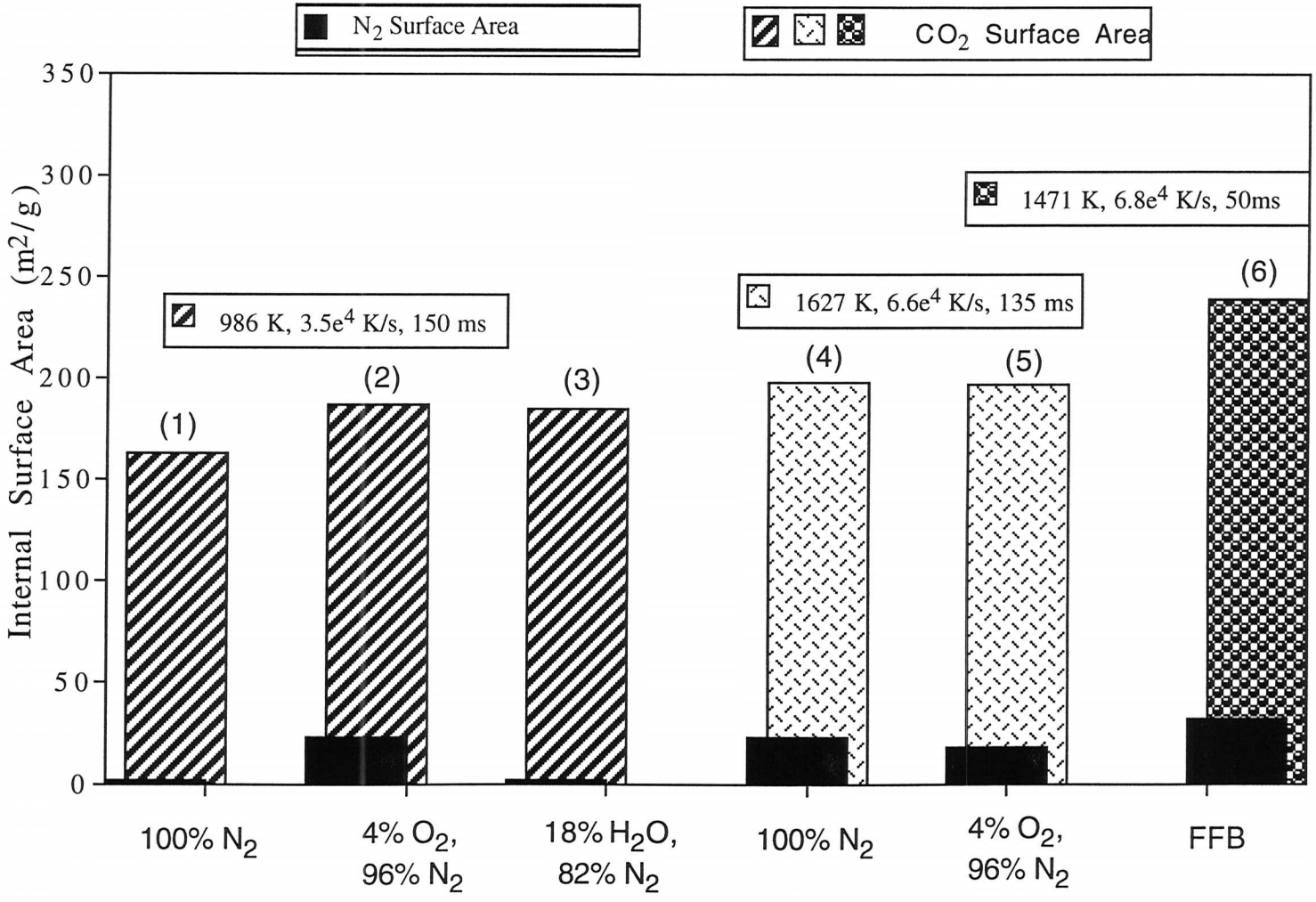

Figure 4.4. Effects of pyrolysis atmosphere on internal surface areas of Pittsburgh No. 8 chars. Chars were prepared in the HPCP in the different atmospheres shown or in the FFB in 4% O_2, 7.5% CO_2, 18% H_2O and 70.5% N_2. Maximum particle temperatures, heating rates and residence times are listed in the legend.

effect on CO_2 and N_2 surface areas for UBC char prepared at 1000 K and 294 ms (see Fig. 4.5, Samples 1 and 2) as shown in Figure 4.5. However, once again the surface areas for FFB char are much higher. Sample 3 was prepared in the HPCP at a similar heating rate, higher temperature and longer residence time than the FFB char (Sample 4). The N_2 surface area of the FFB char is 37 m^2/g (336%) higher, while the CO_2 surface area is approximately 123 m^2/g (54%) higher than the comparable HPCP char (see Samples 3 and 4).

The greater part of the investigation of pyrolysis gas effects on char internal surface area focused on Zap (23% moisture content) coal because of its propensity to undergo large increases in both N_2 and CO_2 surface areas. However, some of the results may extrapolate qualitatively to bituminous coals, because as will be discussed, the mechanisms accounting for increases or decreases in internal surface area during pyrolysis in the presence of a reactive gas may be similar. Figure 4.6 compares surface areas of Zap chars prepared under different pyrolysis atmospheres. Addition of oxygen to the pyrolysis atmosphere decreases both CO_2 and N_2 surface areas by 27 and 108%, respectively (see Samples 7 and 8), while steam addition (see Samples 3 and 4) increases N_2 surface area by 68%. Moreover, pyrolysis with 18% steam in the HPCP results in a N_2 surface area 25% higher than that for FFB char (see Samples 4 and 6). However, the CO_2 surface area of the FFB char is still 21% higher than the char prepared in steam in the HPCP.

Figure 4.6 also compares the effects of steam addition to the pyrolysis atmosphere on surface areas at low and high residence times. At short residence times (i.e., 150 ms -- see Samples 1 and 2), addition of 18% steam causes only slight (33 and 7 m^2/g, i.e., 13% and 33%) increases in CO_2 and N_2 surface areas. However at a longer residence time (490 ms, see Samples 3 and 4), an 18% steam atmosphere increases CO_2 surface area by 67 m^2/g (19%) and N_2 surface area by 96 m^2/g (68%).

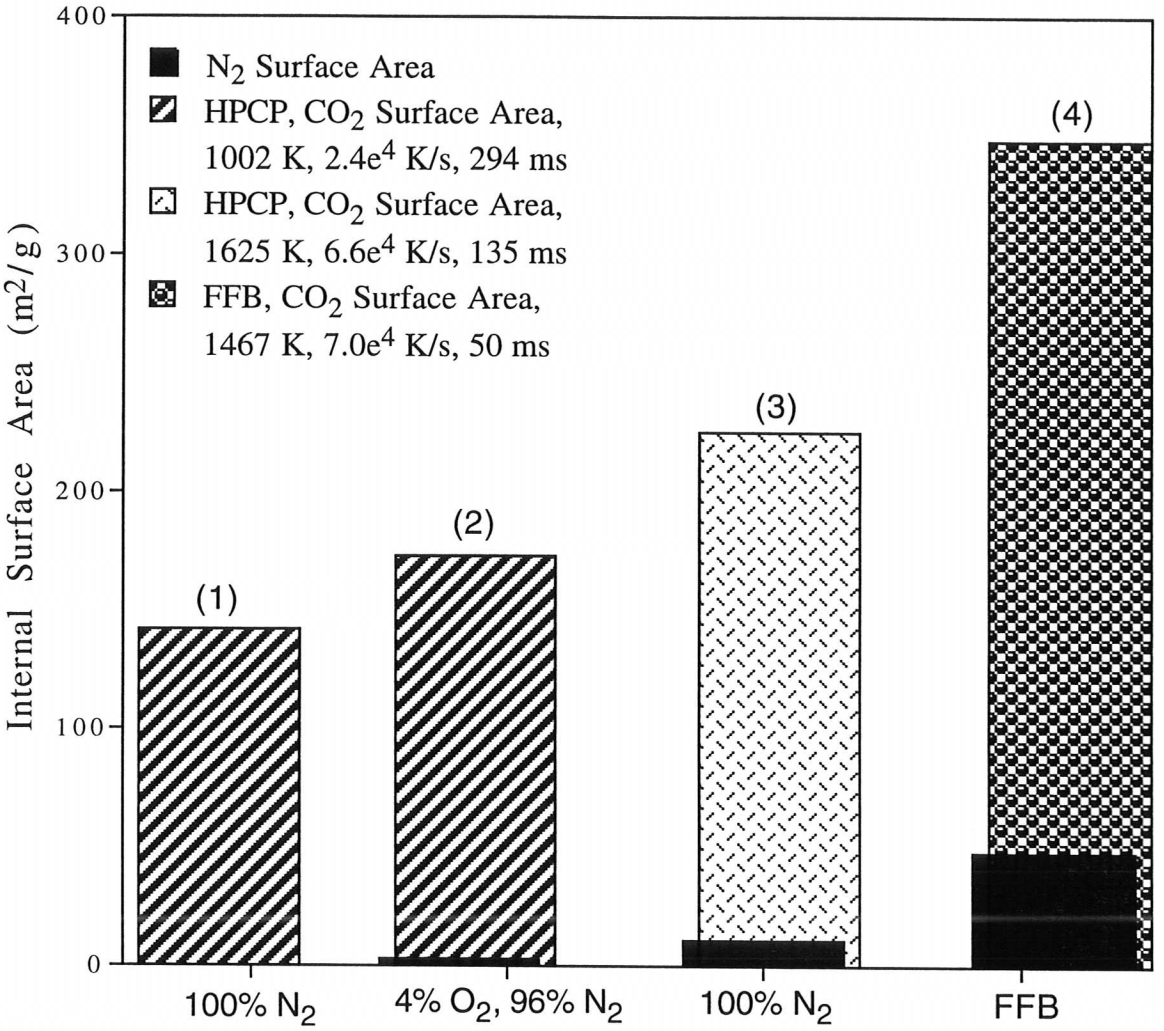

Figure 4.5. Effects of pyrolysis atmosphere on internal surface areas of Utah Blind Canyon chars. Chars were prepared in the HPCP in the different atmospheres shown or in the FFB in 4% O_2, 7.5% CO_2, 18% H_2O and 70.5% N_2. Maximum particle temperatures, heating rates and residence times are listed in the legend.

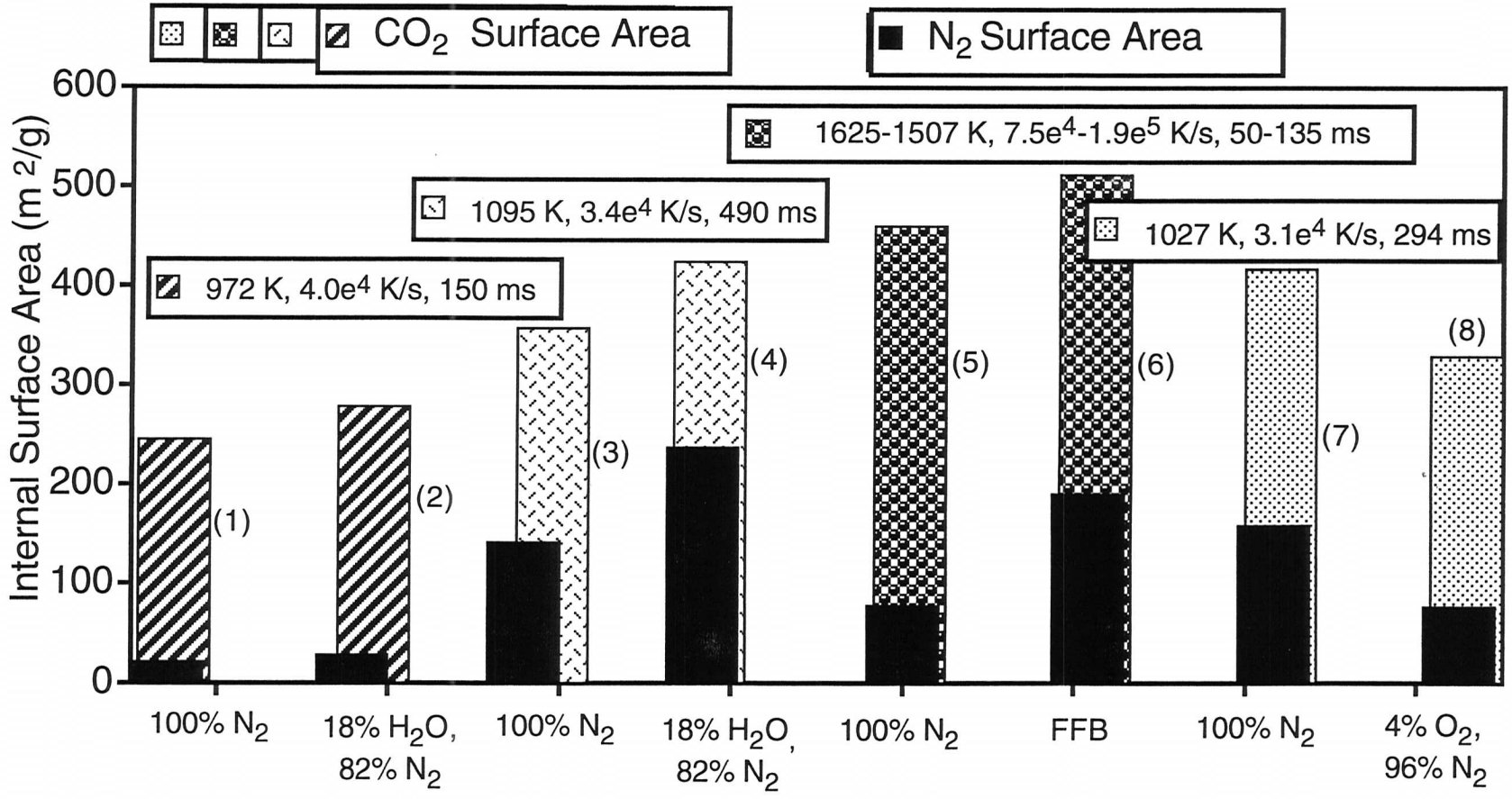

Figure 4.6. Effects of pyrolysis atmosphere on internal surface areas of North Dakota (Zap) chars. Chars were prepared in the HPCP in the different atmospheres shown or in the FFB in 4% O_2, 7.5% CO_2, 18% H_2O and 70.5% N_2. Maximum particle temperatures, heating rates and residence times are indicated above each bar.

Table 4.1 compares the effects of parent coal moisture content and pyrolysis in 18% steam on surface areas of Zap char. Pyrolysis of coal with 23% moisture produces a char having high CO_2 and N_2 surface areas. Drying at 110 °C for 2 h in air prior to pyrolysis causes a significant reduction of surface area, the most significant reduction being in the N_2 surface area; it also significantly reduces mass release. Devolatilization of the 23% moisture containing coal in 18% steam results in higher CO_2 and N_2 surface areas, although measured daf mass release is slightly lower. Another North Dakota lignite with a lower moisture content (7.0%) was also pyrolyzed under somewhat conditions. However, in order to ensure that the mass release of char prepared from the 7% Zap lignite was higher than that for char prepared from 23% moisture content Zap lignite, it was prepared at a preparation temperature several hundred degrees higher than Zap char prepared from the 23% moisture content lignite. Other than the moisture content, the analysis of this coal is

Table 4.1

Effects of Parent Coal Moisture Content During Pyrolysis of North Dakota Lignite

% Moisture of Parent Coal	Char Properties			Pyrolysis Gas Atmosphere
	CO_2 Surface Area (m^2/g)	N_2 Surface Area (m^2/g)	Total Mass Release (% daf)	
23.3[a]	357	141	55	100% N_2
0.0[b]	249	7	31	100% N_2
23.3	424	237	51	18% H_20, 82% N_2
7.0[c]	468	4	72	[d]100% N_2

a. Chars were prepared from North Dakota (Zap) lignite at 1095 K for 490 ms.
b. This char was prepared from the same lignite as above following drying for two hours in a muffle furnace at 110 °C.
c. Prepared from a similar North Dakota (Zap) lignite with a different moisture content. The ultimate analysis of this coal, along with the other coals, is contained in Table 3.2. All (Zap) chars in this study, except this one, were prepared from the lignite with a higher moisture content.
d. Char prepared under similar pyrolysis conditions to those above.

similar to that of the 23% moisture content Zap coal (see Table 3.2). However, the carbon, oxygen and ash content of the two Zap lignites differ by 3 to 4% (absolute), and the 23% moisture content Zap was weathered. Consistent with its higher mass release, the CO_2 surface area of char prepared from the 7% moisture content coal is higher than for the other

chars; however, its N_2 surface area is barely above that of the parent coal.

True densities are plotted versus mass release in Figure 4.7 for Pitt. 8, UBC and Zap coals. There is a clear trend of increasing density with increasing mass release independent of coal rank, ash content, and pyrolysis conditions. Measured values for the ash true density were obtained from helium pycnometry analysis of pure ash samples. One value of ash true density was used to calculate ash free true densities for HPCP chars and one value was used for FFB chars. Inspite of over 1.0 g/cc difference in ash true density between HPCP and FFB char ash, calculated ash-free char true densities for the FFB data are very similar to the ash-free HPCP char data, as shown in Figure 4.7b. This finding of ash free true density increasing with increasing mass release regardless of coal type, ash content, or preparation conditions is an indication of ordering of layered carbon planes within the coal char matrix due to an increase in carbon aromatization during devolatilization. Carbon aromatization increases as aliphatic carbon is released along with hydrogen and oxygen that is preferentially released from the char during pyrolysis [72].

Discussion

Effects of Pyrolysis Temperature, Heating Rate, Residence Time and Mass Release on Surface Area

The general trend is for char micro-pore surface area to increase with maximum particle temperature and heating rate. This effect is partly related to mass release and residence time (Fig. 4.1-4.2). For example, as maximum particle temperature and heating rate increase, mass release increases somewhat and completion of pyrolysis occurs at a shorter residence time. For a constant residence time, the sooner complete pyrolysis occurs, the longer will be the post-pyrolysis baking of the chars [75]. The effects of maximum particle temperature and corresponding heating rate appear to be somewhat less at longer residence times than shorter residence times. At longer residence times, the potential to further increase mass release is somewhat less, and additional post-pyrolysis bake time reaches diminishing returns in terms of increasing surface area.

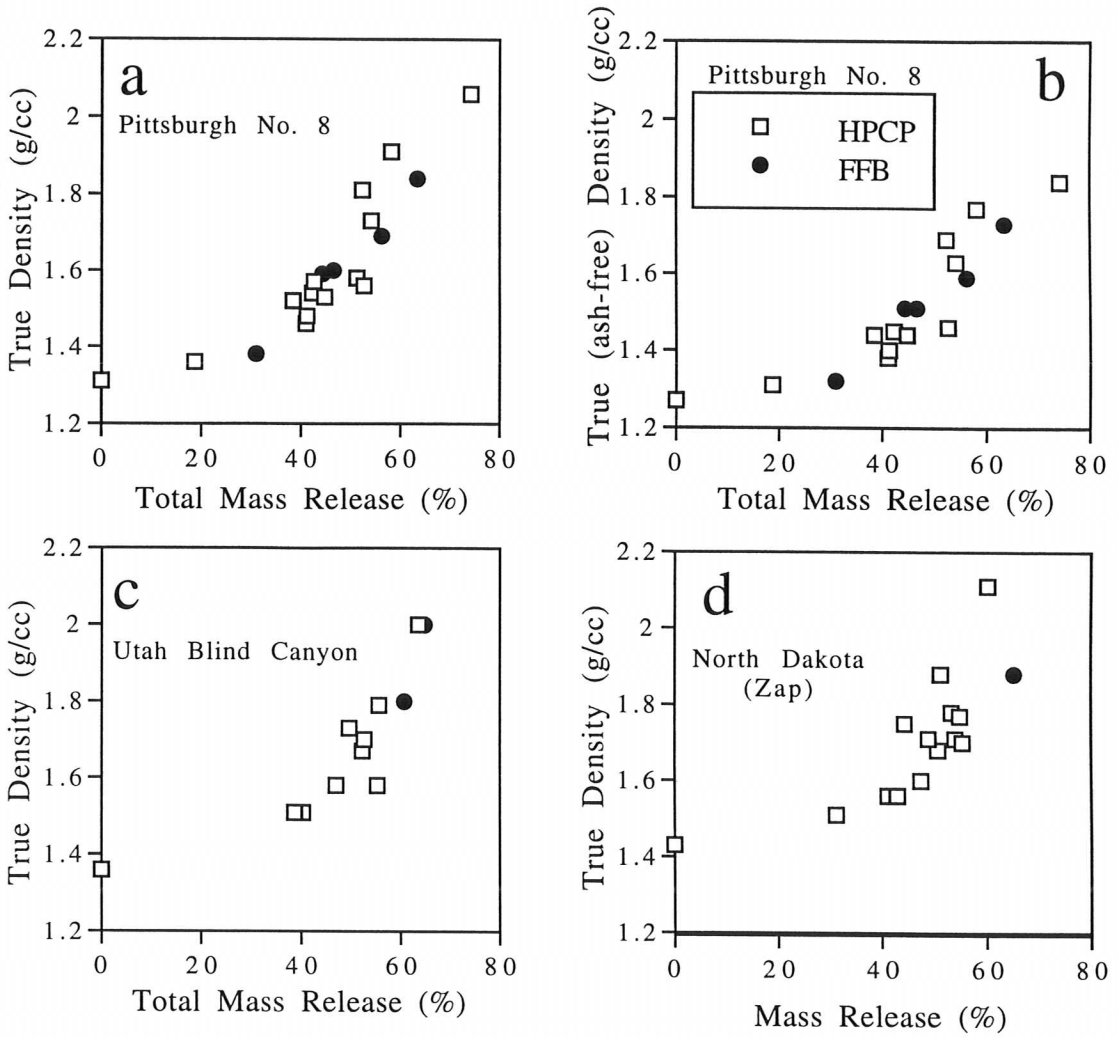

Figure 4.7a, b, c, d. True density and ash free true density versus total mass release for chars prepared under a variety of different pyrolysis conditions in the HPCP and FFB.

In physical terms, the CO_2 surface area results may be explained as follows. As a coal particle is heated and kept at temperatures high enough to cause chemical restructuring in the carbon matrix, gases are released from the coal particle. The nature of this release is such that many micro-pores having pore diameters less than 2.0 nm are opened. These micro-pores have a large surface to volume ratio. The amount of micro-pore surface area opened is dependent upon the extent of mass release which in turn is somewhat dependent upon pyrolysis temperatures, heating rates and residence times. Even if mass release is only increased by a few percent due to increased temperature, heating rate and residence time, it may have a significant effect on CO_2 surface area. The few percent increase in mass release may be mass which was blocking the opening of micro-pores. In addition to the kinetics controlling pyrolysis and the effects of temperature on the vaporization of potential volatile matter, at low temperatures and heating rates, crosslinking reactions occur, incorporating organic material into the char matrix that might otherwise be released as volatile matter. At higher temperatures and heating rates, more volatiles (than at lower temperatures and heating rates) are expelled from the particle before crosslinking can occur to solidify the reacting material into a solid porous char matrix. Longer residence times also somewhat increase the amount of volatile matter released. Even small increases in devolatilization may increase micro-pore surface area.

N_2 surface areas only substantially increase relative to the parent coal during char formation in inert gas atmospheres for Zap chars. This is probably due to the Zap's higher 23% moisture content compared to 1.49 and 2.36% for the Pitt. 8 and UBC coal (see Table 4.1), although the effects of plastic and non-plastic coals between Pitt. 8 and Zap coal char is also significant, as discussed earlier. More specifically, the results of this work indicate that N_2 surface area of Zap char increases with increasing mass release, increases rapidly with residence time to about 300 ms and declines slowly thereafter, and declines slowly or remains about the same between maximum particle temperatures and heating rates of 950 to 1650 K and 10^4 to 7.5 x 10^4 K/s, respectively.

N_2 surface area is contained in meso-pores, which have pore diameters between 2 and 50 nm and are probably formed from micro-pore coalescence or widening. N_2 surface area, therefore, correlates to some extent with mass release, as does CO_2 surface area. However, an increase in N_2 surface area may require an additional chemical reaction to those strictly associated with devolatilization, such as gasification reactions involving the moisture contained in the Zap lignite or in a reactive devolatilization gas atmosphere as in the FFB.

Effects of Reactive Gas Atmosphere on Surface Area

The two bituminous coals form chars with small increases in N_2 surface area at the temperatures, heating rates and residence times considered in this study (see Figs. 4.1-4.3). However, the most significant increases were observed for chars which experienced mild H_2O or CO_2 gasification or O_2 oxidation. From the results of the internal surface area comparison of Zap chars prepared in different gas atmospheres (see Fig. 4.6) it appears that the high N_2 surface areas of chars prepared in the FFB may be due to steam gasification. However, the high char CO_2 surface areas produced in the FFB are probably a result of a high mass release as discussed in the previous section. The effect of oxygen addition to the pyrolysis atmosphere for all three chars is to sometimes slightly increase and sometimes slightly decrease both N_2 and CO_2 surface area. This erratic behavior was also observed by others [12]. Oxygen may increase N_2 surface area by aiding in micro-pore coalescence or widening and may increase both N_2 and CO_2 surface area by removing material blocking meso- and micro-pores. Alternatively, oxygen may decrease both N_2 and CO_2 surface area by removing bulk carbonaceous material containing open meso- and micro-pores from the external char surface or from large macro-pore surfaces.

Zap char prepared in the FFB containing 18% steam in its post flame gases (see Fig. 4.6, Sample 6) has a fairly high meso-pore surface area, although 47 m^2/g (25%) less than the char prepared in 18% steam in the HPCP (Sample 4). However, the micro-pore

surface area of the Zap FFB char is 88 m^2/g (21%) higher than the meso-pore surface area of Sample 4. The maximum temperature for preparation of Zap FFB chars was 1507 K, while the maximum particle heating rate was $1.9x10^5$ K/s. Maximum particle temperature, heating rate and residence time are the most significant factors affecting char micro-pore surface area for a given coal type. The lower micro-pore surface area of char prepared in 18% steam in the HPCP (Sample 4) is consistent with its lower preparation temperature and heating rate. The higher meso-pore surface area of the HPCP char (Sample 4) is consistent with a larger extent of steam gasification possible at longer residence times. Furthermore, the lower preparation temperatures and heating rates allow more time for diffusion of steam into pores before reaction, which would encourage production of larger meso-pore surface areas.

As discussed before, Zap char prepared in the HPCP with 18% steam (see Fig. 4.6, Sample 3-4) has a 96 m^2/g (68%) larger meso-pore surface area than char prepared in 100% nitrogen under otherwise similar conditions in the HPCP. The increase in N_2 surface area is attributed to partial steam gasification. However, the amount of steam gasification necessary to cause the increase in N_2 surface area was smaller than could be detected by Ti tracer mass release measurements. The measured values of mass release for Samples 3 and 4 are 54.8 and 50.6%, respectively. These values are essentially equal, considering the uncertainty of preparation conditions and repeatability limits for preparation of char in steam compared to nitrogen.

It is of interest to consider which gasification or oxidation reactions predominate under the conditions of this study. Three different reaction zones exist for gas/carbon reactions [76] depending on mass transport conditions determined by the temperature of reaction:

Zone I. This is the chemically-controlled reaction zone in which the controlling process is surface reaction, i.e., chemisorption of a reacting gas molecule onto a carbon

free site to form a surface oxygen complex, a rearrangement of chemisorbed species on the surface to desorbable product or products, and desorption of product or products from the surface. This process is the rate-determining at low reaction temperatures. The controlling part of this process may be the formation of the surface oxygen complex (First or Second order reaction), rearrangement and desorption of products (Zero or First order reaction), or a combination of both (Reaction order = 0 to 2).

Zone II. This is the reaction zone influenced by pore diffusion, involving mass transport of reacting gas from the exterior surface to active sites inside the pores and mass transport of the products out of the particle. The rate is determined by a combination of the chemical reaction rate and the pore diffusion rate.

Zone III. In this zone, the rate is controlled by film diffusion. Film diffusion dominates at high reaction temperatures and involves mass transport of reacting gas and product or products from the main gas stream across a boundary layer to the exterior surface of the solid, where reaction occurs instantaneously.

Table 4.2 contains approximate relative rates of gas-carbon reactions at 800 K and 0.1 atm. pressure, and their true activation energies. Even if there were considerable error in the relative rates provided in Table 4.2, it is clear that any steam or carbon dioxide

Table 4.2

Relative Rates and Activation Energies of Gas-Carbon Reactions

Reaction	True Activation Energies, kcal/mole[a]	Relative Rates at 800 K and 0.1 atm. Pressure[b]
$C+CO_2 \rightarrow 2CO$	86	1
$C+H_2O \rightarrow CO+H_2$	80	3
$C+1/2O_2 \rightarrow CO$	50-58	1×10^5

a. Reference 76. True activation energy means activation energies experimentally determined in the chemical reaction controlled Zone I.
b. Reference 76. Approximate relative rates averaged from different investigators.

gasification occurring at that temperature and pressure would be totally insignificant compared to O_2 oxidation. However, because of the higher activation energies of the first two reactions, as the temperature of the reaction increases, the difference in the overall reaction rates of the different gas-carbon reactions gradually decreases. According to

Walker and Rusinko [76], the carbon-oxygen, carbon-steam and carbon-carbon dioxide reactions are quite similar at extremely high temperatures where all reaction rates are under Zone III film diffusion control. The carbon-hydrogen reaction however, is much less significant [76] even at high temperatures.

The temperature range of experiments for the present work was between 950 and 1627 K. Reaction rates were calculated for oxygen oxidation and steam and CO_2 gasification of chars prepared from all three coals considering diffusional effects and partial pressures (18% H_2O, 7.5% CO_2, and 4% O_2) from global kinetic parameters obtained from Goetz et al. [77] for Pittsburgh No. 8 coal char. Goetz et al. and coworkers did not present kinetic parameters for steam. Therefore, the surface reaction rate constant k_s for steam was determined by multiplying the k_s value for carbon dioxide by two, since the surface reaction rate of steam is approximately twice as large as that for carbon dioxide regardless of temperature. At a particle temperature of 1500 K, essentially the same as FFB particle temperatures (1507 K) in this research, the carbon-oxygen rate was 267 times higher than the carbon-steam reaction rate, and 1295 times higher than the carbon-carbon dioxide reaction rate. In addition to the differences in reaction rate at the same temperature, particle temperatures will be higher in oxygen than in steam or carbon dioxide due to the exothermic carbon-oxygen reaction. Of course, in the FFB the particle temperature will be the same for all reactions because the gases are mixed. Therefore, experiments performed in the HPCP or FFB where reactant gases were present would be more significantly affected by O_2 oxidation than by steam or carbon dioxide gasification in terms of mass removed. Nevertheless, at 1500 K, film diffusion partially controls the carbon-oxygen reaction but does not affect the carbon-carbon dioxide and carbon-steam reactions.

Even though rates of carbon-oxygen and carbon-steam reactions in Zone III may be [76] about the same, film diffusion reaction control of the carbon-steam reaction may not occur until temperatures over 3000 K. Steam is probably more effective at increasing meso-pore surface area than oxygen if the carbon-steam reaction takes place in Zone II as

opposed to Zone III. Steam diffusivity at 1500 K in nitrogen is somewhat higher than in oxygen. The higher diffusivity and lower intrinsic reactivity of steam allows greater penetration of H_2O molecules into the porous char matrix, allowing deeper steam gasification than O_2 oxidation. This deeper gasification by steam promotes micro-pore widening and coalescence and/or opening of blocked meso- and micro-pores and hence increased surface area. The higher intrinsic reactivity and lower diffusivity of oxygen cause it to experience film and pore diffusion limitations at lower temperatures than steam. Consequently, for the temperatures and heating rates investigated in this research, oxygen may only react with the char matrix at the external char particle surface or with macro-pore surfaces, thereby reducing CO_2 and perhaps N_2 surface area to some extent by eroding away char mass containing small open pores.

Conventional flat flame burners typically have a higher percentage of steam than carbon dioxide or oxygen in their post flame gases due to the combustion of air and methane (in this case 18% steam, 7.5% CO_2 and 4% O_2). The carbon-steam reaction therefore, may have the greatest effect on the creation of meso-pore surface areas in such burners prior to significant carbon conversion due to gas-carbon reaction.

Another factor to consider is the production of carbon dioxide via the water-gas shift reaction, which could change the H_2O/CO_2 ratio at the surface of the char particle. It has been shown [78] that a carbon surface accelerates the water-gas shift reaction. Rodriguez [21] however, reports that at temperatures higher than 1100 K, the water-gas shift reaction is at equilibrium and therefore not a factor.

Interaction of Oxygen with Gasifying Reactant Gases

When oxygen and steam or oxygen and carbon dioxide are used to gasify char, it is possible that the O_2 may react with the gasification products (i.e., CO and H_2) in the boundary layer of the particle. This would change the particle temperature and overall reaction rate. Mitchell et al. [79] however, concluded that for particles of less than 100 μm

in diameter, (1) any CO_2 formation must occur on the particle surface, not in the surrounding gas, and (2) little CO conversion occurs in the boundary layer, and hence no thermal energy from boundary layer reactions is transferred back to the particle surface. Since the particle size used in the current research is 63-74 μm, it is highly unlikely that there was any significant interaction between oxidation and gasification reactions.

Effects of Drying and Coal Moisture Content on Surface Area

Drying Zap coal at 110 °C for 2 h prior to pyrolysis caused a significant reduction of surface area (Table 4.1), the most significant reduction being in the N_2 surface area. Drying also significantly reduced mass release (daf basis). Cross-linking during the drying process [44] can significantly reduce the volatile yield during pyrolysis. Pre-oxidation during drying can [7] promote cross-linking during the early stages of pyrolysis. However, pre-oxidation has less of an effect when pyrolysis occurs under rapid heating rates [65] such as were used in this study. Another factor is that drying causes significant shrinkage [80,81] of coal particles.

When pyrolyzed under similar conditions, Zap coal with 23% moisture produced char (Table 4.1) with a higher N_2 surface area than Zap coal with 7% moisture. In order to ensure that the mass release of char prepared from the 7% Zap lignite was higher than that for char prepared from 23% moisture content Zap lignite, it was prepared at a preparation temperature several hundred degrees higher than Zap char prepared from the 23% moisture content lignite. The measured mass release of the char prepared from 7% moisture content Zap was higher than char prepared from 23% moisture content Zap coal. This was consistent with its higher preparation temperature. Both N_2 and CO_2 surface areas have been shown to increase with increasing mass release, and the CO_2 surface area of the char prepared from the 7% moisture content Zap coal was indeed higher than that for the Zap char with a lower mass release. In spite of the higher mass release and CO_2 surface area, the N_2 surface area of char prepared from the lower moisture content Zap lignite was barely

above that of the parent coal.

As discussed by Fletcher et al. [17], lignite and sub-bituminous coals tend to increase their N_2 surface area by expulsion of tar and gases from a rigid char matrix when exposed to rapid heat treatment in an inert gas environment, while bituminous (especially plastic coals) tend to accommodate mass release by at least a partial coal melt, which keeps the size of most of the pores within the char in the micro-pore size range. Along with coal rank, it appears that parent coal moisture content is very important and may even be more critical than coal rank. The moisture contents of Fletcher et al's. [17] size graded Zap and New Mexico sub-bituminous coal were 18% and 9.3% respectively. Sub-bituminous coals have been shown to have a higher propensity to increase in N_2 surface area by several investigators [17,18]. Unfortunately, Nsakala et al. [16], who reported increases in N_2 surface area for Zap char prepared in an inert atmosphere, did not report the moisture content of the parent coal. McDonald et al.'s [18] coals contained 23.7 and 32.2% moisture for the sub-bituminous and Zap lignite coals respectively, but since their inert gas drop tube experiments were performed under less severe pyrolysis conditions than for chars prepared in their reactive gas atmosphere or for chars prepared in the present study, no conclusive information about the effects of parent coal moisture content can be made from their data.

From the data in Table 4.1, it appears that a high parent coal moisture content significantly increases meso-pore surface area, but not necessarily the micro-pore surface area. Once again a distinction can be made between the mechanisms involved in creating micro-pore surface area and in creating meso-pore surface area. Micro-pore surface area, at high conversion, is more a function of mass release, rather than coal type, moisture content or mineral matter. Meso-pore surface area, while affected by mass release and coal rank, may be mostly a function of chemical reaction, i.e. steam gasification, and parent coal moisture content.

Gasification Mechanisms that Increase Meso-pore Surface Area

As discussed earlier, micro-pore surface area is created directly from the release of volatile matter and chemical restructuring of the char matrix during devolatilization. It appears, however, that this process does little to increase meso-pore surface area unless the parent coal has a high moisture content or reactive gases (i.e., H_2O, CO_2, O_2, etc.) are present in the devolatilization gas atmosphere. Figure 4.8 contains a schematic illustrating possible mechanisms involved in the creation of meso-pore surface area during gasification. In Zone I or the transition between Zone I and Zone II, gasification of micro-pore walls (Fig. 4.8a) may contribute to micro-pore widening or coalescence, thereby increasing micro- and meso-pore surface area. In Zone II or the transition from Zone II to Zone III, diffusion limitations keep the reactant gas from penetrating the micro-pores. However, meso-pore surface area may be increased by partial widening of pores by gasification at the mouth of micro-pores (Fig. 4.8b) or by removing constricted or blocked meso-pore channels (Fig. 4.8c). In Zone III, the effects are limited to micro-pore widening or coalescence and meso-pore opening that can take place due to external surface gasification. Since external gasification can also remove micro- and meso-pores due to bulk carbonaceous material removal, gasification or oxidation in Zone II and Zone III may sometimes increase and sometimes decrease internal surface area. According to Rodriguez [21], the exothermic nature of the carbon-oxygen reaction produces a continuous and localized removal of material from the char external surface, thus reducing micro-pore volume to a larger extent than CO_2 gasification under the same gasification conditions, i.e., temperature, heating rate and residence time.

Hurt et al. [46] reported micro-pore widening during CO_2 gasification of sucrose carbon in Zone I. The effect of gasification was to increase N_2 surface area at almost constant CO_2 surface area. In another paper by Hurt et al. [49] on non-uniform carbon gasification, three modes of gasification were considered: (1) uniform pore widening, (2) large pore widening, and (3) large channel production. The largest increase in surface

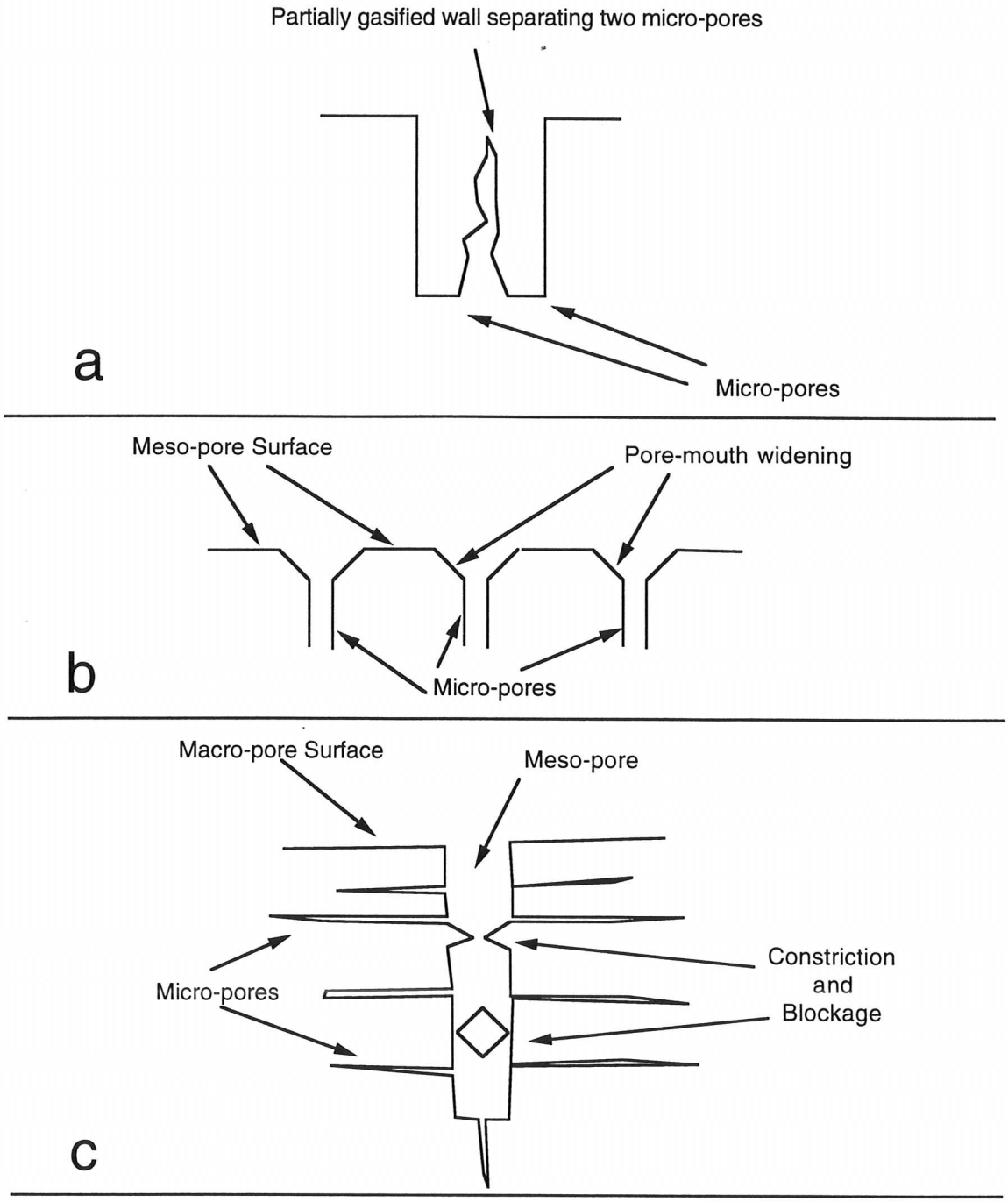

Figure 4.8a,b,c. Pore models illustrating the effects of gasification on pore structure during gasification in different reaction zones. Fig. 8a: Gasification of a micro-pore wall causing micro-pore coalescence and creation of a larger pore; Fig. 8b: Partial widening of micro-pores by gasification around the mouth of micro-pores in the transition from Zone I to Zone II; Fig. 8c: Opening of meso-pore passages by removing, via gasification, restrictions or blockages during transition from Zone II to Zone III.

areas were obtained for uniform pore widening. Uniform pore widening may increase mainly micro-pore surface area or meso-pore surface area depending upon the extent of gasification. Extensive gasification will remove surface area by destroying walls separating pores. Large pore widening occurs during gasification exclusively on the surface of macro-pores, which significantly decreases micro-pore surface area by "engulfment" of the carbonaceous material containing the micro-pores. Sintering of mineral matter and migration to large pore surfaces was cited as a possible mechanism that causes large pore widening in impure carbons such as coal. Catalytic mineral matter is also responsible for creating channels larger than 10 nm in diameter. Gasification of impure carbons often occurs in the immediate vicinity of catalytically active particles of inorganic matter. Along with the formation of channels of definite shape and possibly orientation, the formation of pits of indefinite shape have been observed following catalyzed gasification. However, uniform pore widening is not consistent with catalyzed gasification. Catalyzed gasification by channeling decreases micro-pore surface area by removing material containing micro-pores as channels are formed. In the case of very low surface area carbons such as graphite, channeling would probably increase the total internal surface area.

Effects of Coal Type on Surface Area

All three coals (see Fig. 4.1-4.3) increase in CO_2 surface area with increasing mass release and residence time. However, the Pitt. 8 char is the only one that initially decreases in CO_2 surface area, followed by a net increase. This is probably due to the plasticity of the coal, i.e. it is likely that during the early stages of pyrolysis, the coal melts and fills some of the micro-pores. As pyrolysis continues, however, these pores are reopened and additional pores are formed as volatile products are released and the surface area increases.

Micro-pore surface area of significantly devolatilized chars is affected more by pyrolysis conditions (i.e., temperature, heating rate and residence time) than by parent coal type. However, parent coal type is quite significant since the lignite formed chars with micro-pore surface areas as much as 150 m^2/g higher than for the bituminous coal chars.

The largest CO_2 surface areas of the bituminous coal chars were about the same.

As discussed earlier, Zap (23% moisture content) lignite formed chars with the highest meso-pore surface areas. Coal moisture content was a significant factor in increasing the meso-pore surface area. However, the organic matter in the Zap coal may also be a factor in creating high meso-pore surface areas. Zap mineral matter is much more effective at catalyzing gasification reactions than the organic matter in UBC or Pitt. 8 coal, largely because it is more disperse in Zap coal. Inorganic matter in char may catalyze conversion of small pores to large pores [26]. The effect of parent coal moisture content on the N_2 surface area of bituminous coal chars needs to be examined.

Correlation of True Density with Mass Release

Along with internal surface area, true (skeletal) density is a good measure [1,2] of the physical restructuring of chars during devolatilization. Attempts have been made to correlate true density [11] with char crystallite structure. As reported earlier [2,16], true density increases with increasing pyrolysis temperature. As illustrated in Figure 4.8, this phenomena is probably due to an increased mass release with increased pyrolysis temperature. True density for all three coals correlates well with total mass release even though chars were prepared in a variety of different pyrolysis conditions, including different reactive gas atmospheres. Figure 4.8b contains the ash-free true densities of the Pittsburgh No. 8 chars. The true densities of the char ash used to calculate the ash-free densities was determined experimentally to be 5.26 and 4.06 g/cc respectively for the HPCP and FFB chars. As expected, the ash-free true densities are lower than the true densities from which they were calculated. More importantly, the trend of increasing true density with increasing mass release still exists. Therefore, the increase in true density is not merely a function of increasing ash content but of densification in a manner similar to graphitization. While coal chars generally do not become genuinely graphitic even at high conversion, as mass release proceeds, the orientation of the layered planes in the carbon matrix of the char becomes more ordered.

There may be a difficulty in measuring the actual true density using helium pycnometry. Helium may not be able to penetrate micro-pores that are completely enclosed. Therefore, if a char has a significant closed pore volume, the helium density will be lower than the true density. In this respect, it may be convenient to partially gasify chars so that less micro-porosity is completely closed to helium adsorption, and hence, make the helium density a better indication of densification. Carbon dioxide adsorption penetrates pores as small as helium adsorption at room temperature (as conducted in this research), and gasification had only minor effects on CO_2 surface areas of chars in this research. Therefore, the true densities obtained by helium pycnometry may still be considered as a good measure of the extent of densification. Furthermore, helium densities of partially-gasified chars correlate with mass release just as well as helium densities of chars prepared in an inert environment.

For each coal the increase in true density is small for low mass release and then increases to a greater extent above 40% mass release as shown in Figure 4.8. The initial small increase in true density corresponds to the release of tar along with lighter molecular weight volatile gases. Tar release is completed in the early stages of pyrolysis. As devolatilization continues, lighter molecular weight hydrocarbons are released along with hydrogen without the accompanying tar yield, thus increasing true density with increasing mass release at a higher rate than at the early stages of devolatilization.

Conclusions

1) Micro-pore surface areas increase with mass release and with residence time for coals of different rank. However, CO_2 surface areas of chars prepared from Pittsburgh No. 8, a plastic coal, initially decrease, likely due to the initial coal melt during pyrolysis.

2) While the general trend is for CO_2 surface area to increase with increasing pyrolysis temperature and heating rate, the increase is small at temperatures between 840 and 1650 K, and heating rates between 10^4 and $7x10^4$ K/s for all coals considered.

3) Large N_2 surface areas obtained in flat flame burners are probably caused mostly by

mild char steam gasification causing micro-pore widening and coalescence and/or opening of unavailable meso-porosity. Internal surface areas are also influenced by mild oxidation. However, mild char oxidation sometimes slightly increases and sometimes slightly decreases N_2 and CO_2 surface areas subsequent to rapid pyrolysis under conditions representative of typical flat flame burners. Oxidation may destroy micro-porosity by removal of carbon material from external char surface or from the walls of large pores.

4) The North Dakota (Zap) lignite examined here has a higher potential to form chars with increased meso-pore surface area than do the hv-bituminous coals even when prepared in an inert environment, as shown by others [16,17]. However its high moisture content (23% compared to 1.5 and 2.4% for Pitt. 8 and UBC respectively) may be a significant reason for its propensity to form chars with high N_2 surface area.

Chars prepared in nitrogen from Zap lignite with 23% moisture content have higher N_2 surface areas than chars prepared from a similar Zap lignite with 7% moisture content, although, parent coal moisture content does not necessarily affect CO_2 surface area. The measured mass release of the char prepared from 7% moisture content Zap was higher than char prepared from 23% moisture content Zap lignite. This was consistent with its higher preparation temperature. Both N_2 and CO_2 surface areas have been shown to increase with increasing mass release, and the CO_2 surface area of the char prepared from the 7% moisture content Zap lignite was indeed higher than that for the Zap char with a lower mass release. In spite of the higher mass release and CO_2 surface area, the N_2 surface area of char prepared from the lower moisture content Zap lignite was barely above that of the parent coal.

Drying Zap lignite prior to pyrolysis causes the char to have a significantly lower internal surface area, probably due to lower mass release because of crosslinking [44] or particle shrinkage [80,81] during drying. The measured mass release of Zap char prepared from dried coal was much less than that prepared from the original Zap lignite.

5) True density increases with increasing mass release during devolatilization

regardless of coal type for Pitt. 8, UBC and Zap coals, pyrolysis conditions or gas atmosphere for the range of temperatures, heating rates and residence times considered in this study. This is due to carbon densification and aromatization rather than increasing ash percentage. During the early stages of devolatilization (below 40% mass release), the true density increase is small. Beyond about 40% mass release, the increase in true density is greater with increasing mass release.

Chapter 5

Effects of Pyrolysis Conditions on Intrinsic Reactivities of Coal Chars

Introduction

Char oxidation and gasification are typically studied at a laboratory scale in the coal science community to research a wide variety of combustion concerns ranging from char reactivity to pollution control. Concern about comparability and validity of different methods for preparing coal chars for such experiments has led to research on effects of devolatilization conditions on char intrinsic reactivity, as well as physical and chemical structure. Models are being developed to extrapolate from rates obtained in the intrinsic regime to coal combustion reaction rates at high temperatures where pore and film diffusion limitations are present and catalytic effects are less dominant. A main complication in modeling intrinsic reactivities is that of separating the devolatilization step from the oxidation step. While chars prepared for further oxidation studies are essentially devolatilized, they generally still contain significant amounts of hydrogen and oxygen that affect the carbon matrix structure and hence reactivity. Such elements are preferentially released during the early stages of char oxidation, but prior to their release their presence may dominate char intrinsic reactivity by altering the structure, such as increasing the number of active carbon sites.

This chapter focuses on the effects of particle heating rate and gas environment (i.e., N_2, He, H_2O, etc.) during pyrolysis on intrinsic reactivity of chars prepared under carefully controlled conditions from coals of representative ranks. Specifically, pyrolysis heating rate and gas environment were varied independently of residence time and pyrolysis temperature. Finally, an attempt was made to identify correlations of char properties or pyrolysis conditions with intrinsic reactivity for use in modeling.

Much of the data and findings of this chapter are not new, but are presented here in support of data already published. However, in view of the extensive previous work on

coal char reactivity, it is appropriate to address here the unique contributions of this work:

(1) First of all, devolatilization conditions were separated from reactor type. A comparison of reactivity for chars prepared in a flat flame burner and in a drop tube furnace was made entirely on the basis of preparation conditions such as temperature, heating rate, residence time, gas atmosphere (N_2, O_2, CO_2, H_2O), and coal type. A major goal was to promote comparisons of char properties, including reactivity, surface areas, densities, etc., on the basis of pyrolysis conditions and precursor properties such as coal type rather than by reactor type.

(2) It was found that, for the preparation and collection conditions and procedures utilized in this work, tar condensation onto or into char was insignificant in the collection system of the HPCP following pyrolysis and a rapid quench even when pyrolysis took place in an inert atmosphere. In other words, any tar condensation that may have occurred had no effect on intrinsic reactivities, element release or internal surface areas of chars compared to those of chars prepared by pyrolysis in reactive gases where volatiles were burned.

(3) A set of intrinsic reactivity and physical property data for chars prepared at relatively high temperatures and low residence times from three different coal types under well-defined conditions in two different reactors are presented. This set of data will be useful to other researchers investigating the same coals.

(4) Extensive correlations of the reactivity data with physical properties and preparation parameters are provided; these correlations address the apparent contradictions from previous studies regarding the effects of pyrolysis heating rate on reactivity and the relationship between porosity and internal surface area and intrinsic reactivity. It will be shown, for the range of heating rates investigated, that intrinsic reactivity decreases with increasing heating rate, and an explanation for the confusion in the literature will be given. Furthermore, it will be shown that there is no basis for correlating intrinsic reactivity with meso- or micro-pore surface area for the chars prepared in this research.

Results

The pyrolysis conditions at which the chars in this research were prepared are listed in Tables A1.1-A1.3 (see Appendix A1). Chars were prepared by pyrolysis of UBC, Pitt. 8, Zap (23% moisture content), and dried Zap (ZD) coals in N_2, He, O_2/N_2, and H_2O/N_2 atmospheres in the HPCP reactor and in the $O_2/CO_2/H_2O/N_2$ atmosphere of the FFB reactor at temperatures ranging from 840 to 1627 K, heating rates of $9x10^3$ to $2x10^5$ K/s and residence times of 25 to 1000 ms. Char properties, total percentage mass release, element analysis, and element release data of these chars are summarized in Tables A1.4-A1.6. Intrinsic O_2 reactivities and kinetic parameters for the three coals investigated are found in Tables A1.7-A1.9 (see Appendix A1).

The data in Table A1.4 (see Appendix A1) provide a basis for relating densities, porosities and surface areas of chars to pyrolysis conditions (Tables A1.1-A1.3 in Appendix A1) and reactivity (Tables A1.7-A1.9 in Appendix A1). This chapter focuses on relationships between char physical properties, preparation conditions and reactivity.

Effects of Char/Tar Separation on Internal Surface Area

N_2 surface area is generally higher for chars prepared in reactive environments. This fact raises questions as to (1) whether or not tar is more completely removed by oxidation from the pores of chars prepared in the presence of oxygen-containing species and (2) whether tar is condensed in the pores during collection in inert atmosphere in the HPCP. To address the second question, Zap char and tar were collected together in one experiment, i.e., a valve was closed in the HPCP collection system so that char and tar were collected together in a water cooled filter. Visually, char and tar appeared to be separated. All visible tar stuck either to cold metal surfaces or to the glass fiber filter, while all of the char was loose and fell out of the filter upon opening. The same visual separation was observed for hv-bituminous coals when the char and tar were collected together. The N_2 surface area of this char (158 m^2/g) was consistent with its preparation conditions and

comparable to chars (116 to 146 m^2/g) prepared in inert atmosphere with advanced mechanical char/tar separation.

Following a rapid quench in the HPCP, small amounts of tar remain entrained in the char-gas flow and subsequently stick to the metal surfaces of the cyclone where the char is collected, even when the advanced tar-char separation system is used. In order to determine effects of burning the volatiles during pyrolysis as opposed to separating them, 4% O_2 (the same amount as is in the post flame gases of the FFB) was added to the flow gases of the HPCP. Table 5.1 compares N_2 surface areas for Zap char prepared in a 4% O_2 atmosphere (all the volatiles were burned) with Zap char prepared in an inert

Table 5.1

N_2 Surface Area of Zap Chars Collected with or without Tar

[a]Tar Separation Condition	Pyrolysis Gas Composition	N_2 Surface Area (m^2/g)	Total Volatile Yield (%)
Not Separated	100% N_2	158	53.9
Separated	100% N_2	141	54.8
Burned	4% O_2, 96% N_2	76	47.4
Burned	[b]FFB	190	65.2

a. All chars except FFB were prepared in the HPCP at: 1027-1095 K, 3.1-3.4e4 K/s, and 294-490 ms.
b. Prepared in the flat flame burner at 1507 K, 1.94e5 K/s, and 50 ms in pyrolysis gases consisting of: 4% O_2, 7.5% CO_2, 18% H_20 and 70.5% N_2.

environment but separated from the tar or with Zap char collected with its tar. The FFB char data are also presented for comparison. The N_2 surface area of the char collected with the tar is slightly higher than that for the separated char and nearly as high as that of the FFB char. Char prepared in the 4% O_2 atmosphere has a much lower surface area and surprisingly slightly lower mass release than the char prepared in the inert environment.

Effect of Oxygen in Pyrolysis Atmosphere on Intrinsic Reactivity

Apparently, for chars prepared at similar temperatures, residence times, and heating rates, char intrinsic reactivity is reasonably independent of gas atmosphere during pyrolysis as long as oxidation or gasification is minimal. For example, Zap char collected with tar, and char prepared in an inert environment have similar intrinsic reactivities. Moreover,

Pitt. 8 char prepared with 4% O_2, and the same char prepared in an inert environment under similar conditions have the same intrinsic reactivity of 2.1 to $2.3x10^{-3}$ g/g.s at 25% burnout and 500 °C.

Effect of Coal Pretreatment

Coal pretreatment can greatly affect char reactivity, other factors being equal. For example, five grams of the Zap lignite used in this research was dried at 110 °C for two hours and then pyrolyzed under the same conditions as the above chars. The char prepared from dried coal was found to have a much higher reactivity than that prepared from undried coal. Significantly less mass release during devolatilization was also observed for the dried lignite. Therefore the char prepared from dried coal experienced less carbon aromatization (see Chapter 4) than char that experienced a higher mass release.

Effects of Heating Rate and Temperature on Intrinsic Reactivity

Figure 5.1 contains plots correlating intrinsic reactivity with maximum particle heating rate, temperature, true density, and mass release for all three coals. Intrinsic char reactivity clearly decreases with either increasing pyrolysis temperature or heating rate (see Figs. 5.1a and b). Intrinsic char reactivity is also known to be a function of residence time [31,32,37]. However, the HPCP and FFB data in this project do not correlate very well with residence time (135 to 1000 ms) because of the more dominating effects of particle temperature and heating rate. However, the scatter in the heating rate and temperature data is attributed mainly to residence time differences. Plots of intrinsic reactivity versus true density and versus mass release are also shown (see Figs. 5.1c and d). Mass release increases with increasing temperature and heating rate [75], and true or skeletal density increases with increasing mass release as shown in Chapter 4. Thus, intrinsic reactivity decreases with increasing true density and mass release. Moreover, the correlation of decreasing intrinsic reactivity with either increasing density or mass release is as good if not better than the correlation with maximum particle temperature or heating rate.

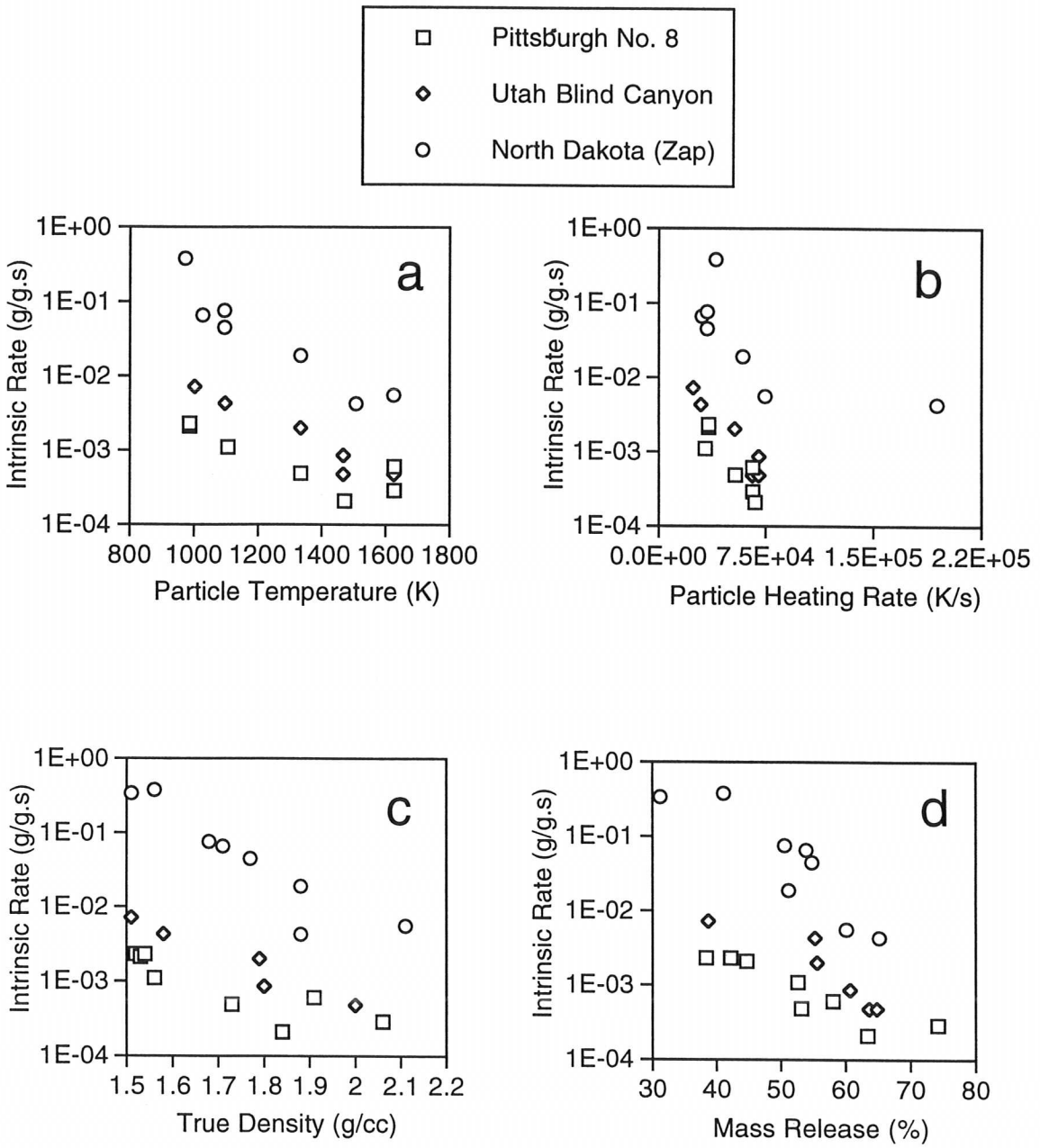

Figure 5.1a,b,c,d. Intrinsic reactivities of Pitt. 8, Zap, and UBC coal chars in oxygen plotted versus maximum particle pyrolysis temperature, heating rate, true density, and total mass release. Intrinsic oxidation rates were obtained by TG analysis in 10% oxygen at 500 °C and 25% burnout.

Correlations of Element Release Versus Mass Release

Figures 5.2 contains plots of hydrogen, oxygen, nitrogen and carbon release versus mass release for all three coals. Data points that fall on the 45° line represent element release in the same percentage as the total mass release. Consequently, data points above the 45° line represent elements that are preferentially released to total char mass, and data points below the 45° line represent elements that are preferentially retained in the char matrix in comparison to other elements. The elemental release versus total mass release trends for all of the data are consistent with previous work reported for similar coals [17,38]. The slightly higher hydrogen release of the Pitt. 8 FFB chars relative to HPCP chars in Figure 5.2a is consistent with higher maximum particle heating rates in the FFB. Consistent with previously reported data [17,38], hydrogen and oxygen are preferentially released relative to carbon and nitrogen for all three coals. Also consistent with data reported elsewhere [17,38], UBC and Pitt. 8 carbon and nitrogen release data follow the 45° line fairly closely or perhaps are slightly below it, while data for carbon and nitrogen release from Zap char are well below the 45° line. It should be noted that some of these data are for partially-devolatilized chars as well as fully-devolatilized chars. Thus, the percentage release of hydrogen and oxygen is as low as 25% for some chars and extends to nearly 100% for chars prepared from all three coal types.

Correlations with Intrinsic Reactivity

Figure 5.3 contains plots correlating intrinsic reactivity with elemental release for all three coals. Increasing elemental release relates directly to a decrease in the absolute amount of that element in the char. Elemental ratios however, such as those contained in Fig. 5.4, are more useful for considering the amount of a certain element in the char compared to the amount of carbon. The data in Figure 5.3 indicate that intrinsic reactivity decreases with increasing hydrogen, oxygen, nitrogen, and carbon release for all coal char types. However, the correlation is better for certain char types and for specific elements.

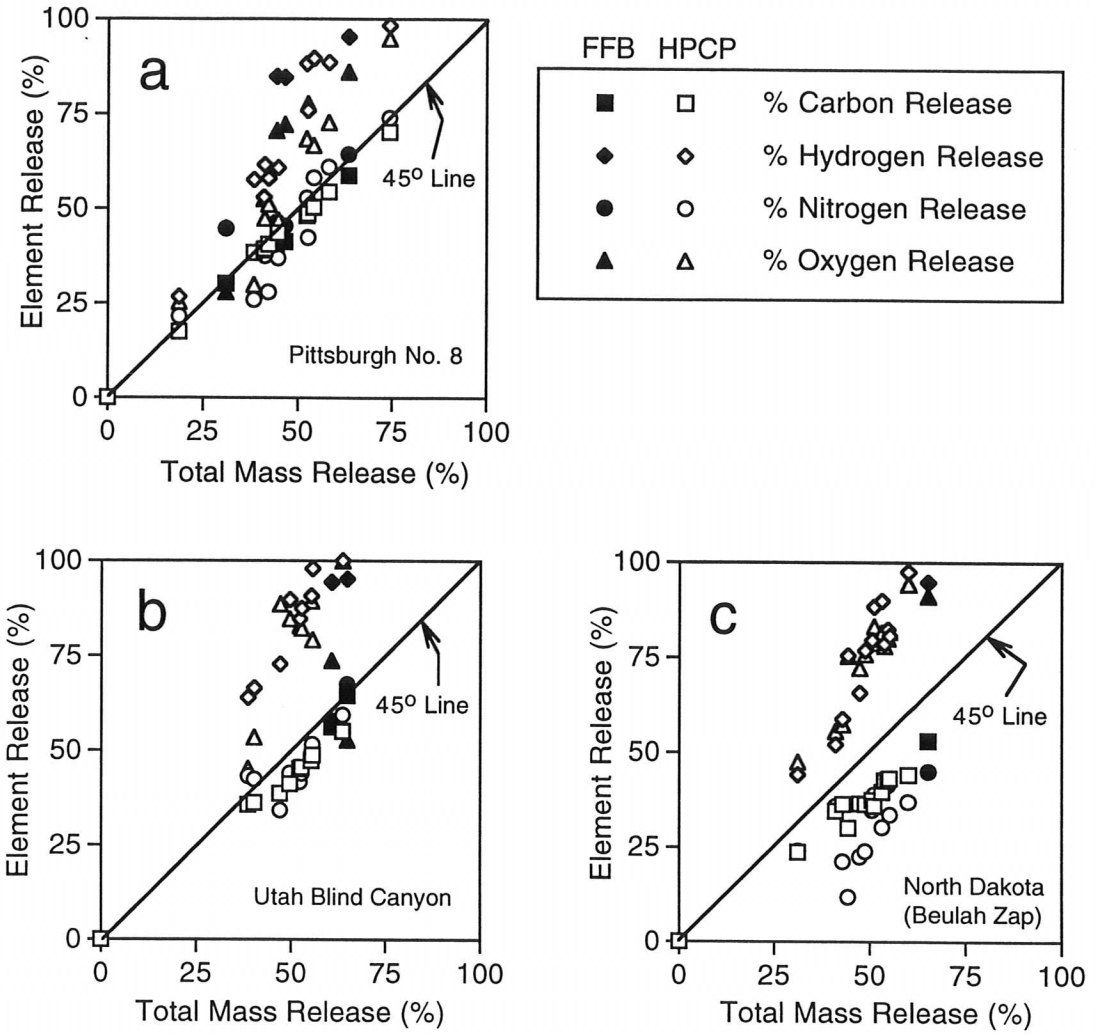

Figure 5.2a,b,c. Hydrogen, oxygen, carbon and nitrogen release versus total mass release for Pitt. 8, Zap and UBC Coal chars.

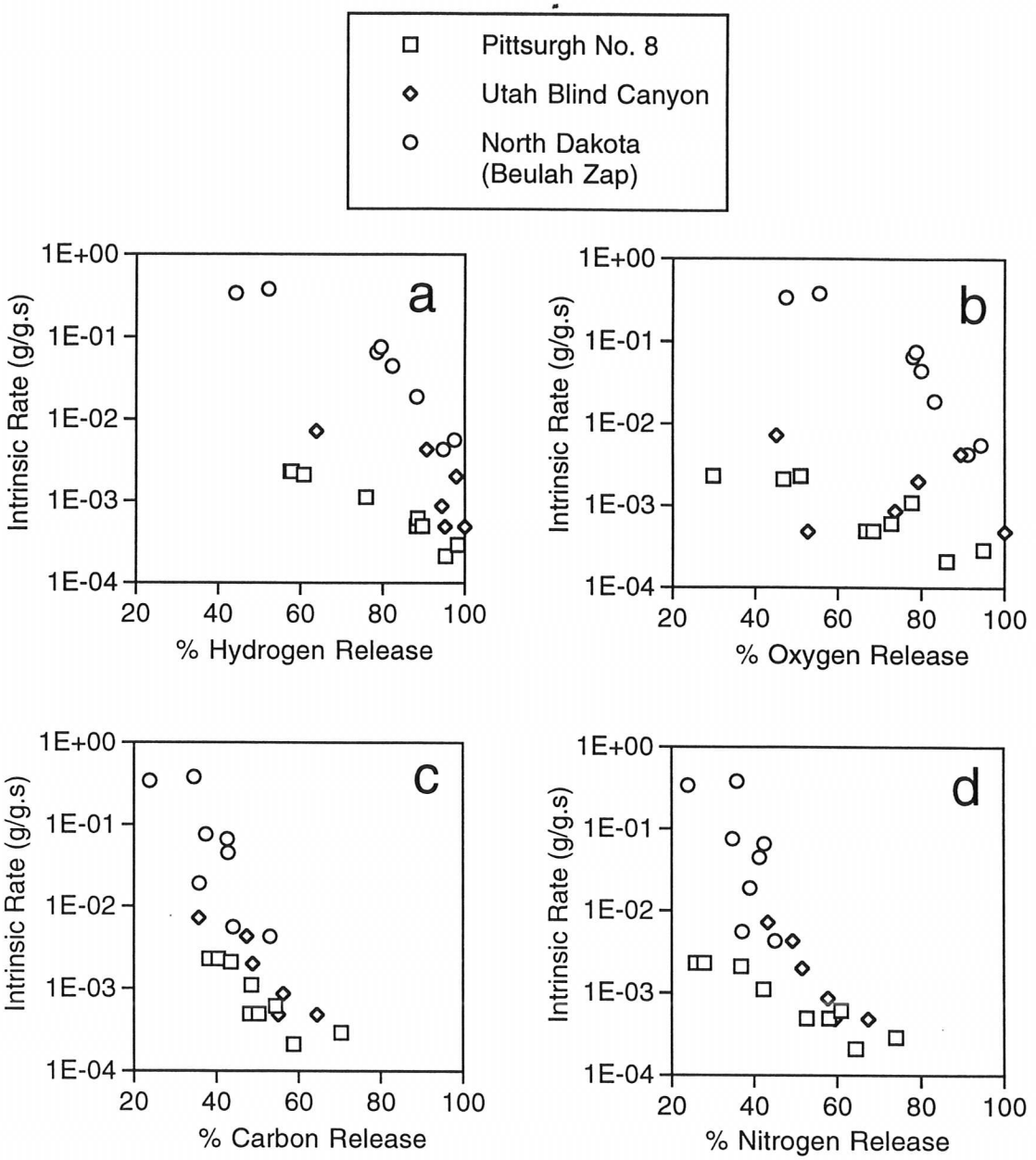

Figure 5.3a,b,c,d. Intrinsic reactivity in oxygen versus hydrogen, oxygen, carbon and nitrogen release for Pitt.8, Zap and UBC chars prepared in the HPCP and FFB under a variety of different conditions. Intrinsic oxidation rates were obtained by TG analysis in 10% oxygen at 500 ^{o}C and 25% burnout.

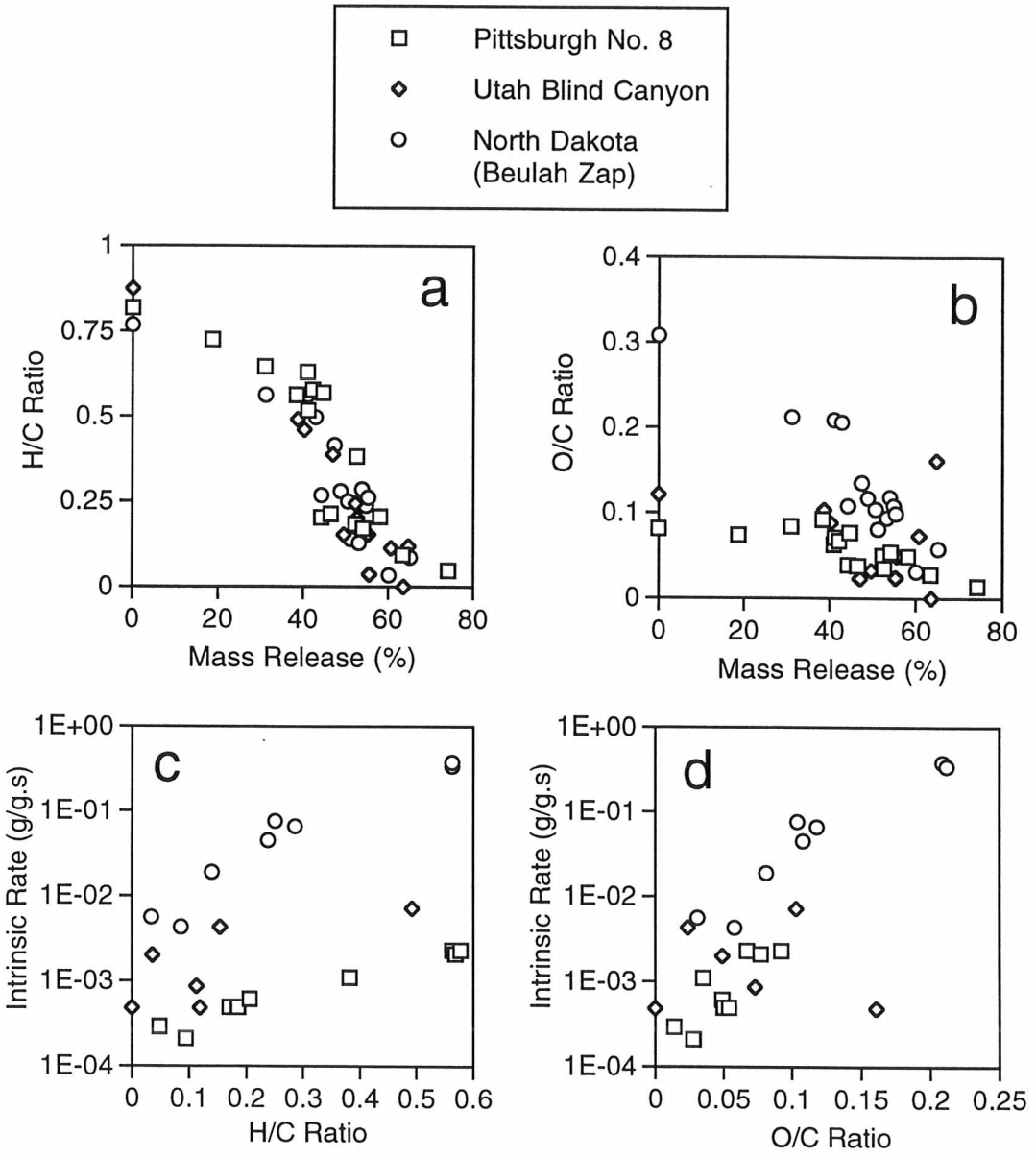

Figure 5.4a,b,c,d. H/C and O/C ratios versus total mass release, and intrinsic oxidation rate in oxygen versus H/C and O/C ratios for chars prepared in the FFB and HPCP under different conditions. Intrinsic oxidation rates were obtained by TG analysis in 10% oxygen at 500 °C and 25% burnout.

For example, Pitt. 8 reactivity correlates well with either hydrogen or nitrogen release, but its correlation with oxygen release is somewhat scattered. Zap char reactivity correlates best with hydrogen or oxygen release, but its correlation with carbon release is only fair and with nitrogen release is relatively poor. UBC char reactivity on the other hand correlates well with carbon or nitrogen release, but its correlation with hydrogen release is only modest and with oxygen release fairly scattered. Thus, the reliability of release correlations for a given element varies with coal rank; however, in every case, a linear correlation exists.

Figures 5.4a and b contain plots of H/C ratio and O/C ratio versus mass release for all three chars. A good correlation of decreasing ratio with increasing mass release is evident for all coal chars except for a few stray data points representing UBC chars in Figure 5.4b. A few of the chars represented, for all three coals, were prepared with 4% oxygen (see Tables A1.1-A1.3 and A1.7-A1.9 in Appendix A1) either in the FFB or in the HPCP. During devolatilization of these chars, the char was slightly oxidized and consequently oxygen was chemisorbed as part of the oxidation process. This probably explains why the O/C ratios of two UBC char samples prepared with oxygen are higher than the rest. This could also explain the scatter in the intrinsic rate versus oxygen release or O/C ratio curve for the UBC char (Fig. 5.4d). It is interesting however, that the same phenomena was not observed for the other coal chars even though some oxidation of some of these chars occurred as well. Perhaps the UBC char has a relatively small chemical reactivity (i.e. it takes longer for the carbon oxygen complex on the surface of the char particle to rearrange and desorb) at the temperatures and heating rates observed for its devolatilization. Therefore, more oxygen chemisorption may occur during oxidation of UBC chars than occurs on other coal chars, even though its overall reactivity is probably between that of Pitt. 8 and Zap coal char.

Also contained in Figure 5.4 (Fig. 5.4c and d) are correlations of H/C and O/C ratios with intrinsic reactivity for all three coal chars. Except for UBC coal char, intrinsic

char reactivity, as shown in Figure 5.4c and by other investigators [29,37,40], is strongly correlated with H/C ratio. Intrinsic reactivity for Pitt. 8 and Zap char also correlates with O/C ratio. Because of the larger range of element ratios, reactivity correlates better with H/C ratio than with O/C ratio for Pitt. 8 char. UBC intrinsic reactivity does not correlate well with O/C ratio.

In order to understand the effects of increasing available char surface area for oxidation and increasing total porosity (opening up more pores in the char particle or making open pores bigger) on intrinsic O_2 reactivity, reactivity is plotted versus CO_2 and N_2 surface area and porosity. Figure 5.5 contains plots of intrinsic O_2 reactivity versus total (CO_2) surface area, meso-pore (N_2) surface area, and total porosity. Intrinsic reactivity declines almost linearly with increasing CO_2 surface area for each coal type. It does not, however, correlate with N_2 surface area. Intrinsic reactivity declines with increasing porosity for Zap and UBC (non-swelling) coals, but not with Pitt. 8, which is a swelling coal. Figure 5.3 shows that the intrinsic reactivity of Zap char is much higher than that of the hv-bituminous chars for most available values of element release for the three coal chars, and UBC char is slightly more reactive than the Pittsburgh No. 8 char.

Discussion

Effects of Tar/Char Separation and/or Oxidation on Reactivity

Internal surface areas of Zap chars prepared in the HPCP were similar when collected with tar or separated from tar during collection (see Table 5.1). Therefore, it appears that use of the advanced tar/char separation system employed by the HPCP does not significantly enhance lignite char surface area that might be otherwise reduced by tar condensation onto char. Others [16] have reported high N_2 surface areas for chars collected with tar.

Char prepared in N_2 gas in the HPCP had slightly higher N_2 surface areas than chars prepared in 4% O_2 at a sufficiently long residence time to combust all volatiles, i.e.,

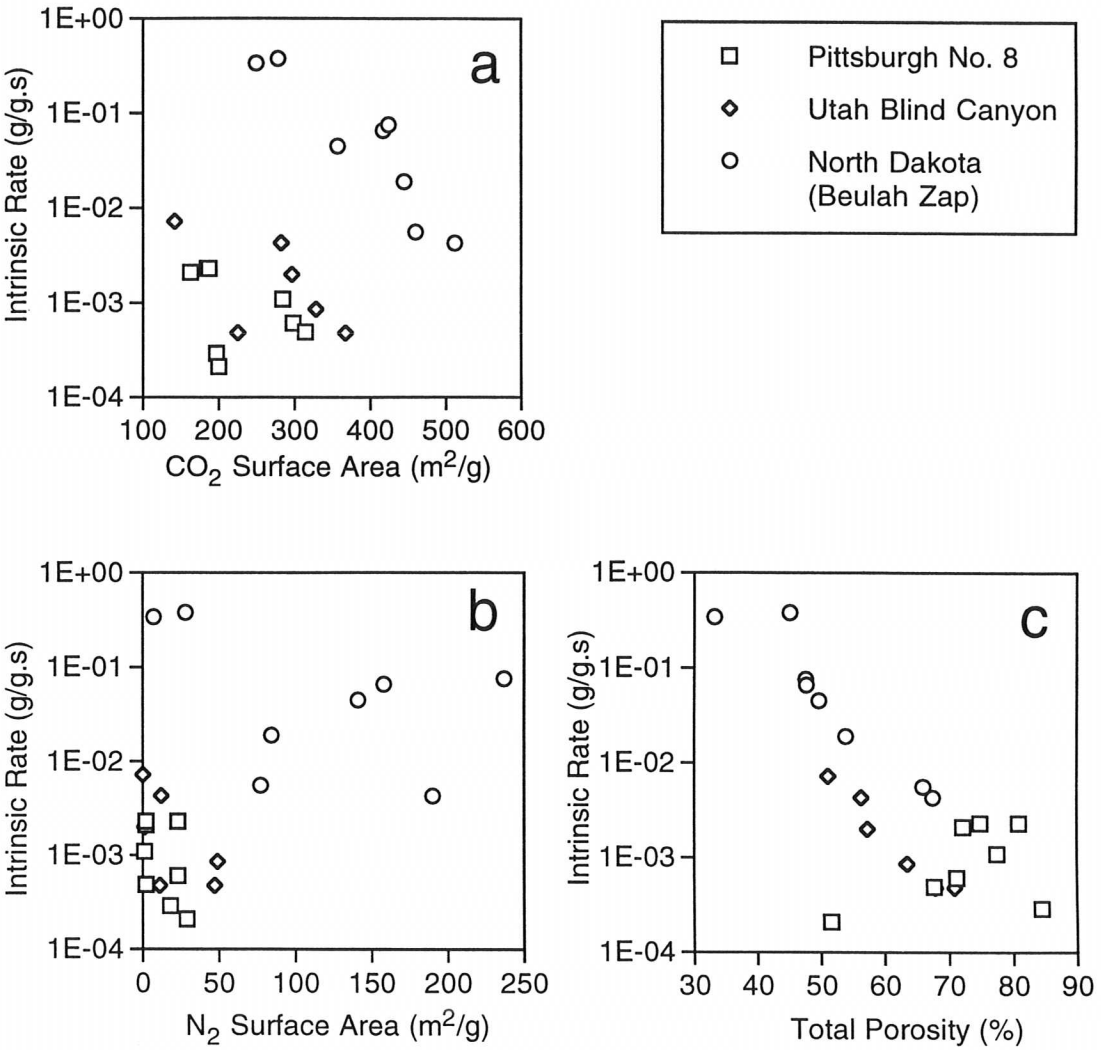

Figure 5.5a,b,c. Intrinsic reactivities in oxygen of Pitt. 8, Zap, and UBC coal chars versus CO_2 and N_2 surface area and total porosity. Intrinsic oxidation rates were obtained by TG analysis in 10% oxygen at 500 °C and 25% burnout.

no tar was collected on the glass fiber filters. Char collected with tar, char pyrolyzed in 4% O_2 (with some accompanying char oxidation), and char prepared in an inert environment under similar conditions all had similar intrinsic reactivities at 25% burnout (see Tables A1.1-A1.9). Moreover, slight oxidation was observed by others [82] not to affect reactivity. Both the surface area and reactivity data strongly suggest that tar does not significantly condense onto or into pores of chars in the collection system of the HPCP following preparation in inert atmosphere.

Considering the significantly higher hydrogen and oxygen contents of tar compared to char [39], had tar condensation occurred during inert atmosphere devolatilization, the values of apparent hydrogen and oxygen release should have decreased to a greater extent as a function of mass release than for chars prepared in an oxidizing atmosphere or in the FFB, where the tars are burned. The maximum error in %H and %O release measurements for data in Figure 5.2 is only ±2%. Zap char hydrogen release correlations would be particularly affected by tar condensation, since Zap coal tar [39] has over twice the percentage of hydrogen than the coal itself. Zap char, on the other hand, has a significantly lower amount of hydrogen than does the coal, the magnitude of which depends upon the extent of devolatilization. In this research, nearly all chars prepared from all three coals had less than half the percentage of hydrogen and oxygen as the parent coal. Consequently, if more than 2% of the Zap char were to consist of condensed tar, the predicted hydrogen release would be lower than the actual measured value by more than the error in the measurement. Thus, hydrogen release data for chars with extensive tar condensation would be expected to be below the 45° line in Figure 5.2c. Instead, the hydrogen release data for Zap chars in Figure 5.2c, including char collected with tar, are comparable with values for other chars, including those prepared with 4% O_2 in the HPCP. Similar logic applies to the oxygen release data in Figure 5.2, i.e., tar condensation, accounting for more than 5% of char mass, should [39] decrease the apparent oxygen release for Pitt. 8 and UBC chars.

Therefore, it is unlikely that more than 2% of Zap char or more than 5% of UBC or Pitt. 8 char consisted of condensed tar following preparation in the HPCP in this research regardless of the gas atmosphere used during pyrolysis. Furthermore, any tar condensation onto or into char that may have occurred in the HPCP collection system did not affect char surface areas or reactivities in this particular research.

Modeling Char Initial Intrinsic Reactivity

Relationships of Intrinsic Reactivity to Surface Area and Porosity. It has been argued [52] that CO_2 gasification occurs outside micro-pores on active sites located on the surfaces of larger pores. This may also be the case for intrinsic oxidation. The correlation between CO_2 surface area and reactivity (Fig. 5.5a) is probably an artifact due to a common dependence of both parameters on maximum particle temperature or total mass release. As the maximum particle pyrolysis temperature increases, the total mass release [75] and total surface area both increase (see Chapter 4), and the intrinsic reactivity decreases. Intrinsic rate however, does not correlate well with meso-pore surface area.

The reactivity of the non-plastic coals, Zap and UBC, correlates well with porosity, i.e., reactivity decreases as porosity increases. However, the correlation exists merely because both reactivity and porosity are functions of mass release. There is no other fundamental reason why intrinsic reactivity would correlate with total porosity unless porosity is related to the active surface area. The reactivity of Pitt. 8 char does not correlate with porosity because it is a swelling coal and its porosity does not correlate as well with mass release. It may be that intrinsic oxidation takes place preferentially on the surfaces of macro-pores where more active and catalytic [52] sites are present.

Due to catalytic mineral matter lying preferentially on large pore surfaces [49-51], micro- and meso-pore surface areas may not be part of the active surface area during measurements of coal char intrinsic rates for bituminous and lower rank coals. At higher temperatures however, catalytic effects become less important so that the reaction does not take place exclusively in the presence of catalytic particles as is nearly the case at low

temperatures. As a matter of fact, at temperatures above approximately 1500 K, catalytic effects may be insignificant. Film diffusion limitations make micro-pore access unavailable at temperatures above 2000 to 3000 K depending upon the reactant gas and char reactivity. Therefore, pore diffusional effects and internal surface areas may only be important within a gasification temperature window in which catalytic sites have become somewhat or totally inactive but diffusion limitations are still fairly small.

Correlations of Intrinsic Reactivity with True Density and Mass Release. As shown in Fig. 5.1c, intrinsic reactivity correlates with true (skeletal) density (ash free or not). It has been shown [2] that true density is a good measure of ordering of layered carbon planes within the char matrix due to increased carbon aromatization (see Chapter 4). It has been shown in Chapter 4 that true density (ash free or not) correlates very well with total mass release regardless of devolatilization conditions or atmospheres employed to prepare the char. Consequently, intrinsic reactivity should and does correlate well with mass release (Fig. 5.1d); moreover, any parameter that correlates well with mass release will also correlate well with intrinsic reactivity. For example, CO_2 surface area correlates with intrinsic reactivity (Fig. 5.5a), but in a fashion opposite from that expected if the CO_2 surface area is part of the active surface area. Another example is nitrogen release. Even though there is no mechanistic reason why nitrogen content or release should correlate with intrinsic reactivity, it does because they both correlate with total mass release. It seems reasonable to use true density to model intrinsic reactivity because true density is a measure of what actually changes reactivity [2,76], namely, ordering of layered planes.

Correlation of Reactivity with Severity of Devolatilization Conditions

Consistent with the concept of reactivity correlating with mass release, intrinsic reactivity for all coals studied decreases with increasing severity of pyrolysis conditions. As discussed earlier, reactivity decreases as maximum particle pyrolysis temperature, heating rate and residence time increase. In other words, whatever combination of pyrolysis conditions exist to increase mass release will be those that decrease reactivity

most. However, towards the end of devolatilization, mass released may consist mainly of hydrogen which doesn't contribute much to the total mass released but still corresponds to an increase in carbon aromatization. It has been reported [43] that rapid heat treatment of previously pyrolyzed chars increases their intrinsic reactivity due to disordering of the carbon matrix. The resulting increase in carbon active sites increases the intrinsic reactivity. A distinction must be made, however, between maximum particle heating rate during devolatilization and following devolatilization. During pyrolysis experiments in which the char is quenched and collected for further study, an increased heating rate increases total mass release, which increases carbon aromatization and hence decreases reactivity. However, after devolatilization is complete and crosslinking has set the char in a rigid structure, a higher heating rate may induce higher reactivity as discussed above, but the magnitude of increase is expected to be much less than the decrease in reactivity which occurs due to devolatilization.

Effects of Coal Type on Reactivity

Char intrinsic reactivity is highest for the Zap lignite and decreases with increasing rank, as shown in Figure 5.3 and by others [29,30,37]. Intrinsic reactivity for all three coals, however, correlates well with elemental release, mass release and true (skeletal) density as illustrated in Figures 5.1-5.3.

Conclusions

1. For a given coal, the initial intrinsic char reactivity may be correlated to any parameter that correlates with mass release and true density. The mechanism which causes a decrease in reactivity during devolatilization is ordering of the layered carbon planes of the char matrix as aliphatic carbon is released and true density increases.

2. For coals of varying rank, mineral matter content, moisture content and plasticity, char intrinsic reactivity decreases with increasing particle pyrolysis temperatures between 850 and 1627 K, heating rates between 10^4 and $2x10^5$ K/s, and residence times between 50 and 1000 ms, as shown by many other investigators for other coals and conditions except in the

case of heating rate.

3. Meso-pore (N_2) and micro-pore (CO_2) surface area may not be part of the active surface area during intrinsic rate measurements.

Chapter 6

Decreases in the Swelling and Porosity of Bituminous Coals During Devolatilization at High Heating Rates

Introduction

Swelling of a bituminous coal during pyrolysis can affect the reactivity, particle size, and density of the resulting char. Under certain pyrolysis conditions, chars prepared from bituminous coals form low apparent density, glassy, balloon-like cenospheres with transparent thin walls and large inner cavities, which fragment easily during combustion. Accurate char oxidation models require knowledge of both porosity and the swelling characteristics of coal char to predict combustion behavior [83].

This investigation reports further research on the effects of pyrolysis conditions on the swelling characteristics of hv-bituminous coals for heating rates in excess of 10^4 K/s. It will be demonstrated that effects of particle heating rate on particle diameter and porosity change markedly in a relatively narrow region of heating rate. The work presented in this chapter is accepted for poster presentation at the 25th International Symposium on Combustion, and publication in Combustion and Flame [84].

Results

At a given particle temperature, a swelling coal particle initially swells during the early stages of pyrolysis, and then shrinks slightly during the later stages of devolatilization [17,58,59]. The same results were observed in this study (see Appendix A1). Moreover, all samples represented by data in the following figures were obtained at long enough residence time to include slight shrinkage.

Swelling ratios and porosities are plotted versus maximum particle temperature for Pittsburgh No. 8 and UBC chars in Figure 6.1. Experimental conditions for each legend symbol are shown in Table 6.1. Figures 6.1a and 6.1b show a general trend of decreasing swelling ratio and porosity with increasing particle temperature for the Pittsburgh No. 8 char. A slight decrease in swelling ratio with increasing temperature is also observed for

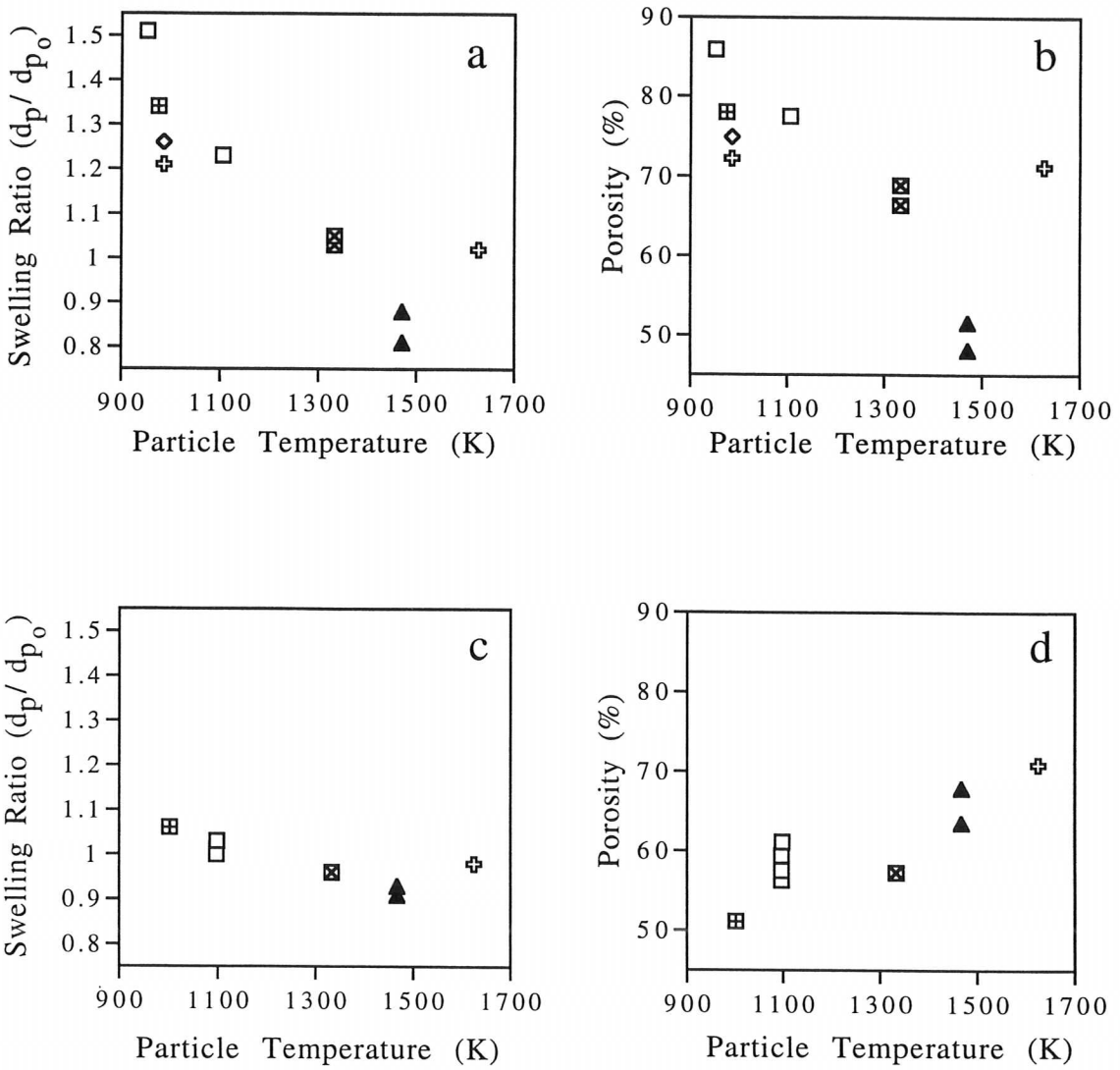

Figure 6.1a,b,c,d. Changes in swelling and porosity as a function of maximum particle temperature for Pittsburgh No. 8 coal chars (a and b) and UBC coal chars (c and d). Open symbols are data from the HPCP, filled symbols are data from the FFB (see Table 6.1).

Table 6.1

Summary of Experimental Conditions for Swelling Experiments

Symbol	Reactor	Maximum Particle Temperature	Residence Time (ms)	Gas Atmosphere Composition
□	HPCP	950 - 1100 K	[a]480 - 490	100% N_2
✣	HPCP	986 - 1626 K	135 - 150	100% N_2
◇	HPCP	986 K	150	100% N_2
⊠	HPCP	1333 K	490	100% He
⊞	HPCP	975 K	350	100% N_2
▲	FFB	1467 K	50	[b]Vitiated Air

a. Between 480 and 600 ms for UBC coal char.
b. 18% H_20, 4% O_2, 7.5% CO_2, and 70.5% N_2

the UBC chars in Figure 6.1c, however, the porosity of the UBC char *increases* with increasing particle temperature as shown in Figure 6.1d, in contrast to that for the Pittsburgh No. 8 char. The particle porosity for the UBC char increases to 70% even though swelling is minimal. The FFB char data (solid symbols) agree with the HPCP data for the UBC chars, but are lower than the HPCP data for the Pittsburgh No. 8 char.

Zap lignite does not swell or even experience a plastic state during devolatilization. Values for Zap char swelling ratios obtained in this research range from 0.85 to 0.97. Swelling ratio values obtained in this study agree with values obtained elsewhere [17,59] for all three coals.

Swelling ratio and porosity for Pittsburgh No. 8 chars decrease markedly with increasing heating rate (see Figs. 6.2a and b). In entrained flow systems, it is difficult to separate effects of heating rate and maximum temperature. The correlation of swelling with heating rate for the Pittsburgh No. 8 char is approximately linear and less scattered than that with temperature. Conversely, the UBC char swelling ratios and porosities appear to be better correlated with particle temperature than with heating rate.

Porosities of UBC and Zap coal chars (Figure 6.3) generally increase with increasing maximum particle temperature and heating rate, while Pitt. 8 porosities decrease for the temperatures, heating rates and residence times considered.

Table 6.2 compares effects of pyrolysis on coal char swelling and porosity in 100% nitrogen with pyrolysis in 4% oxygen and 96% nitrogen. The presence of oxygen in the pyrolysis gases increases swelling of Pitt. 8 char considerably at 986 K, but only slightly at the higher temperature of 1627 K. At a lower preparation temperature (~1000 K) but at a longer residence time, UBC char swells more with oxygen in the pyrolysis gas. At the low temperature condition, Pitt. 8 char prepared in an inert environment has a higher mass release. At higher temperature, oxidation is more severe, causing char prepared with oxygen to experience a much higher mass release. At a longer residence time than the Pitt. 8 char preparation condition but at a

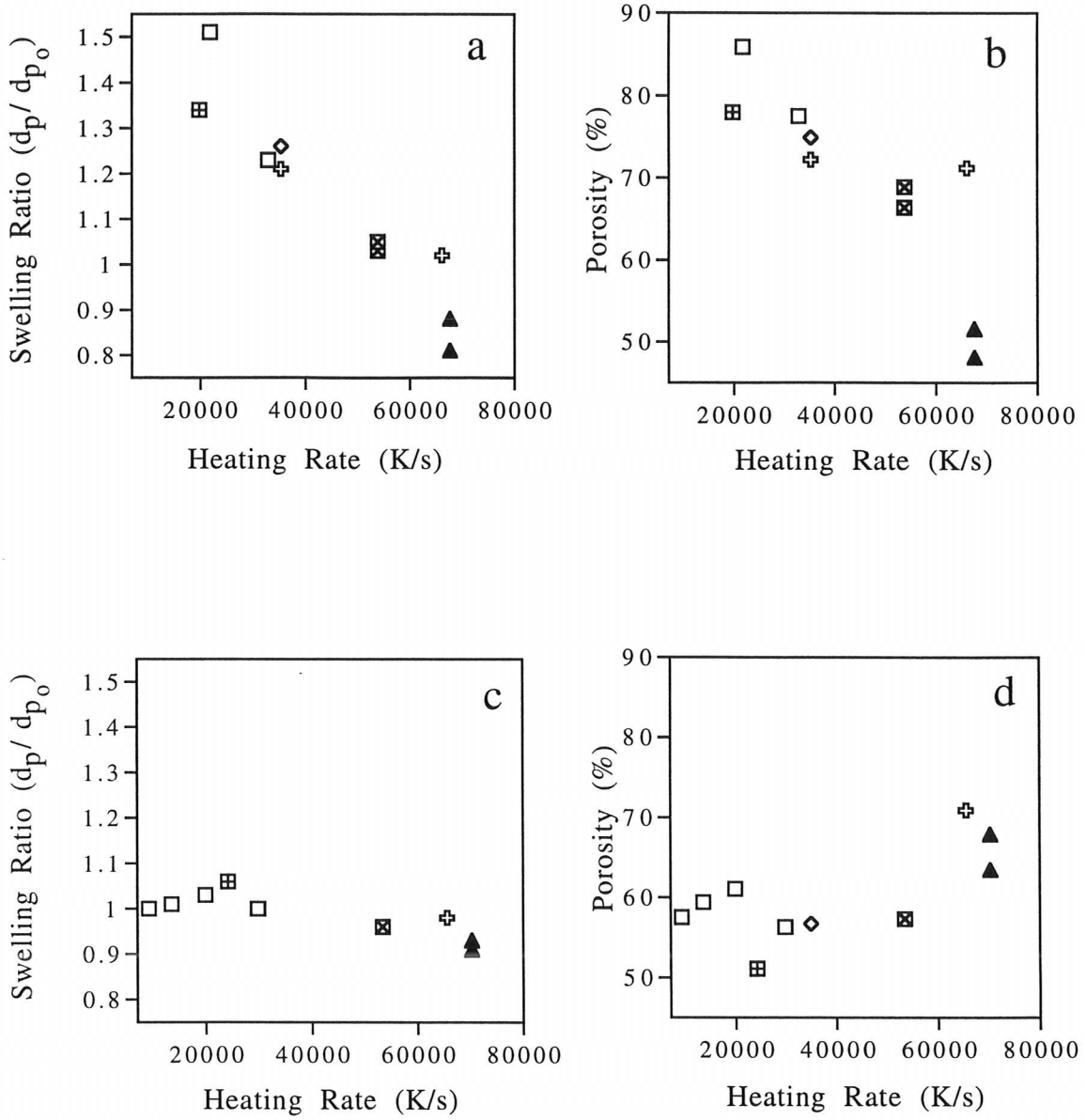

Figure 6.2a,b,c,d. Changes in swelling and porosity as a function of maximum particle heating rate for Pittsburgh No. 8 coal chars (a and b) and UBC coal chars (c and d). Open symbols are data from the HPCP, filled symbols are data from the FFB (see Table 6.1).

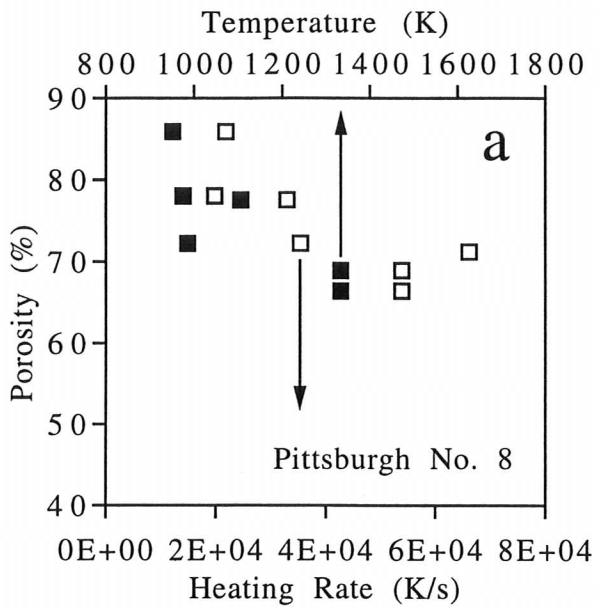

Darkened symbols are plotted versus maximum particle temperature and open symbols are plotted versus maximum particle heating rate.

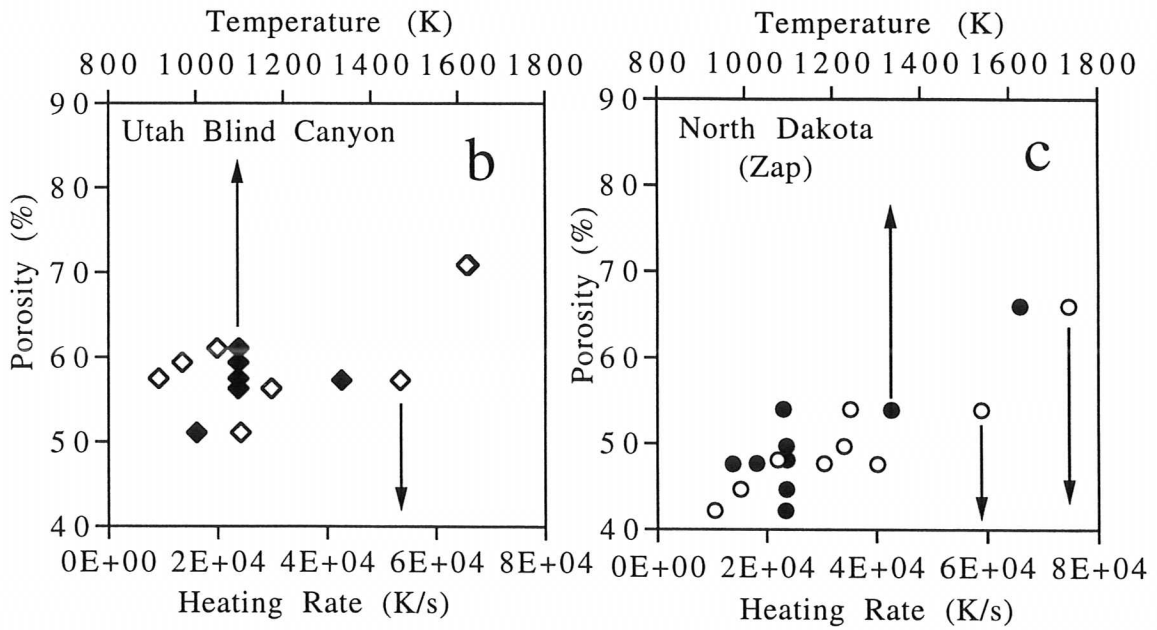

Figure 6.3. Porosity versus maximum particle temperature and heating rate for chars prepared in an inert environment in the HPCP from Pitt. 8, UBC, and Zap coals.

relatively low temperature, UBC char experiences a higher mass release when prepared with oxygen than when prepared in an inert environment. As with Pitt. 8, Zap char experiences a higher mass release when prepared in an inert environment. However, the Zap char swelling ratio is not affected by oxygen in the pyrolysis gas. Furthermore, Zap char porosity is higher when prepared in an inert environment, which is consistent with its higher mass release. As expected, for the non-swelling coals, the largest porosities are observed for chars which experience the highest mass release. Porosity and mass release were independently calculated such that they may be used as a check for each other. Due to swelling, however, plastic coals such as Pitt. 8 generally increase in porosity consistent with their swelling ratio, and porosity is therefore less dependent on mass release.

Table 6.2
Effects on Swelling of Oxygen in the Pyrolysis Gas

Coal Type	Swelling Ratio D_p/D_{po}	Porosity (%)	Mass Release (%)	Residence Time (ms)	Particle Temp. (K)	Gas Atmosphere (%)
Pitt. 8	1.21	72.2	44.7	150	986	100 N_2
Pitt. 8	1.41	80.9	38.4	150	986	4 O_2, 96 N_2
Pitt. 8	1.02	71.2	58.1	135	1627	100 N_2
Pitt. 8	1.06	84.5	74.2	135	1627	4 O_2, 96 N_2
UBC	1.06	51.1	38.7	294	1002	100 N_2
UBC	1.17	68.5	47	294	1002	4 O_2, 96 N_2
Zap	0.91	47.7	53.9	294	1027	100 N_2
Zap	0.91	41.4	47.4	294	1027	4 O_2, 96 N_2

Discussion

Swelling Ratio and Porosity Versus Heating Rate

Data from Zygourakis [62] indicate a continual *increase* in porosity with increasing heating rate between 0.1 and 1000 K/s for chars prepared from Illinois No. 6 hv-bituminous coal. In the present study, at maximum particle heating rates of $2x10^4$ to $7x10^4$ K/s, a *decrease* in both porosity and swelling for Pittsburgh No. 8 chars was observed. UBC chars, however, underwent a moderate decrease in swelling and an increase in

porosity with increasing heating rate. Zygourakis [62] also reported particle radii for the Illinois No. 6 char, from which swelling ratios can be calculated using his initial coal particle size fraction. The initial particle sizes used by Zygourakis are five times larger than those used in this research. However, the trends between his work and this work (Fig. 6.4) qualitatively indicate an increase in swelling and porosity versus heating rate up to 10^3 K/s and a decrease in swelling and porosity at higher heating rates for swelling coals. Industrial entrained-flow coal furnaces have even higher heating rates of 10^5 to 10^6 K/s. Therefore, these findings indicate that swelling is not important at high heating rates, which is the case in industrial furnaces. Additional experiments using identical particle sizes and coal types are suggested for more quantitative comparisons.

Swelling and porosity both increase initially with particle heating rate because the total volatile yield increases with increasing heating rate [75]. The increased volatile matter contributes to the swelling by expanding the outer shell of the char particles as it escapes. The temperature at which devolatilization occurs increases with heating rate because of the distributed nature of the coal bonding structure [39,85]. At very low heating rates, swelling does not occur even though there may be significant devolatilization because pressure build-up from the release of volatiles is too small to expand the particle shell, i.e., there is sufficient time for volatiles to escape through small pores in the surface before pressure can build up. At the heating rates observed in this study, both swelling and porosity decrease with increasing heating rate because the chemical release rate of volatiles is faster than the relaxation time involved in expansion of the particle shell. This results in either solidification before significant swelling, or else popping of gas bubbles to release the internal pressure. Significant internal particle temperature gradients may also affect particle behavior at the high heating rates. After rapid devolatilization at these high heating rates, crosslinking quickly solidifies the particle structure.

The heating rate range of 2×10^4 to 7×10^4 K/s studied in this work is typical of

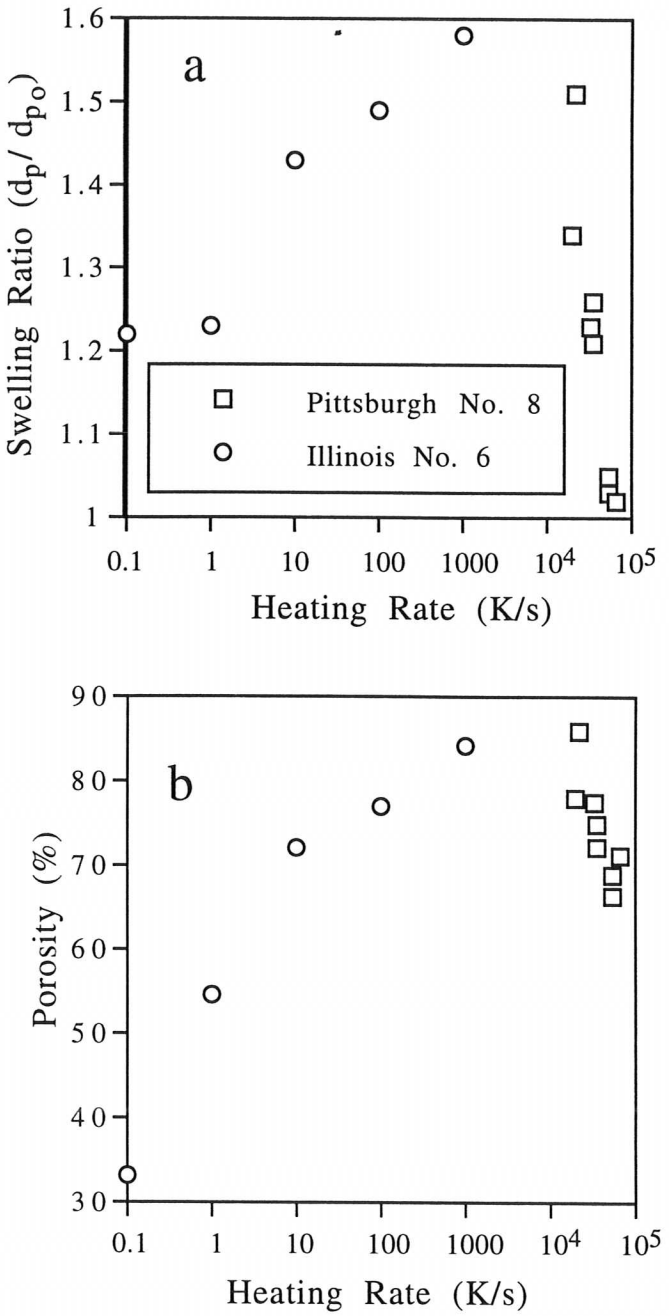

Figure 6.4a,b. Swelling ratio and porosity versus maximum particle heating rate for two coals. The Illinois No. 6 char data were obtained from Zygourakis [62].

the heating rate difference between many flat flame burners and drop tubes. Therefore, the difference in swelling ratios of chars prepared in flat flame burners and drop tubes is largely due to the heating rate difference. However, if sampling does not take place before the onset of char oxidation or gasification in flat flame burner experiments, fragmentation of char particles may reduce both swelling and porosity. This may explain why swelling and porosity of Pittsburgh No. 8 is less for the FFB chars than for the HPCP chars prepared at identical heating rates (see Fig. 6.1 and 6.2). Although attempts were made to sample the FFB char before significant gasification and/or oxidation occurred, the mass release and nitrogen surface area, both indicators of char oxidation [58, see Chapter 4], were higher for the FFB char than for the HPCP char. On the other hand, the swelling and porosity values of UBC FFB char are in line with those for UBC HPCP chars. The Pittsburgh No. 8 char is probably more susceptible than the UBC char to fragmentation during the early stages of char gasification because it is a plastic coal, which quickly forms thin-walled cenospheres in the early stages of devolatilization.

Correlations of Porosity and Surface Area

The decrease in Pitt. 8 char porosities (see Fig. 6.3) over the same range of heating rates that UBC and Zap char porosities increase is probably due to the plasticity of Pittsburgh No. 8 coal. Because Pitt. 8 is a plastic coal, it has the potential to form cenospheres during heat treatment. Cenospheres are very porous balloon-like spheres, some with thin walls and some with thick. As a char particle porosity approaches one, the char particle becomes more hollow, spherical and possessing thin walls. Consequently, Pitt. 8 char, at heating rates between 10^3 and 10^4 K/s, forms chars that are much more porous than UBC and Zap (non-plastic) chars. At higher heating rates such as employed in these experiments, swelling is less or not at all. However, large voids are known to exist in chars prepared from plastic coals at high heating rates, even though little swelling occurs. Pitt. 8 char porosity decreases with increasing heating rate between $2x10^4$ to $7x10^4$ K/s. UBC and Zap chars, however, have less potential to form cenospheres than

Pitt. 8 char, and increase in porosity only as volatile matter is released leaving open pore volume once occupied by gas and tar. For the range of heating rates observed in this research, Pitt. 8 char porosity decreases with increasing heating rate due to decreased swelling. UBC and Zap chars become more porous with increasing heating rates due to an increase in open pore volume as mass is released.

N_2 and CO_2 surface areas do not correlate with total porosities for any of the three coal chars. It must not be assumed, therefore, that an increase in meso-pore surface area always accompanies an increase in total porosity. This is particularly true for swelling coals that may have a very large porosity but essentially no N_2 surface area.

Oxygen Experiments

Even though chars were prepared at high heating rates, it has been suggested that a very small amount of oxidation occurred prior to pyrolysis in the 4% O_2 HPCP experiments. A small amount of oxidation just prior to pyrolysis could cause crosslinking that may account for the decrease in mass release for a Pitt. 8 and a Zap char prepared with 4% O_2 in the pyrolysis gases of the HPCP. In addition to decreasing mass release, crosslinking reactions prior to pyrolysis might cause increased swelling at the heating rates considered in this work. However, it has been shown [59] that oxygen in the pyrolysis gas atmosphere has no affect on swelling until char oxidation occurs. Further understanding of swelling during transition from devolatilization to char oxidation is needed. Perhaps titanium is an unsuitable tracer to determine mass release in the transition between devolatilization and oxidation. Char prepared in 4% O_2 in the HPCP did experience mild oxidation following pyrolysis.

Another difficulty with the above explanation of the effect of oxygen in the pyrolysis gas on coal char swelling is the behavior of the UBC char. UBC char increased in swelling considerably in the presence of a small amount of oxygen during pyrolysis, but UBC char did not swell at any heating rate investigated when prepared in an inert environment. Large particles of UBC coal char have been observed to swell considerably

and even explode during combustion at low heating rates [86]. However, UBC char significantly increased in porosity with increasing heating rate during pyrolysis in an inert environment even though the swelling ratio stayed near one; such behavior is consistent with a rigid particle that increases in porosity as mass is released.

The presence of steam in the pyrolysis gas under the conditions of this research had no effect on char swelling ratios for any of the three coals investigated.

Conclusions

1) The swelling ratio and porosity of Pittsburgh No. 8 char decrease (by 35 and 15%, respectively) as maximum particle heating rates increase from 2 x 10^4 K/s to 7 x 10^4 K/s. This factor of 4 increase in heating rate is enough to explain why particles swell in drop tube reactors and not in flat flame burner experiments.

2) For Pittsburgh No. 8 coal, the heating rate at which maximum particle swelling and porosity occurs in an inert environment is less than 10^4 K/s, and is probably greater than 10^3 K/s based on data at lower heating rates.

3) For UBC coal, porosity continued to increase with increasing heating rate for all heating rates examined ($2x10^4$ to $7x10^4$ K/s). The maximum particle heating rate corresponds to a maximum particle temperature of 1625 K in this study.

4) Swelling and porosity correlate better with maximum particle heating rate than with particle temperature for highly swelling coals such as Pittsburgh No. 8.

Chapter 7

Summary

The effects of devolatilization temperature, heating rate, residence time, and gas atmosphere on coal char swelling, internal surface area, porosity, density, elemental composition, and intrinsic reactivity have been determined, and correlations were defined for Pittsburgh No. 8, Utah Blind Canyon hv-bituminous coals, and Zap lignite. In addition, correlations of coal char properties with intrinsic reactivity have been identified for these three coals. This information will allow improved modeling of the coal combustion process. Improved control, via better computer models, of the coal combustion process will allow cleaner and more efficient use of coal as an energy source.

In addition to new fundamental information about the coal combustion process to aid in modeling, this work provides information for those performing coal char oxidation studies for application to full scale industrial boilers. It is clear that pyrolysis conditions significantly effect the char oxidation process by affecting char properties following pyrolysis. Specifically, pyrolysis affects coal char intrinsic reactivity, porosity, internal surface area, and swelling, all of which affect reaction rates, burnout times, and temperatures in industrial boilers and in laboratory scale char oxidation reactors. Those who perform char oxidation experiments for industrial boiler application should consider the effects of char preparation conditions on the resulting char properties and combustion characteristics provided in this work. Care should be taken to prepare chars at conditions similar to those of industrial boilers. Some specific preparation guidelines that must be considered are:

(1) Heating rate significantly affects swelling of plastic coals. The heating rate should be higher than 7×10^4 K/s to be representative of industrial pulverized coal boilers.

(2) Temperature, heating rate, residence time and gas atmosphere (O_2, H_2O, CO_2) significantly affect internal surface areas and porosities. It is not clear what the gas atmosphere is in industrial furnaces, but certainly some steam is present.

(3) Temperature, heating rate and residence time during pyrolysis significantly affect intrinsic coal char reactivities. The combination of intrinsic reactivity, porosity, density, and internal surface area significantly affect the overall char reactivity at high temperatures. This means that chars for high temperature reactivity experiments should be prepared at relevant conditions.

Finally, it is important to understand that in modeling, all of the fundamental information about the coal combustion process is related. Even though the most direct application to full scale industrial boilers of the data obtained in this research is to coal reaction rates, this data will indirectly aid in the improvement of the entire coal combustion process including NO_x and SO_x control as well as control of boiler slagging and deposition characteristics.

References

1. Franklin, R. E., "Crystallite Growth in Graphitizing and Non-Graphitizing Carbons," *Proc. Roy. Soc.* A 209: 196-218 (1951).

2. Franklin, R. E., "A Study of the Fine Structure of Carbonaceous Solids by Measurements of True and Apparent Densities," *Trans. Faraday Soc.* 45: 668-682 (1949).

3. Walker Jr., P. L. and Geller, I., "Change in Surface Area of Anthracite on Heat Treatment," *Nature*, Lond. 178: 1001 (1956).

4. Anderson, R. B., Hall, W. K., Lecky, J. A., and Stein, K. C., *J. Phys. Chem.* 60: 1548 (1956).

5. Anderson, R. B., Hofer, L. J. E. and Bayer, J., "Surface Area of Coal," *Fuel* 41: 559 (1962).

6. Walker Jr., P. L. and Kini, K. A., "Measurement of the Ultrafine Surface Area of Coals," *Fuel* 44: 453-459 (1965).

7. Mahajan, O. P., Komatsu, M., and Walker Jr., P. L., "Low-Temperature Air Oxidation of Caking Coals. 1. Effect on Subsequent Reactivity of Chars Produced," *Fuel* 59: 3-10 (1980).

8. White, W. E., Bartholomew, C. H., Hecker, W. C., and Smith, D. M., "Changes in Surface Area, Pore Structure and Density during Formation of High-Temperature Chars from Representative U.S. Coals," *Adsorption Sci. Tech.* 7: 180-209 (1991).

9. Brunauer, S., Emmett, P.H. and Teller, E., *J. Am. Chem. Soc.* 60: 309 (1938).

10. Dubinin, M. M., *Chemistry and Physics of Carbon* 2: 51-120 (1966).

11. Nandi, S. P., Ramadass, V., and Walker Jr., P. L., "Changes in the Ultrafine Structure of Anthracites upon Heat Treatment," *Carbon* 2: 199-210 (1964).

12. Ludvig, M. M., Gard, G. L., and Emmett, P. H., "Use of Controlled Oxidation to Increase the Surface Area of Coal," *Fuel* 62: 1393-1396 (1983).

13. Sahu, R., Levendis, Y. A., Flagan, R. C., and Gavalas, G. R., "Physical Properties and Oxidation Rates of Chars from Three Bituminous Coals," *Fuel* 67: 275-283 (1987).

14. Kojima, T., Yamashita, S., Adschiri, T., and Furusawa, T., "Structural Difference Among Chars Produced at Various Heating Rates and Its Effect on Gasification Rate of Char," *1989 International Conference on Coal Science*: 465-468 (1989).

15. Zygourakis, K., "The Effects of Pyrolysis Conditions on the Macropore Structure of Coal Chars," *ACS Div. Fuel Chem. Preprints* 33 (4): 951-959 (1988).

16. Nsakala, Y. N., Essenhigh, R. H., and Walker Jr., P. L., "Characteristics of Chars Produced from Lignites by Pyrolysis at 808 °C Following Rapid Heating," *Fuel* 57: 605-611 (1978).

17. Fletcher, T. H., and Hardesty, D. R., "Compilation of Sandia Coal Devolatilization Data Milestone Report", Sandia National Laboratories Report No. SAND92-8209, 1992.

18. McDonald, K. M., Hyde, W. D., and Hecker, W. C., "Low Temperature Char Oxidation Kinetics: Effect of Preparation Method," *Fuel* 71: 319-323 (1992).

19. Hecker, W. C., McDonald, K. M., Reade, W., Swensen, M. R., and Cope, R. F., "Effects of Burnout on Char Oxidation Kinetics," *24th Symp. (Intl.) on Comb.*, The Combustion Institute, Pittsburgh, PA, 1992, pp. 1225-1231.

20. Mitchell, R. E., Hurt, R. H., Baxter, L. L., and Hardesty, D. R., "Compilation of Sandia Coal Devolatilization Data Milestone Report", Sandia National Laboratories Report No. SAND92-8208, 1992.

21. Rodriguez-Reinoso, F., "Controlled Gasification of Carbon and Pore Structure Development," *NATO Adv Study Inst Ser E* : (1991).

22. Marsh, H., and Rand, B., "The Process of Activation of Carbons by Gasification with CO_2--I. Gasification of Pure Polyfurfuryl Alcohol Carbon," *Carbon* 9: 47-85 (1971).

23. Tomkov, K., Jankowska, C., and Siemieniewska, T., "Activation of Brown-Coal with Oxygen," *Fuel* 56: 101-106 (1977).

24. Almela-Alarcon, M., *Ph. D. Thesis.* University of Alicante(Spain) : (1988).

25. Wigmans, T., Hoogland, A., Tromp, P., and Moulijn, J. A., "The Influence of Potassium Carbonate on Surface Area Development and Reactivity During Gasification of Activated Carbon by Carbon Dioxide," *Carbon* 21: 13-22 (1983).

26. Holmes, J., and Emmett, P. H., "Investigation of Low-Temperature Nitrogen Adsorption at High Relative Pressures," *J. Phys. Colloid Chem.* 57: 1276 (1947).

27. Wigmans, T., "Industrial Aspects of Production and Use of Activated Carbons," *Carbon* 27, 13-22 (1989).

28. Tomkov, T., Siemieniewska, T., Czechowski, F., and Jankowska, A., "Formation of Porous Structures in Activated Brown-Coal Chars Using O_2, CO_2 and H_2O as Activating Agents," *Fuel* 56: 121-124 (1977).

29. Hyde, W. D., Hecker, W. C., Cope, R. F., Painter, M. M., McDonald, K. M., and Bartholomew, C. H., "The Effects of Rank and Preparation Method on Coal Char Oxidation Rates," *1989 Western States Catalysis Meeting*, 1989.

30. Jenkins, R. G., Nandi, S. P., and Walker Jr., P. L., "Reactivity of Heat-Treated Coals in Air at 500 °C," *Fuel* 52: 288-293 (1973).

31. Radovic, L. R., Walker Jr., P. L., and Jenkins, R. G., "Importance of Carbon Active Sites in the Gasification of Coal Chars," *Fuel* 62: 849-856 (1983).

32. Chitsora, C. T., Muhlen, H. J., Van Heek, K. H., and Juntgen, H., "The Influence of Pyrolysis Conditions on the Reactivity of Char in H_2O," *Fuel Processing Technology* 15: 17-29 (1987).

33. Rybak, W., "Reactivity of Heat-Treated Coals," *Fuel Processing Technology* 19: 107-122 (1988).

34. Kothandaraman, G., and Simons, G. A., "Evolution of the Pore Structure in PSOC-140 Lignite During Pyrolysis," *20th Symp. (Intl.) on Comb.*, The Combustion Institute, Pittsburgh, PA, 1984, pp. 1523-1529.

35. Agrawal, R. K., "Effect of Pyrolysis Conditions on Gasification Reactivity of Chars," *Eighth Annual (Intl.) Pittsburgh Coal Conference* : 76-82 (1991).

36. Young, B. C., and Smith, I. W., "Pulverized Coal Char Combustion : The Effect of Coal Rank and Pyrolysis Conditions," *1987 (Intl.) Symp. on Coal Comb.* (1987).

37. Solomon, P. R., Serio, M. A., and Heninger, S. G., "Variations in Char Reactivity with Coal Type and Pyrolysis Conditions," *ACS Preprints* 31 (3): 200-209 (1986).

38. Smoot, L. D., Hedman, P. O., and Smith, P. J., "Pulverized-Coal Combustion Research at Brigham Young University," *Progr. Energy Combust. Sci.* 10: 359-441 (1984).

39. Freihaut, J. D., Proscia, W. M., and Seery, D. J., "Chemical Characteristics of Tars Produced in a Novel Low-Severity, Entrained-Flow Reactor," *Energy Fuels* 3: 692-703 (1989).

40. Charpenay, S. and Solomon P., "The Prediction of Coal Char Reactivity Under Combustion Conditions," *24th Symp. (Intl.) on Comb.*, The Combustion Institute, Pittsburgh, PA, 1992, pp. 1189-1197.

41. Serio, M. A., Solomon, P. R., and Suuberg, E. M., "Variations in Char Reactivity with Coal Type and Pyrolysis Conditions," 1987 *International Conference on Coal Science*: 597-600 (1987).

42. Thiele, E. W., *Ind. Eng. Chem.* 31: 916 (1939).

43. Ashu, J. T., Nsakala, N. Y., Mahajan, O., P., and Walker Jr., P. L., "Enhancement of Char Reactivity by Rapid Heating of Precursor Coal," *Fuel* 57: 50-51 (1978).

44. Solomon, P. R., Serio, M. A., Despande, G. V., and Kroo, E., "Cross-Linking Reactions During Coal Conversion," *Energy Fuels* 4: 42-54 (1990).

45. Kamishita, M., Mahajan, O. P., and Walker Jr., P. L., "Effect of Carbon Deposition on Porosity and Reactivity of a Lignite Char," *Fuel* 56: 444-450 (1977).

46. Hurt, R. H., Sarofim, A. F., and Longwell, J. P., "Role of Microporous Surface Area in Uncatalyzed Carbon Gasification," *Energy Fuels* 5: 290-299 (1991).

47. Hippo, E., and Walker, P. L. Jr., "Reactivity of Heat-Treated Coals in Carbon Dioxide at 900 °C," *Fuel* 54: 245 (1975).

48. Gopalakrishnan, R., Fullwood, M. J., and Bartholomew, C. H., "Catalysis of Char Oxidation by Calcium Minerals: Effects of Calcium Compound Chemistry on Intrinsic Reactivity of Doped Spherocarb and Zap Chars," In Press, *Energy Fuels* (1994).

49. Hurt, R. H., Sarofim, A. F., and Longwell, J. P., Effect of Nonuniform Surface Reactivity on the Evolution of Pore Structure and Surface Area during Carbon Gasification," *Energy Fuels* 5: 463-468 (1991).

50. Wigmans, T., Auwerda, D., Geus, J. W., and Moulign, J. A., *15th Biennial Conf. Carbon*, Extended Abstr. 1981, 144.

51. Radovic, L. R., Ph.D. *Thesis*, Department of Marerials Science and Engineering, The Pennsylvania State University, 1982.

52. Hurt, R. H., Sarofim, A. F., and Longwell, J. P., "The Role of Microporous Surface Area in the Gasification of Chars from a Sub-Bituminous Coal," *Fuel* 70: 1079-1082 (1991).

53. Sinnatt, F.S., McCulloch, A. and Newall, H. E., "The Carbonisation of Particles of Coal. The Study of Cenospheres. Part 5.," *J. Soc. Chemical Ind. Trans.*, 46: 331-335 (1927).

54. Brookes, F. R., "The Combustion of Single Captive Particles of Silkstone Coal," *Fuel* 48: 139-149 (1969).

55. Kallend, A. S., and Nettleton, M. A., *Sixth Intl. Conf. on Coal Sci.* Paper 6 (1965).

56. Street, P. J., Weight, R. P., and Lightman P., "Further Investigations of Structural Changes Occurring in Pulverized Coal Particles during Rapid Heating," *Fuel* 48: 343-365 (1969).

57. Shibaoka, M., "An Investigation of the Combustion Processes of Single Coal Particles," *J. Inst. Fuel*, 42: 59-66 (1969).

58. Tsai, C. Y., and Scaroni, A. W., "The Structural Changes of Bituminous Coal Particles during the Initial Stages of Pulverized-Coal Combustion," *Fuel* 66: 200-206 (1987).

59. Fletcher, T. H., "Swelling Properties of Coal Chars During Rapid Pyrolysis and Combustion," *Fuel* 72: 1485-1495 (1993).

60. Hamilton, L. H., "A Preliminary Account of Char Structures Produced from Liddell Vitrinite Pyrolysed at Various Heating Rates," *Fuel* 59: 112-116 (1980).

61. Hamilton, L. H., "Char Morphology and Behavior of Australian Vitrinites of Various Ranks Pyrolysed at Various Heating Rates," *Fuel* 60: 909-913 (1981).

62. Zygourakis, K., "Effect of Pyrolysis Conditions on the Macropore Structure of Coal-Derived Chars," *Energy Fuels* 7: 33-41 (1993).

63. Solomon, P. R., and Hamblen, D. G.,"Chemistry of Coal Conversion" by Richard H. Schloberg , Chapter: Pyrolysis, section 3.6 Swelling: 195-203 (Plenum 1985).

64. Furmisky, E., MacPhee, J. A., Vancea, L., Ciavaglia, L. A., and Nandi, B. N., "Effect of Oxidation on the Chemical Nature and Distribution of Low-Temperature Pyrolysis Products from Bituminous Coal," *Fuel* 62: 395-400 (1983).

65. Maloney, D. J., and Jenkins, R. G., "Influence of Coal Preoxidation and the Relation Between Char Structure and Gasification Potential," *Fuel* 64: 1415-1422 (1985).

66. Hurt, R. H., and Mitchell, R. E., "Unified High-Temperature Char Combustion Kinetics for a Suite of Coals of Various Rank," *24th Symp. (Intl.) on Comb.*, The Combustion Institute, Pittsburgh, PA, 1992, pp. 1243-1250.

67. Fletcher, T. H., "Time-Resolved Particle Temperature and Mass Loss Measurements of a Bituminous Coal During Devolatilization," *Combust. Flame* 78: 223-236 (1989).

68. Cope, R. F., Dissertation Chem. Eng. in Progress, Brigham Young University, Provo UT (1994).

69. Monson, C. R., and Germane, G. J., "A High-Pressure Drop-Tube Facility for Coal Combustion Studies," *Energy Fuels* 7: 928-936 (1993).

70. Hyde, W. D., "Effects of Preparation Method and Parent Coal Rank on Coal Char Reactivity" M.S. Thesis, Brigham Young Univ., Provo, UT (1990).

71. Selph, C., "Generalized Thermochemical Equilibrium Program for Complex Mixtures," Rocket Propulsion Laboratory, Edwards Air Force Base, CA (1965).

72. Fletcher, T. H., Kerstein, A. R., Pugmire, R. J., Solum, M. S., and Grant, D. M., "Chemical Percolation Model for Devolatilization. 3. Direct Use of ^{13}C NMR Data to Predict Effects of Coal Type," *Energy Fuels* 6: 414-431 (1992).

73. Spalding, D. B., *Some Fundamentals of Combustion, Butterworths*, London, 1955.

74. Tsai, C. Y., and Scaroni, A. W., "Pyrolysis during the Initial Stages of Pulverized-Coal Combustion," *20th Symp. (Intl.) on Comb.* The Combustion Institute, 1984, pp. 1455-1462.

75. Gibbins-Matham, J., and Kandiyoti, R., "Coal Pyrolysis Yields from Fast and Slow Heating in a Wire-Mesh Apparatus with a Gas Sweep," *Energy Fuels* 2: 505 (1988).

76. Walker Jr., P. L., Rusinko, F., Jr., and Austin, L. G., "Gas Reactions of Carbon," *Advan. Catal.* 11: 133-178 (1959).

77. Goetz, G. J., Nsakala, N. Y., Patel, R. L., and Lao, T. C., "Combustion and Gasification Kinetics of Chars from Four Commercially Significant Coals of Varying Rank," Second Annual Contractors' Conference on Coal Gasification, Palo Alto, California 1982.

78. Ingles, O. G., *Trans. Faraday Soc.* 48, 706 (1952).

79. Mitchell, R. E., Kee, R. J., Glarborg, P., and Coltrin, M. E., "The Effect of CO Conversion in the Boundary Layers Surrounding Pulverized-Coal Char Particles," *23rd Symp. (Intl.) on Comb.*, The Combustion Institute, Pittsburgh, PA, 1990, pp. 1169-1176.

80. Deevi, S. C., and Suuberg, E. M., "Physical Changes Accompanying Drying of Western US Lignites," *Fuel* 66: 454-460 (1987).

81. Suuberg, E. M., Otake, Y., Yun, Y., and Deevi, S. C., "Role of Moisture in Coal Structure and the Effects of Drying Upon the Accessibility of Coal Structure," *Energy Fuels* 7: 384-392 (1993).

82. Su, J. L., and Perlmutter, D. D., "Effect of Chemisorbed Oxygen on Char Reactivity," *AIChE Journal* 31: 1725-1727 (1985).

83. Bailey, J. G., Tate, A., Diessel, C. F. K., and Wall, T. F., "A Char Morphology System with Applications to Coal Combustion," *Fuel* 69: 225-239 (1990).

84. Gale, T. K., Bartholomew, C. H., Fletcher, T. H., "Decreases in the Swelling and Porosity of Bituminous Coals During Devolatilization at High Heating Rates," *Combust. Flame* In Press, 1994.

85. Fletcher, T. H., Kerstein, A. R., Pugmire, R. J., and Grant, D. M., "Chemical Percolation Model for Devolatilization. 2. Temperature and Heating Rate Effects on Product Yields," *Energy Fuels* 4: 54-60 (1990).

86. Smoot, L. D., Personal Communication, Brigham Young University 1994.

Appendicies

Appendix A1

Char Preparation Conditions, Temperature Profiles, and Data

This appendix contains the preparation conditions for each char. Labels provided in Tables A1.1, A1.2, and A1.3 for each char are used throughout the appendices to report further information on each char. Gas temperature profiles for each preparation condition are also provided.

Table A1.1
Pyrolysis Conditions of Pittsburgh No. 8 Coal Chars

Char Label (P#)	Maximum Particle Temperature (K)	Maximum Particle Heating Rate (K/s)[a]	Residence Time (ms)	Pyrolysis Gas Atmosphere (%)[b]	Temperature Profile of Pyrolysis Condition
P	---	---	---	---	Parent Coal
P2	1106	3.29e4	490	100 N_2	E
P3				100 N_2	
P4	840	1.73e4	280	100 N_2	A
P5	975	1.98e4	350	100 N_2	C
P6	952	2.18e4	480	100 N_2	D
P7	1333	5.38e4	490	100 He	J
P8	1333	5.38e4	490	100 He	J
P9	986	3.53e4	150	100 N_2	L
P10	986	3.53e4	150	4 O_2, 96 N_2	L
P11	986	3.53e4	150	18 H_2O, 82 N_2	L
P12				100 He	
P13	1627	6.61e4	135	100 N	M
P14	1627	6.61e4	135	4 O_2, 96 N_2	M
P15	1090	6.90e4	26	FFB[c]	B
P16	1471	6.76e4	50	FFB	B
P17	1471	6.76e4	50	FFB	B
P18	1471	6.90e4	75	FFB	B
P19	1471	6.90e4	100	FFB	B

a. 3.3e4 = 3.3×10^4
b. Prepared in the HPCP unless otherwise noted.
c. FFB = Flat Flame Burner: 4% oxygen, 7.5% carbon dioxide, 18% Steam, 70.5% nitrogen

Tables A1.TPa-m contain the gas and wall temperature profiles for each of the conditions listed above and for Tables A1.2 and A1.3.

Table A1.2

Pyrolysis Conditions of Utah Blind Canyon Coal Chars

Char Label (U#)	Maximum Particle Temperature (K)	Maximum Particle Heating Rate (K/s)[a]	Residence Time (ms)	Pyrolysis Gas Atmosphere (%)[b]	Temperature Profile of Pyrolysis Condition
U	---	---	---	---	Parent Coal
U2	1097	2.98e4	490	100 N_2	E
U3	1098	1.99e4	525	100 N_2	F
U4	1097	1.35e4	560	100 N_2	G
U5	1097	9.17e3	595	100 N_2	H
U6	1002	2.42e4	294	100 N_2	K
U7	1002	2.42e4	294	4 O_2, 96 N_2	K
U8	1333	5.34e4	490	100 He	J
U9	980	3.49e4	150	18 H_2O, 82 N_2	L
U10	1625	6.56e4	135	100 N_2	M
U11	1467	7.03e4	50	FFB[c]	B
U12	1467	7.03e4	50	FFB	B
U13	1467	7.03e4	100	FFB	B

a. 3.3e4 = 3.3×10^4

b. Prepared in the HPCP unless otherwise noted.

c. FFB = Flat Flame Burner: 4% oxygen, 7.5% carbon dioxide, 18% Steam, 70.5% nitrogen

Table A1.3

Pyrolysis Conditions of North Dakota (Beulah Zap) Coal Chars

Char Label (Z#)	Maximum Particle Temperature (K)	Maximum Particle Heating Rate (K/s)[a]	Residence Time (ms)	Pyrolysis Gas Atmosphere (%)[b]	Temperature Profile of Pyrolysis Condition
Z	---	---	---	---	Parent Coal
ZD	---	---	---	---	Dried Coal
ZD3			490	100 N_2	E
Z4	1027	3.05e4	294	100 N_2	K
Z5	1095	3.41e4	490	100 N_2	E
Z6	1097	2.20e4	525	100 N_2	F
Z7	1095	1.52e4	560	100 N_2	G
Z8	1093	1.04e4	595	100 N_2	H
Z9	1088	3.53e4	980	100 N_2	I
Z10	1027	3.05e4	294	4 O_2, 96 N_2	K
Z11	1334	5.90e4	490	100 He	J
Z12	972	4.02e4	150	100 N_2	L
Z13	972	4.02e4	150	18 H_2O, 82 N_2	L
Z14	1095	3.41e4	490	18 H_2O, 82 N_2	E
Z15	1625	7.47e4	135	100 N_2	M
Z16	1507	1.94e5	50	FFB[c]	B

a. 3.3e4 = 3.3×10^4

b. Prepared in the HPCP unless otherwise noted.

c. FFB = Flat Flame Burner: 4% oxygen, 7.5% carbon dioxide, 18% Steam, 70.5% nitrogen

Tables A1.TPa-m: Temperature Profile Listings

a. Wall Temperature = 850 °C

Distance from injection (mm)	Gas Temperature (K)
5	673
20	683
40	728
60	718
80	726
100	737
120	748
140	726
160	855
180	822
200	619
220	876
240	759
260	753

b. Wall Temperature = 850 °C

Distance from injection (mm)	Gas Temperature (K)
0.0	300
3.18	383.5
15.88	800
28.58	1689
41.28	1705
53.98	1662
79.38	1621
104.78	1556
130.18	1532
155.58	1505
180.98	1472
200	1450
220	1430
250	1400
260	1400

c. Wall Temperature = 850 °C

Distance from injection (mm)	Gas Temperature (K)
5	720
20	750
40	770
60	800
80	825
100	846
120	862
140	874
160	894
180	900
200	879
220	975
240	948
260	750
280	985
300	878
320	870

d. Wall Temperature = 850 °C

Distance from injection (mm)	Gas Temperature (K)
5	677
10	682
20	655
40	688
60	704
80	704
100	677
120	688
140	762
160	778
180	789
200	810
220	831
240	846
260	862
280	862
300	862
320	841
340	841
360	815
380	661
400	852
420	741
440	730

e. Wall Temperature = 1050 °C			
Distance from injection (mm)	Gas Temperature (K)	Distance from injection (mm)	Gas Temperature (K)
0.0	393.15	290	962
5	939	330	986
10	921	370	1038
20	932	390	1050
30	920	410	1079
40	873	430	1055
50	880	450	1011
70	847	470	953
90	780	490	889
130	759	510	852
170	806	530	957
210	901	550	744
250	902		

f. Wall Temperature = 1050 °C	
Distance from injection (mm)	Gas Temperature (K)
0.0	393.15
5	555
10	787
20	787
30	800
40	817
50	834
60	842
70	829
90	878
110	853
130	847
150	780
190	759
230	806
270	902
310	903
350	962
390	986
430	1038
450	1050
470	1079
490	1055
510	1011
530	953
550	889
570	852
590	957
610	744

g. Wall Temperature = 1050 °C	
Distance from injection (mm)	Gas Temperature (K)
0.0	393.15
5	597
10	612
20	636
30	654
40	673
50	691
70	722
90	764
110	780
130	798
150	818
170	847
190	780
230	759
270	806
310	902
350	903
390	962
430	986
470	1038
490	1050
510	1079
530	1055
550	1011
570	953
590	889
610	852
630	957
650	744

h. Wall Temperature = 1050 °C	
Distance from injection (mm)	Gas Temperature (K)
0.0	393.15
5	499
10	533
20	561
30	580
40	591
50	621
70	634
90	654
110	686
130	705
150	669
170	705
190	763
210	847
230	780
270	759
310	806
350	902
390	903
430	962
470	986
510	1038
530	1050
550	1079
570	1055
590	1011
610	953
630	889
650	852
670	957
690	744

i. Wall Temperature = 1050 °C	
Distance from injection (mm)	Gas Temperature (K)
0.0	393.15
5	1054
10	1056
20	1070
30	1048
40	1066
50	1032
70	1068
90	809
130	715
170	776
210	832
250	856
290	900
330	971
370	1019
390	1060
410	1060
430	1049
450	1040
470	1020
490	998
510	936
530	940
550	772

j. Wall Temperature = 1050 °C	
Distance from injection (mm)	Gas Temperature (K)
5	628
10	636
20	673
30	705
40	743
50	788
70	864
90	932
130	1046
170	1138
210	1207
250	1259
290	1295
330	1318
370	1332
390	1334
410	1333
430	1325
450	1309
490	1286
510	1257
530	824
550	887
570	804

k. Wall Temperature = 1050 °C	
Distance from injection (mm)	Gas Temperature (K)
0.0	393.15
5	812
10	823
20	798
30	784
40	763
50	758
70	769
90	779
130	801
170	821
210	901
250	895
290	923
330	948
370	988
390	1004
410	999
430	990
450	974
470	936
490	944
510	834
530	947
550	781

l. Wall Temperature = 1050 °C	
Distance from injection (mm)	Gas Temperature (K)
0.0	922.15
5	902
10	889
20	879
30	892
40	929
50	895
60	916
80	899
100	933
120	969
140	918
160	925
180	914
200	896
220	939
240	882
260	965
280	899

m. Wall Temperature = 1450 °C	
Distance from injection (mm)	Gas Temperature (K)
0.0	1247.15
5	1247
10	1352
20	1352
30	1405
40	1379
50	1432
60	1490
80	1532
100	1596
120	1607
140	1602
160	1570
180	1511
200	1416
220	1331
240	1279
260	1263
280	1048

Tables A1.H
Predicted Gas and Particle Temperature Histories*

Table A1.H.1
Predicted Gas and Particle Temperature History for P2

Residence Time (ms)	Distance (mm)	Particle Temperature (K)	Gas Temperature (K)	Volatile Yield (%)
0.0	0.0	375	375	0.0
33	38	845	882	9.8
66	76	895	828	26.7
99	113	850	768	28.9
132	151	845	784	29.2
165	189	888	850	30.0
198	226	947	901	34.5
231	264	965	923	37.1
264	301	1006	969	41.0
297	339	1032	998	44.9
330	377	1073	1042	47.6
363	414	1106	1074	49.9
396	452	1066	1006	51.0
429	489	974	891	51.1
462	527	962	942	51.1
490	550	895	745	51.1

Table A1.H.2
Predicted Gas and Particle Temperature History for P4

Residence Time (ms)	Distance (mm)	Particle Temperature (K)	Gas Temperature (K)	Volatile Yield (%)
0.0	0.0	375	375	0.0
19	17	583	681	0.0
38	34	671	715	0.0
57	51	720	722	0.2
76	68	738	721	1.2
95	85	747	729	3.0
114	103	757	738	4.5
133	120	766	748	6.0
152	137	766	730	7.1
171	154	786	815	8.1
190	171	833	837	11.8
200	180	839	824	13.8
209	188	824	740	15.3
228	205	745	685	15.6
247	222	808	863	15.8
266	239	821	763	17.1
280	252	802	755	17.5

* These histories were taken from computer predictions using the CPD model. Values in these tables are only a subset of the entire predictions.

Table A1.H.3

Predicted Gas and Particle Temperature History for P5

Residence Time (ms)	Distance (mm)	Particle Temperature (K)	Gas Temperature (K)	Volatile Yield (%)
0.0	0.0	373	375	0.0
23	21	644	751	0.0
46	41	741	772	0.5
69	62	787	803	6.4
92	83	824	828	1.1
125	112	862	856	18.5
148	113	881	870	23.9
171	153	898	888	28.2
194	174	914	898	31.5
227	204	913	899	33.8
250	224	970	868	35.8
258	232	975	959	36.8
273	245	955	892	38.0
296	266	843	825	38.2
319	287	960	947	38.4
342	308	915	875	38.8
350	315	907	872	38.9

Table A1.H.4

Predicted Gas and Particle Temperature History for P6

Residence Time (ms)	Distance (mm)	Particle Temperature (K)	Gas Temperature (K)	Volatile Yield (%)
0.0	0.0	375	375	0.0
32	29	688	739	0.0
64	58	759	754	3.2
96	86	800	786	8.5
128	115	787	755	10.7
160	144	826	835	12.8
192	173	864	855	19.6
224	202	889	882	26.1
256	230	918	909	31.4
288	259	943	931	34.7
320	288	951	932	36.6
330	297	952	932	37.0
352	317	943	914	37.7
384	346	932	904	38.2
416	374	862	774	38.4
448	403	899	904	38.4
480	432	850	804	38.4

Table A1.H.5

Predicted Gas and Particle Temperature History for P7 and P8

Residence Time (ms)	Distance (mm)	Particle Temperature (K)	Gas Temperature (K)	Volatile Yield (%)
0.0	0.0	375	375	0.0
33	38	728	734	0.2
66	75	873	882	14.6
99	113	994	997	36.9
132	150	1092	1093	48.2
165	188	1169	1169	53.3
198	226	1227	1227	55.9
231	263	1270	1271	57.2
264	301	1300	1301	57.7
297	339	1320	1321	58.0
330	376	1331	1333	58.1
345	393	1333	1334	58.2
363	414	1331	1331	58.2
396	451	1309	1308	58.2
429	489	1288	1287	58.2
462	527	944	898	58.2
490	559	869	852	58.2

Table A1.H.6

Predicted Gas and Particle Temperature History for P9 through P11

Residence Time (ms)	Distance (mm)	Particle Temperature (K)	Gas Temperature (K)	Volatile Yield (%)
0.0	0.0	375	375	0.0
10	19	624	880	0.0
20	37	752	919	0.3
30	56	825	908	7.8
40	75	875	903	14.5
50	93	906	922	22.5
60	112	941	955	29.8
70	131	971	941	34.9
80	150	972	921	37.0
90	168	974	920	38.1
100	186	970	908	38.9
110	206	962	908	39.4
120	224	974	927	39.8
130	243	961	894	40.3
140	262	981	959	40.7
144	269	986	935	41.0
150	280	978	900	41.3

Table A1.H.7

Predicted Gas and Particle Temperature History for P13 and P14

Residence Time (ms)	Distance (mm)	Particle Temperature (K)	Gas Temperature (K)	Volatile Yield (%)
0.0	0.0	375	375	0.0
10	20	859	1352	7.6
20	40	1122	1379	46.6
30	60	1390	1491	58.9
40	80	1526	1533	59.9
50	101	1591	1596	60.0
60	121	1621	1607	60.0
69	139	1627	1602	60.0
70	141	1626	1601	60.0
80	161	1612	1567	60.0
90	181	1577	1505	60.0
100	201	1517	1410	60.0
110	221	1450	1327	60.0
120	242	1396	1278	60.0
130	262	1367	1245	60.0
135	272	1327	1136	60.0

Table A1.H.8

Predicted Gas and Particle Temperature History for U2

Residence Time (ms)	Distance (mm)	Particle Temperature (K)	Gas Temperature (K)	Volatile Yield (%)
0.0	0.0	375	375	0.0
33	38	843	884	7.8
66	75	888	830	23.4
99	113	844	768	25.8
132	150	834	783	26.1
165	188	872	849	26.8
198	226	930	901	30.8
229	261	950	919	33.7
262	299	991	967	36.8
295	336	1018	994	41.2
328	374	1059	1040	44.6
361	411	1094	1077	47.5
368	419	1097	1068	48.1
394	449	1068	1013	49.1
427	487	980	900	49.3
460	524	940	927	49.3
490	550	895	744	49.3

Table A1.H.9

Predicted Gas and Particle Temperature History for U3

Residence Time (ms)	Distance (mm)	Particle Temperature (K)	Gas Temperature (K)	Volatile Yield (%)
0.0	0.0	375	375	0.0
33	38	744	813	0.3
66	75	854	842	12.2
99	113	896	852	24.7
132	150	873	780	28.6
165	188	835	760	28.9
198	226	846	801	29.0
231	263	903	886	29.8
264	301	944	903	33.0
297	339	971	945	35.2
330	376	1006	978	39.3
363	414	1038	1017	43.0
396	451	1074	1052	46.1
420	479	1098	1069	48.1
429	489	1094	1056	48.6
462	527	1031	963	49.3
490	550	971	889	49.3
525	550	971	889	49.3

Table A1.H.10

Predicted Gas and Particle Temperature History for U4

Residence Time (ms)	Distance (mm)	Particle Temperature (K)	Gas Temperature (K)	Volatile Yield (%)
0.0	0.0	375	375	0.0
35	40	651	673	0.0
70	80	755	742	1.6
105	120	818	789	8.3
140	160	858	832	15.8
175	199	852	775	22.4
210	239	830	770	23.3
245	279	858	828	24.2
280	319	924	902	29.1
315	359	949	916	33.3
350	399	992	967	36.7
385	439	1021	997	41.5
420	479	1064	1043	45.0
455	519	1097	1069	48.0
490	559	1049	986	49.2
525	598	950	873	49.3
560	638	957	869	49.3

Table A1.H.11

Predicted Gas and Particle Temperature History for U5

Residence Time (ms)	Distance (mm)	Particle Temperature (K)	Gas Temperature (K)	Volatile Yield (%)
0.0	0.0	375	375	0.0
40	46	612	608	0.0
80	91	699	656	0.1
120	137	750	693	2.4
160	182	768	741	5.2
200	228	847	787	13.3
240	274	827	763	17.6
280	319	855	828	20.2
320	365	926	902	28.9
360	410	959	933	33.8
400	456	1004	978	38.8
440	502	1045	1027	43.5
480	547	1089	1075	47.2
490	559	1097	1069	48.0
520	593	1061	1003	49.2
560	638	951	874	49.3
595	678	957	870	49.3

Table A1.H.12

Predicted Gas and Particle Temperature History for U6 and U7

Residence Time (ms)	Distance (mm)	Particle Temperature (K)	Gas Temperature (K)	Volatile Yield (%)
0.0	0.0	375	375	0.0
20	37	645	769	0.0
40	75	727	771	0.2
60	112	767	791	3.7
80	150	797	811	6.4
100	187	825	855	9.3
120	224	871	899	15.7
140	262	892	903	22.9
160	299	916	929	27.9
180	337	942	955	31.6
200	374	977	991	34.4
220	411	1001	998	37.9
225	421	1002	994	38.7
240	449	996	975	40.3
260	486	965	942	41.0
280	523	910	910	41.1
294	550	891	784	41.1

Table A1.H.13

Predicted Gas and Particle Temperature History for U8

Residence Time (ms)	Distance (mm)	Particle Temperature (K)	Gas Temperature (K)	Volatile Yield (%)
0.0	0.0	375	375	0.0
33	38	728	734	0.2
66	75	873	882	12.8
99	113	994	997	34.8
132	150	1092	1093	46.1
165	188	1169	1169	52.0
198	226	1227	1227	55.1
231	263	1270	1271	56.5
264	301	1300	1301	57.2
297	339	1320	1321	57.5
330	376	1331	1333	57.6
345	393	1333	1334	57.7
363	414	1331	1331	57.7
396	451	1309	1308	57.7
429	489	1288	1287	57.8
462	527	946	898	57.8
490	559	869	852	57.8

Table A1.H.14

Predicted Gas and Particle Temperature History for U9

Residence Time (ms)	Distance (mm)	Particle Temperature (K)	Gas Temperature (K)	Volatile Yield (%)
0.0	0.0	375	375	0.0
10	19	622	880	0.0
20	37	750	919	0.3
30	56	826	908	6.1
40	75	874	903	12.6
50	93	903	922	20.2
60	112	935	955	27.1
70	131	963	941	32.1
80	150	966	921	34.3
90	168	968	920	35.4
100	187	965	908	36.1
110	206	958	908	36.6
120	224	969	927	37.1
130	243	958	894	37.6
140	262	975	959	38.0
145	271	980	929	38.3
150	280	974	900	38.6

Table A1.H.15

Predicted Gas and Particle Temperature History for U10

Residence Time (ms)	Distance (mm)	Particle Temperature (K)	Gas Temperature (K)	Volatile Yield (%)
0.0	0.0	375	375	0.0
10	20	861	1352	58.8
20	40	1116	1379	43.4
30	60	1368	1491	57.4
40	80	1514	1533	59.1
50	101	1585	1596	59.1
60	121	1618	1607	59.2
70	141	1625	1601	59.2
80	161	1612	1567	59.2
90	181	1578	1505	59.2
100	201	1519	1410	59.2
110	221	1452	1327	59.2
120	242	1399	1278	59.2
130	262	1368	1245	59.2
135	272	1330	1136	59.2

Table A1.H.16

Predicted Gas and Particle Temperature History for Z4 and Z10

Residence Time (ms)	Distance (mm)	Particle Temperature (K)	Gas Temperature (K)	Volatile Yield (%)
0.0	0.0	375	375	0.0
20	37	702	769	0.0
40	75	776	771	9.5
60	112	819	791	13.4
80	150	843	811	18.3
100	187	867	855	23.6
120	224	909	899	31.6
140	262	927	903	37.3
160	299	951	929	40.7
180	337	974	955	43.7
200	374	1005	991	46.8
220	411	1027	998	50.1
240	449	1019	975	51.8
260	486	987	942	52.3
280	523	933	910	52.4
294	550	914	784	52.4

Table A1.H.17

Predicted Gas and Particle Temperature History for Z5 and Z14

Residence Time (ms)	Distance (mm)	Particle Temperature (K)	Gas Temperature (K)	Volatile Yield (%)
0.0	0.0	375	375	0.0
33	38	862	884	15.4
66	75	889	830	29.5
99	113	837	768	30.9
132	150	828	783	31.0
165	188	869	849	31.4
198	226	928	901	34.7
231	263	947	922	37.8
264	301	988	969	42.1
297	340	1017	997	46.1
330	376	1058	1042	49.5
363	414	1094	1074	52.1
367	418	1095	1069	52.4
396	451	1058	1007	53.3
429	489	965	892	53.5
462	527	943	939	53.5
490	550	884	744	53.5

Table A1.H.18

Predicted Gas and Particle Temperature History for Z6

Residence Time (ms)	Distance (mm)	Particle Temperature (K)	Gas Temperature (K)	Volatile Yield (%)
0.0	0.0	375	375	0.0
35	40	771	817	5.5
70	80	868	853	20.4
105	120	896	850	30.7
140	160	852	775	32.7
175	199	825	770	32.8
210	139	858	828	32.9
245	179	929	902	34.9
280	319	947	916	38.0
315	359	990	967	42.2
350	399	1020	998	46.4
385	439	1063	1043	49.9
419	478	1097	1070	52.4
455	519	1044	986	53.4
490	559	942	873	53.5
525	598	954	867	53.5

Table A1.H.19

Predicted Gas and Particle Temperature History for Z7

Residence Time (ms)	Distance (mm)	Particle Temperature (K)	Gas Temperature (K)	Volatile Yield (%)
0.0	0.0	375	375	0.0
35	40	668	673	0.0
70	80	760	742	5.6
105	120	822	789	13.7
140	160	859	832	20.9
175	199	848	775	26.5
210	239	824	770	27.1
245	279	855	828	27.8
280	319	922	902	32.2
315	359	944	916	36.8
350	399	987	967	41.5
385	439	1018	997	46.0
420	479	1062	1043	49.7
455	519	1095	1069	52.3
490	559	1044	986	53.3
525	598	942	873	53.4
560	638	953	869	53.4

Table A1.H.20

Predicted Gas and Particle Temperature History for Z8

Residence Time (ms)	Distance (mm)	Particle Temperature (K)	Gas Temperature (K)	Volatile Yield (%)
0.0	0.0	375	375	0.0
40	46	625	608	0.0
80	91	705	656	0.1
120	137	750	693	5.7
160	182	770	741	94.4
200	228	849	787	18.7
240	274	823	763	22.0
280	319	852	828	24.0
320	365	922	902	31.9
360	410	852	933	37.3
400	456	997	978	43.4
440	502	1040	1027	48.0
480	547	1085	1075	51.5
490	559	1093	1069	52.2
520	593	1055	1003	53.2
560	638	942	874	53.3
595	678	951	870	53.3

Table A1.H.21

Predicted Gas and Particle Temperature History for Z9

Residence Time (ms)	Distance (mm)	Particle Temperature (K)	Gas Temperature (K)	Volatile Yield (%)
0.0	0.0	375	375	0.0
50	28	1040	1052	45.5
100	56	1070	1043	53.5
150	84	984	887	54.8
200	112	827	757	54.8
250	140	787	730	54.8
300	168	823	773	54.8
350	196	859	812	54.8
400	224	888	840	54.8
450	252	903	858	54.8
500	280	930	889	54.8
550	308	966	832	54.8
600	336	1009	978	54.9
650	364	1040	1012	55.1
700	392	1083	1060	55.6
725	406	1088	1060	56.0
750	420	1085	1055	56.3
800	448	1073	1041	56.7
850	476	1051	1013	56.9
900	504	1006	955	57.0
850	532	977	923	57.0
980	549	874	782	57.0

Table A1.H.22

Predicted Gas and Particle Temperature History for Z11

Residence Time (ms)	Distance (mm)	Particle Temperature (K)	Gas Temperature (K)	Volatile Yield (%)
0.0	0.0	375	375	0.0
33	38	730	734	0.5
66	75	874	882	12.1
99	113	992	997	32.4
132	150	1090	1093	41.6
165	188	1168	1169	47.5
198	226	1226	1227	50.7
229	261	1268	1269	52.1
262	299	1299	1300	52.8
295	336	1319	1320	53.2
328	374	1331	1332	53.3
340	388	1333	1334	53.4
361	411	1332	1332	53.4
394	449	1311	1310	53.4
427	487	1289	1288	53.5
463	528	925	873	53.5
490	559	868	852	53.5

Table A1.H.23

Predicted Gas and Particle Temperature History for Z12 and Z13

Residence Time (ms)	Distance (mm)	Particle Temperature (K)	Gas Temperature (K)	Volatile Yield (%)
0.0	0.0	375	375	0.0
10	19	649	880	0.0
20	37	773	919	4.1
30	56	847	908	12.9
40	75	887	903	20.8
50	93	910	922	27.5
60	112	937	955	32.8
70	131	961	941	37.0
80	150	959	921	39.1
90	168	960	920	40.3
100	187	956	908	41.1
110	206	949	908	41.6
120	224	960	927	42.1
130	243	949	894	42.5
140	262	966	959	42.8
145	271	972	929	43.1
150	280	965	900	43.4

Table A1.H.24

Predicted Gas and Particle Temperature History for Z15

Residence Time (ms)	Distance (mm)	Particle Temperature (K)	Gas Temperature (K)	Volatile Yield (%)
0.0	0.0	375	375	0.0
10	20	898	1352	14.3
20	40	1167	1379	53.0
30	60	1415	1491	62.1
40	80	1531	1533	62.8
50	101	1591	1596	62.8
60	121	1620	1607	62.8
70	141	1625	1601	62.8
80	161	1609	1567	62.8
90	181	1573	1505	62.8
100	201	1510	1410	62.8
110	221	1441	1327	62.8
120	242	1387	1278	62.8
130	262	1358	1245	62.8
135	272	1316	1136	62.8

Time temperature histories for the FFB experiments are not presented in this thesis. The FFB contains reactive gases that significantly affects the particle time temperature histories and that are not accounted for in the CPD model. However, Table A1.H.25 contains an example of a typical time temperature history for a Pittsburgh No. 8 FFB experiment.

Table A1.H.25

Predicted Gas and Particle Temperature History for FFB

Residence Time (ms)	Distance (mm)	Particle Temperature (K)	Gas Temperature (K)	Volatile Yield (%)
0.0	0.0	300	300	0.0
6	9	343	574	0.0
12	23	526	1286	0.0
18	38	873	1701	12.0
24	53	1058	1666	45.1
30	68	1282	1639	62.0
36	83	1442	1612	66.3
42	98	1489	1573	66.6
48	113	1485	1548	66.7
50	118	1482	1543	66.7

Table A1.4

Char Properties

Char Type Label[a]	True Density[b] (g/cc)	Apparent Density[c] (g/cc)	Porosity[d] (%)	N_2 Surface Area[e] (m^2/g)	CO_2 Surface Area[f] (m^2/g)	Swelling Ratio (d_p/d_{po})	Total Mass Release[g] (%)
P	1.31	1.30	0.5	0	214	1	0
P2	1.56	0.35	77.5	1	284	1.23	52.6
P3	1.46	0.45	69.2	0	156	1.21	41.0
P4	1.36	0.86	36.5	0	128	1.07	18.7
P5	1.48	0.33	78.0	0	188	1.34	41.2
P6	1.57	0.22	85.9	1	241	1.51	42.6
P7	1.73	0.58	66.4	2	304	1.03	54.1
P8	1.81	0.56	68.9	1	324	1.05	52.3
P9	1.53	0.43	72.2	2	163	1.21	44.7
P10	1.52	0.29	80.9	23	187	1.41	38.4
P11	1.54	0.39	74.9	2	185	1.26	42.2
P12	1.58						51.2
P13	1.91	0.55	71.2	23	298	1.02	58.1
P14	2.06	0.32	84.5	18	197	1.06	74.2
P15	1.38	1.01	27.0	4	185	0.96	31.0
P16	1.69	0.83	48.1	35	278	0.88	56.2
P17	1.84	0.89	51.6	29	200	0.83	63.4
P18	1.60	0.77	51.6	29	225	0.97	46.5
P19	1.59	0.59	62.6	49	282	1.07	44.3
U	1.36	1.36	0.1	1	135	1	0
U2	1.58	0.69	56.3	12	282	1.00	55.3
U3	1.73	0.67	61.1	18	313	1.03	49.6
U4	1.70	0.69	59.4	1	304	1.01	52.7
U5	1.67	0.71	57.5	7	296	1.00	52.3
U6	1.51	0.74	51.1	0	142	1.06	38.7
U7	1.58	0.50	68.5	3	173	1.17	47.0
U8	1.79	0.76	57.3	1	296	0.96	55.6
U9	1.51	0.65	56.7	1	159	1.11	40.3
U10	2.00	0.58	70.9	11	225	0.98	63.6
U11	1.80	0.66	63.5	49	328	0.96	60.7
U12	2.00	0.64	67.9	47	367	0.95	64.8
U13	1.86	0.61	67.2	63	350	0.93	72.9
Z	1.43	1.27	11.4	1	203	1	0
ZD3	1.51	1.01	33.2	7	249	0.96	31.2
Z4	1.71	0.89	47.7	158	417	0.91	53.9
Z5	1.77	0.89	49.7	141	357	0.88	54.8
Z6	1.75	0.91	48.1	146	410	0.93	44.3
Z7	1.71	0.95	44.7	116	409	0.90	48.8
Z8	1.70	0.98	42.2	137	398	0.85	55.3
Z9	1.78	0.82	54.0	119	420	0.92	53.2
Z10	1.60	0.94	41.4	76	329	0.91	47.4
Z11	1.88	0.87	53.9	84	445	0.91	51.2
Z12	1.56	0.82	47.6	21	245	0.97	42.9
Z13	1.56	0.86	45.1	28	278	0.97	41.1
Z14	1.68	0.88	47.6	237	424	0.91	50.6
Z15	2.11	0.72	66.0	77	460	0.91	60.1
Z16	1.88	0.61	67.5	190	512	0.90	65.2

a. See Tables A1.1-A1.3 for preparation conditions of each sample

b. Skeletal or solid density
c. Particle density
d. Porosity = volume of void within particle/total particle volume
e. Calculated using the BET equation from adsorption isotherms of nitrogen gas at 77 K.
f. Calculated using the DP equation from adsorption isotherms of carbon dioxide gas at 298 K
g. Percentage of mass in coal not present in char

Table A1.5

Char Analysis (Dry)

Char Type Label	% Carbon	% Hydrogen	% Nitrogen	%Oxygen and Sulfur	% ASH
P2	82.3	2.6	2.0	3.9	9.3
P4	80.3	4.9	1.6	7.9	5.4
P5	79.6	3.4	1.8	7.5	7.7
P7	82.8	1.2	1.5	6.0	8.5
P8	82.2	1.3	1.6	5.4	9.5
P9	78.2	3.7	1.9	8.0	8.2
P10	77.5	3.6	2.0	9.6	7.3
P11	79.3	3.8	2.1	7.1	7.8
P13	80.5	1.4	1.5	5.2	11.4
P14	80.2	0.3	1.5	1.5	16.5
P15	79.2	4.3	1.3	8.9	6.4
P17	84.7	0.7	1.6	3.1	10.0
P18	83.7	1.5	1.7	4.3	8.9
P19	84.7	1.4	1.6	4.4	7.9
U2	74.7	1.0	1.5	2.4	20.4
U3	79.0	1.0	1.6	3.3	15.0
U4	75.3	1.3	1.7	4.0	17.8
U5	74.3	1.5	1.7	3.8	18.8
U6	71.0	2.9	1.3	9.8	15.0
U7	73.6	2.4	1.7	2.2	20.1
U8	74.2	0.2	1.5	4.9	19.2
U9	75.0	2.9	1.5	8.9	11.8
U10	82.3	0	1.6	0	16.3
U11	72.3	0.7	1.5	7.0	18.5
U12	66.3	0.7	1.3	14.2	17.5
ZD3	68.0	3.2	1.0	19.2	8.6
Z4	75.0	1.8	1.1	11.8	10.3
Z5	75.8	1.5	1.2	10.9	10.7
Z6	75.7	1.7	1.4	10.9	10.2
Z7	75.4	1.8	1.3	11.7	9.8
Z8	74.7	1.6	1.3	9.9	12.5
Z9	77.4	0.8	1.3	9.7	10.7
Z10	71.0	2.5	1.3	12.7	12.5
Z11	79.0	0.9	1.1	8.5	10.5
Z12	67.9	2.8	1.3	18.7	9.3
Z13	67.8	3.2	1.0	18.9	9.1
Z14	76.1	1.6	1.2	10.6	10.6
Z15	83.6	0.2	1.4	3.5	11.3
Z16	78.6	0.6	1.4	6.1	13.4

Table A1.6

Char Element Release and Ratio Data

Char Type Label	% C Release	% H Release	% N Release	% O+S Release	H/C Mole Ratio	O/C Mole Ratio
P2	48.5	76.0	42.3	77.7	0.38	0.035
P4	17.4	26.7	21.5	25.3	0.73	0.074
P5	39.2	61.5	37.5	47.3	0.52	0.071
P7	50.2	89.6	58.1	66.7	0.17	0.054
P8	48.1	88.2	52.7	68.4	0.19	0.050
P9	43.5	60.7	36.8	46.8	0.57	0.077
P10	38.3	57.5	25.9	29.8	0.56	0.092
P11	40.5	57.9	27.9	51.0	0.58	0.067
P13	54.4	88.5	61.0	72.7	0.21	0.049
P14	70.3	98.3	74.0	94.8	0.048	0.014
P15	30.1	44.7	44.6	27.9	0.65	0.084
P17	58.8	95.3	64.4	86.0	0.094	0.028
P18	41.1	84.6	45.3	72.2	0.21	0.038
P19	38.7	84.8	46.4	70.5	0.20	0.039
U2	47.4	90.7	49.2	89.4	0.15	0.024
U3	41.2	89.7	44.0	84.6	0.15	0.032
U4	45.6	87.4	43.9	82.2	0.20	0.040
U5	45.2	84.7	41.7	82.9	0.24	0.038
U6	35.7	63.9	43.3	45.2	0.49	0.10
U7	38.7	72.8	34.2	88.5	0.39	0.023
U8	48.8	97.9	51.6	79.2	0.036	0.049
U9	36.2	66.4	42.4	53.4	0.46	0.088
U10	55.1	100	59.4	100	0.00	0.000
U11	56.2	94.4	57.8	73.7	0.11	0.073
U12	64.5	95.2	67.4	52.7	0.12	0.16
ZD3	23.8	44.1	24.0	47.5	0.56	0.21
Z4	42.6	78.6	42.4	78.0	0.29	0.12
Z5	42.9	82.3	41.3	80.0	0.24	0.11
Z6	30.1	75.5	11.9	75.4	0.27	0.11
Z7	36.3	76.8	23.9	75.8	0.28	0.12
Z8	43.2	80.6	33.6	81.7	0.26	0.099
Z9	39.6	89.9	30.3	81.5	0.13	0.094
Z10	36.4	65.6	22.5	72.2	0.42	0.14
Z11	35.9	88.3	38.9	83.2	0.14	0.081
Z12	36.3	58.7	21.3	57.3	0.50	0.21
Z13	34.6	52.1	35.9	55.5	0.56	0.21
Z14	37.4	79.6	34.8	78.8	0.25	0.10
Z15	44.0	97.5	37.0	94.3	0.034	0.031
Z16	53.0	94.8	45.0	91.1	0.086	0.058

Table A1.7

Kinetic Parameters of Oxidation of Pittsburgh No. 8 Chars Measured in TGA with 10% Oxygen.

Char Type Label	Burnout %	E_a (kcal/mole)	A (g/g.s.atm^n)*	Rate (g/g.s)**
P9	10	29	7.7e5	1.9e-3
	25	32	6.3e6	2.1e-3
	50	33	1.4e7	2.2e-3
	75	33	1.3e7	2.3e-3
	90	32	1.0e7	2.8e-3
P10	10	30	2.0e6	2.1e-3
	25	32	1.4e7	2.3e-3
	50	33	1.6e7	2.4e-3
	75	33	2.1e7	2.6e-3
	90	33	1.7e7	3.1e-3
P11	10	30	1.6e6	2.1e-3
	25	32	1.1e7	2.3e-3
	50	33	2.2e7	2.4e-3
	75	33	2.4e7	2.5e-3
	90	33	1.8e7	2.7e-3
P2	10	30	1.2e6	9.9e-4
	25	32	3.3e6	1.1e-3
	50	32	3.5e6	1.3e-3
	75	30	1.9e6	2.0e-3
	90	28	4.3e5	1.6e-3
P7	10	32	1.1e6	4.0e-4
	25	31	9.5e5	4.9e-4
	50	32	2.3e6	6.0e-4
	75	33	4.9e6	7.7e-4
	90	35	2.9e7	8.8e-4
P17	10	31	4.7e5	2.4e-4
	25	33	1.7e6	2.1e-4
	50	35	5.4e6	1.9e-4
	75	38	3.3e7	2.0e-4
P14	10	35	7.9e6	2.8e-4
	25	35	6.3e6	2.9e-4
	50	34	4.9e6	3.1e-4
	75	35	8.5e6	3.3e-4
	90	32	2.0e6	4.4e-4
P13	10	33	3.5e6	4.9e-4
	25	33	3.0e6	6.1e-4
	50	33	6.3e6	7.3e-4
	75	34	7.8e6	8.7e-4
	90	35	1.7e7	? e-4

* Reaction Order: n = 0.5 ** Normalized Rate at 500 °C.

Table A1.8

Kinetic Parameters of Oxidation of Utah Blind Canyon Chars Measured in TGA with 10% Oxygen.

Char Type Label	Burnout %	E_a (kcal/mole)	A (g/g.s.atm^n)*	Rate (g/g.s)**
U11	10	34	2.4e7	1.6e-3
	25	35	2.0e7	8.6e-4
	50	35	1.3e7	6.5e-4
	70	35	1.3e7	7.5e-4
U12	10	35	1.8e7	6.3e-4
	25	36	1.7e7	4.8e-4
	50	36	2.5e7	5.5e-4
	70	33	3.6e6	6.0e-4
U6	10	31	1.1e7	5.5e-3
	25	32	2.6e7	7.2e-3
	50	31	1.5e7	8.1e-3
	75	31	1.7e7	7.2e-3
	90	33	3.1e7	5.7e-3
U2	10	32	1.2e7	4.1e-3
	25	33	2.9e7	4.3e-3
	50	32	1.7e7	3.9e-3
	75	32	8.9e6	2.9e-3
	90	33	1.5e7	2.5e-3
U8	10	35	3.8e7	1.7e-3
	25	34	2.0e7	2.0e-3
	50	32	1.1e7	2.4e-3
	75	32	7.5e6	2.2e-3
	90	33	1.2e7	1.8e-3
U10	10	33	3.7e6	3.9e-4
	25	33	4.3e6	4.8e-4
	50	34	4.7e6	4.7e-4
	75	33	3.0e6	4.0e-4
	90	34	5.8e6	? e-4

* Reaction Order: n = 0.5 ** Normalized Rate at 500 ^oC.

Table A1.9

Kinetic Parameters of Oxidation of North Dakota (Beulah Zap) Chars Measured in TGA with 10% Oxygen.

Char Type Label	Burnout %	E_a (kcal/mole)	A (g/g.s.atm^n)*	Rate (g/g.s)**
Z4	10	33	6.9e8	2.7e-3
	25	32	2.9e8	2.4e-3
	50	32	2.0e8	2.5e-3
	75	32	1.2e8	1.0e-3
Z11	10	30	2.8e7	1.1e-3
	25	30	2.3e7	1.1e-3
	50	32	1.7e8	1.7e-3
	75	31	5.9e7	1.2e-3
ZD3	10	30	1.9e8	6.7e-3
	25	34	5.5e9	9.4e-3
	50	31	1.4e8	3.5e-3
	75	33	3.5e8	1.6e-3
Z5	10	31	1.4e8	2.3e-3
	25	31	1.1e8	2.0e-3
	50	31	9.6e7	2.0e-3
	75	33	1.8e8	7.1e-4
Z15	10	31	1.9e7	3.5e-4
	25	31	1.3e7	3.8e-4
	50	31	1.2e7	2.8e-4
	75	32	1.8e7	1.2e-4
Z13	10	32	8.6e8	7.2e-3
	25	38	8.4e10	1.0e-2
	50	34	4.3e9	8.4e-3
	75	34	6.3e8	1.1e-3
	90	42	6.5e10	3.2e-4
Z14	10	30	5.6e7	3.2e-3
	25	31	1.8e8	2.5e-3
	50	32	2.2e8	2.3e-3
	75	35	1.2e9	1.0e-3
	90	41	2.1e10	2.2e-4
Z16	10	30	7.0e6	2.4e-4
	25	30	5.2e6	1.9e-4
	50	31	8.5e6	1.7e-4
	75	31	5.8e6	1.6e-4
	90	34	1.3e8	? e-4

* Reaction Order: n = 0.6 ** Normalized Rate at 400 °C.

Appendix A2

Error Analysis

The following tables, A2.1 and A2.2 contain the uncertainties, standard deviations and repeatabilities calculated for all data in this thesis.

Table A2.1
Uncertainties and Standard Deviations

Measurement	Percent Uncertainty (%)	Standard Deviation	Percent Standard Deviation (%)
Bulk Density	0.38	0.008 g/cc	2.9
Packing Factor	5.6[a]	---	---
Apparent Density	4.6	0.015 g/cc	2.9
True Density	0.039	0.025 g/cc	1.4
Mass Release	1.2	2.55 %	4.0
Porosity	4.2	1.06 %	1.5
Swelling Ratio	2.5	0.008 %	0.8
N_2 Surface Area	1.0	0.7 m^2/g	0.7
CO_2 Surface Area	1.0	4.0 m^2/g	1.0
Carbon	0.013	0.48 %	0.6
Hydrogen	0.33	0.33 %	10.8
Nitrogen	0.5	0.19 %	9.5
Oxygen	2.8	0.5 %	3.0
Ash	0.28	0.04 %	0.66
Moisture	0.06	0.47 %	2.0
Reactivity	1.5	---	---
Activation Energy	1.5	---	---
Pre-exponential Factor	1.5	---	---

a. This percent uncertainty is calculated from a packing factor of 0.45 and uncertainty of 0.025, which is based on differences in packing factors commonly used, not porosymetry measurements. Therefore, the percent standard deviation of the apparent density is much lower than its percent uncertainty.

Uncertainties of direct measurements represent the smallest measurement that can be made by the method used and the accuracy to which it can be measured. For example, the uncertainty of a mass measurement is 0.0001g if a balance used to measure it is accurate to within + or - 0.0001 g, and the uncertainty of a flask is 0.05 cc if its finest measurement marks are 0.1 cc. Uncertainties of complicated instruments that make many internal measurements and provide virtually black box results must be determined by the repeatability of the numbers given. Therefore, the uncertainty of the measurement is based more on precision than on accuracy. Uncertainty does not account for machine drift, operator error, equipment calibration errors, or any other such uncertainties not

directly associated with the measurement itself. Uncertainties of char properties obtained from a calculation involving a number of different measurements are obtained via the Pythagorean summation of the discrete uncertainties according to the following equation:

$$\frac{u_f}{f} = \sqrt{\left(\frac{u_{x_1}}{f}\frac{df}{dx_1}\right)^2 + \left(\frac{u_{x_2}}{f}\frac{df}{dx_2}\right)^2 + \cdots + \left(\frac{u_{x_n}}{f}\frac{df}{dx_n}\right)^2}$$

The above equation was used to calculate percent uncertainties, where the function f represents the mean value. Standard deviations are also listed in table A2.1 with the corresponding units of the char property. Percent standard deviations were calculated by dividing the standard deviations by the mean value of the function or measurement. Standard deviations account for a combination of measurement uncertainty, machine drift, operator error, equipment calibration errors and equipment measurement precision. However, it does not account for errors in theory upon which char property measurements are based.

Table A2.2 below contains the repeatabilities for three samples. Repeatability is defined as the similarity of measured char properties between two chars prepared at identical preparation conditions but at different times and in different experimental sets. Repeatabilities account for all of the errors or uncertainties listed above and, in addition, account for actual differences in char properties due to uncontrolled fluctuations in the pyrolysis conditions. These are the only samples repeated due to the high cost and time consuming nature of the high temperature experimental work performed in this research.

All of the repeatabilities are at or above 90% for the Pittsburgh No. 8 char prepared in the HPCP, and most are above 95%. In contrast, the measured parameters for Pittsburgh No. 8 char prepared in the FFB are far less repeatable, especially the internal surface areas. This is probably influenced by surging in the coal feeder and fluctuations in the reactive gas atmosphere of the FFB. The reactivities are not very repeatable and at lower burnouts they are even less repeatable. However, since differences in reactivity are

only considered significant in magnitudes, the repeatability is sufficient to make comparisons.

Table A2.2

Repeatability of Preparation Conditions

Measurement	[a]Repeatabilities (%) for three conditions		
	P7 and P8	U11 and U12	P16 and P17
Bulk Density	96.9	97.8	92.9
Apparent Density	96.6	97.0	93.3
True Density	95.6	90.0	91.8
Mass Release	96.7	93.7	88.6
Porosity	96.4	93.5	93.2
Swelling Ratio	98.1	99.0	94.3
N_2 Surface Area	99.0	95.9	82.9
CO_2 Surface Area	93.8	89.4	71.9
Carbon	99.3	---	---
Hydrogen	92.9	---	---
Nitrogen	93.1	---	---
Oxygen	90.3	---	---
Ash	89.8	---	---
Reactivity[b]	---	82.5	---
Activation Energy	---	96.8	---

a. Calculated from the equation: Repeatability = 100% - %Difference
b. Average from %Differences taken at 50% and 70% TGA burnout.

Appendix B1

Steam Generator Design

Overall Design

The schematic in Figure B1.1 on the following page illustrates the design of the steam generator system. The system is designed to operate at pressures up to 30 atm and water flow rates between 160 ml/hr and 7 liters/hr. A few modifications to the system are required in order to obtain this full range of operating conditions. Currently, the system is fully capable of operating at or near the lower flow rate.

Pressurized water unit

The pressure vessel used to hold the water is an air tank was donated by Whitmore Oxygen. The used tank's structural integrity was tested by Whitmore and found to be the same as that of a new tank. The tank was prepared by cleaning out and coating its inside with a two-party epoxy paint developed for the purpose of coating the inside of water tanks. A special two-way flow bushing was made to allow the tank to be pressurized and water to be extracted from the same port. The nitrogen flow gas used in the HPCP is also used to pressurize the tank. The water is extracted from the bottom of the tank by means of a stainless steel tube that is welded to the bushing at the top of the tank and extends down to the bottom of the tank. A one way liquid check valve follows the bushing.

Filter

Distilled water is used in the system to eliminate salt that is normally in tap water and which would contaminate the reactor. A 0.5 micron filter follows the check valve and eliminates contaminants that might be in the distilled water or in the water tank. The filter is a SS-2TF-LE Nupro in-line filter. The filter element insert is a 2TF-0.5 filter. The torque specification for the filter is 500 in-lbs or 42 ft-lbs. At room temperature the filter is capable of handling flows up to 20 l/hr with only a 10 psi pressure drop.

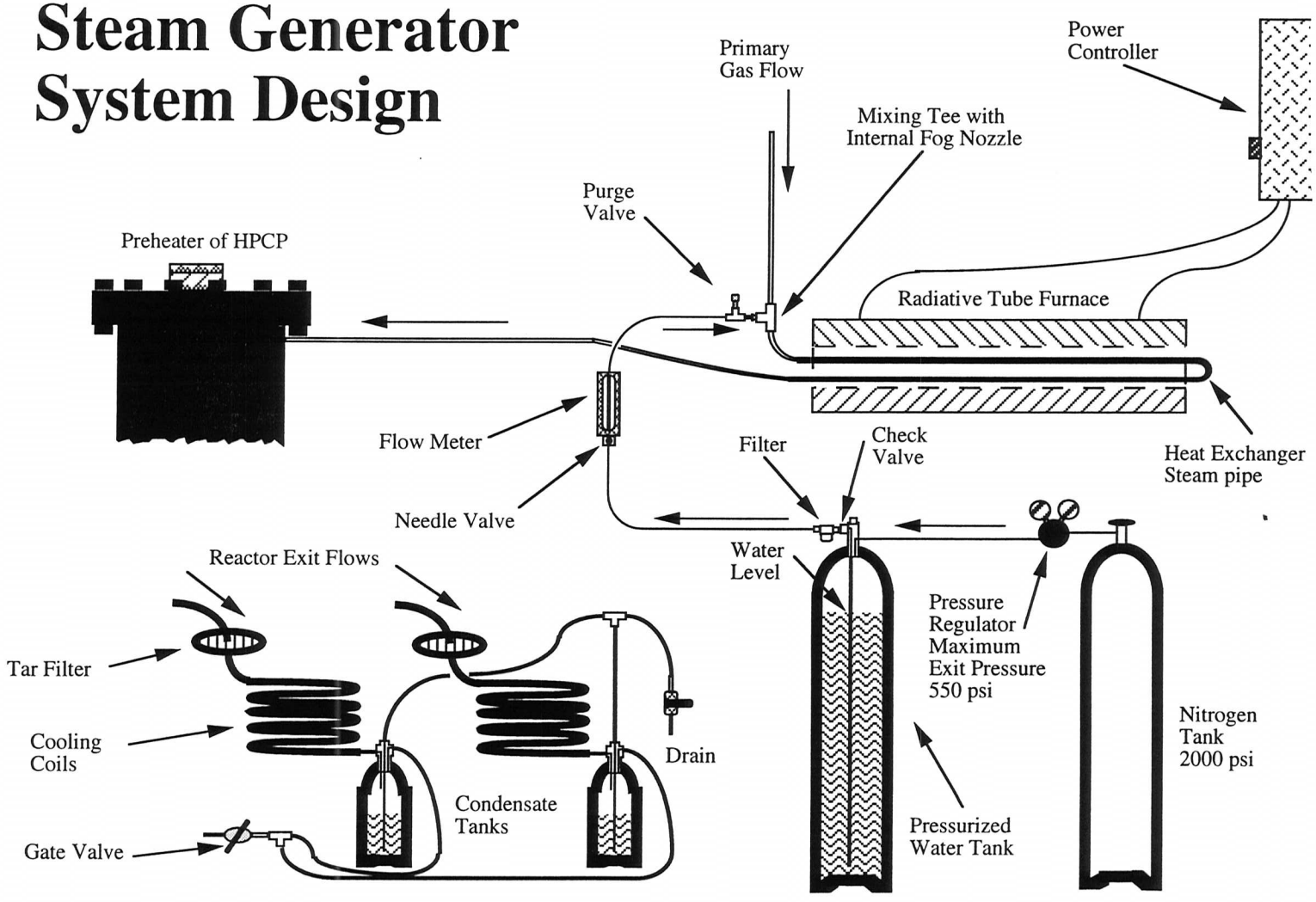

Figure B1.1. Schematic of the steam generator system design.

Flow Meter

Steam flow rates in the HPCP are calculated from the flow of liquid water fed into the steam generator. The flow meter used for measuring the flow of liquid water into the steam generator is a Model 1110 R-Z-15-D with a sapphire float from Brookes instrumentation. Its maximum flow capability is 460 ml/hr with a 10 to 1 turn down ratio. Its accuracy is one percent of full scale, which means that at the maximum operating conditions the accuracy is to within 1%, but at the minimum operating conditions the accuracy is only to within 10%. Its repeatability is 0.25%. For runs performed for this study, flows were above 50% of the flow meter's maximum. When flow rates higher than the maximum are desired, a different flow meter will need to be ordered for the specific flow rates desired. A 1% increase in error is very significant because the volume ratio of steam to liquid water is large.

Power Controller

The power controller is connected directly to a 240 volt source. The power controller is capable of handling a maximum of 60 amps at 240 volts. It is an Athena power controller 91P. Special care must be taken when operating the power controller to ensure that damage is not done to the heater or power control itself by turning the controller up too high without checking the amperage as well as the temperatures of the different components of the heating unit. When maximum operating conditions are desired, the power should be ramped up gradually to avoid destroying the heater. If a temperature controller is added to the system, it would be best to add a soft-start module to the controller.

Mixing Tee & Flow Through the Heater

The mixing tee is a forged stainless steel tee capable of handling up to 5000 psi. Prior to the mixing tee is a Nupro purge valve used to purge gas from the system at start up. Just past the purge valve is a bushing that is connected directly into the tee. A fog nozzle plugs the end of the bushing connected to the tee and forces all of the water that

enters the tee to be atomized through the nozzle tip. The nozzle used is the lowest flow direct pressure nozzle that BET Fog Nozzle makes. The actual flow for which the nozzle was designed is 3 l/hr of water. However, this same nozzle may be used for the complete range of flows mentioned earlier. Through the top of the tee, the main gas flow of the system enters at a much higher flow rate than does the water mist. The water is entrained in the gas flow and immediately enters the heat exchanger pipe being heated by the radiative tube furnace. This flow of gas and water makes two passes through the tube furnace during which time the water is vaporized. Immediately after exiting the tube furnace, the flow enters the pre-heater of the HPCP. This prevents condensation of the water from the gas that might occur if the flow were allowed to contact cold surfaces after exiting the tube furnace prior to entering the HPCP. When larger flows of water are desired, it may be necessary to add length to the heat exchanger pipe and increase the number of times the flow travels through the tube furnace in order to increase heat transfer surface area and residence time.

Appendix B2

Steam Generator: Calculations

Heat Transfer and Flow Considerations

Initial calculations for the design of the steam generator were performed to determine minimum and maximum water consumption and total power required for heat at maximum pressure and water flow rates. The amount of steam flow in the reactor was determined by two different calculations. First, the number of moles of gas at a given temperature and pressure was determined and converted through the ideal gas law to the volume of water required at room temperature and pressure. The flows were also checked by restricting the Reynolds number of the total main reactor gas and steam flow to be less than 2300 so that the flow inside the HPCP would remain laminar; then gas velocities were determined and hence flow rates of water and total reactor flow at room temperature. Both methods of determining flows yielded the same results. At maximum flow conditions: 7 l/hr of water is required. At the minimum flow conditions: 160 ml/hr of water is required. The maximum power requirement was determined by using the specific heats and the heat of vaporization to calculate the energy needed to heat the water up to the vaporization point, vaporize it, and heat the steam beyond that point up to a temperature at which no condensation would occur for the given pressure and flow rate. It was determined that at maximum flow, pressure and 100% steam output, 5.6 KW of power would be required. To compensate for energy losses, the system was designed with a 10 KW power source.

The next phase of the design was to determine the type of heater, the length and diameter of the pipe used for the heat exchanger, and the temperature at which the heater and heat exchanger pipe must be maintained in order to obtain the desired heat transfer. After studying the design, performing calculations, and obtaining information on various types of heaters, a radiative tube furnace was chosen because it allows for variable heat exchanger surface area and flow times. A system of equations was programmed into a

spreadsheet so that incremental steps could be calculated along the flow, and parameters could be changed easily. The first box of the first column of the spreadsheet contained the enthalpy of saturated liquid at the temperature and pressure being considered. This enthalpy was incremented until it reached the value of the enthalpy for saturated vapor at the same temperature and pressure. The specific volume was then calculated by interpolation for each enthalpy between the saturation points, and the flow rate was calculated from the specific volume and the constant mass flow rate of water. An initial amount of energy was calculated to account for the energy necessary to heat the water up to the saturation point. However, this was not critical since the energy is small compared to the amount of energy necessary to vaporize the water.

For heat transfer, vaporization and flow calculations in the steam generator involving a mixture of nitrogen gas and water, an ideal gas law term was added to the flow rate equation to account for the nitrogen. The temperature of the mixture was assumed to be uniform because of turbulent flow inside the flow piping of the steam generator. Therefore, the nitrogen gas temperature was assumed to be constantly at the saturation temperature of the steam. The velocity of the flow in the pipe was calculated from the inside diameter of the pipe and the flow rate. The distance was then determined by dividing the incremental energy increase used in the enthalpy column by the linear energy density along the heat exchanger pipe. The energy density was also multiplied by a correction factor of 0.8 to account for energy loss. This incremental change was then added to the distance already traveled by the flow to obtain the total distance traveled. The quality was calculated directly from the enthalpy. The time was obtained from the sum of the incremental distances multiplied by the respective velocities. The total energy provided by the heater was obtained directly from the distance and the energy density.

The viscosity, thermal conductivity, and Prandtl number were calculated with equations created by curve fitting data found in Fundamentals of Heat and Mass Transfer

by Incropera & DeWitt. The tube was assumed to be smooth. The equation used for the friction factor is as follows:

$$f = \left(0.79\,\mathrm{LN}\left(\mathrm{Re}_D\right) - 1.64\right)^{-2}$$

$2300 \le \mathrm{Re_D} \le 5\mathrm{x}10^6 \qquad 0.5 < \mathrm{Pr} < 2000$

f = Friction factor; $\mathrm{Re_D}$ = Reynolds number; Pr = Prandtl number

Incropera & DeWitt: Page 497

The Nusselt number was calculated for turbulent flow from the following equation:

$$\mathrm{Nu}_D = \frac{\left(f/8\right)\left[\mathrm{Re_D} - 1000\right]\mathrm{Pr}}{1 + 12.7\left(f/8\right)^{1/2}\left(\mathrm{Pr}^{2/3} - 1\right)}$$

$2300 \le \mathrm{Re_D} \le 5\mathrm{x}10^6 \qquad 0.5 < \mathrm{Pr} < 2000$

$\mathrm{Nu_D}$ = Nusselt number

Incropera & DeWitt: Page 497

According to Incropera & DeWitt, this equation for the Nusselt number with the corresponding friction factor will provide Nusselt numbers accurate to within 10%. A Nusselt number of 4.36 was assumed for laminar flow. The convection heat transfer coefficient was calculated from the definition of the Nusselt number. Finally, the temperature of the pipe was calculated from:

$$T_s = \frac{800\,\mathrm{ED}}{\pi \mathrm{Dh}} + T_\infty$$

800 = Conversion & correction factor; T_S = Surface temperature of the heat transfer pipe; = Inside Diameter of the pipe; ED = Energy Density; h = Convection heat transfer coefficient; T_∞ = Temperature of the flow through the pipe.

The corresponding temperature of the radiative tube furnace was calculated from:

$$T_r = \left[\frac{800\,ED}{\sigma \pi D_o} \left(\frac{1}{\varepsilon_s} + \frac{1-\varepsilon_r}{\varepsilon_r} \left(\frac{D_o}{D_r} \right) \right) + T_s^4 \right]^{1/4}$$

T_r = Temperature of tube furnace; 800 = Energy loss correction & conversion factor; D_o = Outside pipe diameter; D_r = Inside diameter of radiative tube furnace; ε_s = Emissivity of heat exchanger pipe; ε_r = Emissivity of radiative tube furnace; σ = Boltzman's constant

Using the above equations, a number of different calculations were performed from which it was determined to use the following dimensions in the steam generator design:

Heat Exchanger Pipe; ID = 1/4" OD = 3/8" L = 2 x 4'

Tube Furnace; ID = 3.5" OD = 9" L = 4' Max Temp = 900 °C

Stainless steel (304 SS) was chosen for the material of the heat exchanger pipe because of potential corrosion problems, even though this material has a lower emissivity than other metals. By highly oxidizing the surface of the pipe, the emissivity can be increased to almost 0.9. The length of the pipe and the conditions of operation were designed such that the water would be completely vaporized about two-thirds of the way through the heat exchanger pipe. It was determined from the calculations of the Reynolds numbers that the flow would be turbulent under most operating conditions.

Theoretical Operating Temperatures and Flow Rates

Table B2.1 contains the theoretical conditions of operation of the steam generator for various flow conditions and percentages of steam in the entrained flow. For the maximum flow conditions, the operating conditions of the equipment will be at their maximum. This will mean that modifications will have to be made to the system in order to operate at these maximum flow conditions. First of all, without a temperature controller it will be very difficult to keep the temperature of the tube furnace exactly at 900 °C without going higher. Even if a temperature controller was added to the system, it would be difficult to keep the temperature exactly at 900 °C because of the

abrupt heat transfer variations that the system will experience at start up. It is unacceptable to allow flow into the reactor before the water has been converted to steam. Allowing liquid water to enter the HPCP could cause considerable damage. Two modifications to

Table B2.1
Steam Generator Operating Parameters

Water Flow Rate (Kg/s)	Pressure, and % Steam	Power Supplied (KW)	Temperature of Pipe (K)	Temperature of Wall (K)
4.4e5	1 atm, 18%	0.25	450	600
1e4	1 atm, 18%	0.44	450	650
2e4	1 atm, 18%	0.79	450	730
2.5e4	1 atm, 100%	1.0	500	800
5e4	1 atm, 100%	1.9	550	950
1e3	1 atm, 100%	3.7	650	1050
2e4	30 atm, 100%	0.7	600	750
5e4	30 atm, 100%	1.5	650	900
1.9e3	30 atm, 100%	5.5	600	1160

the system are suggested to aid in solving this tight tolerance problem. First of all, a number of additional heat exchanger pipes may be added to the tube furnace to increase the heat transfer surface area and the duration of flow through the heater. The radiative tube furnace was chosen so that such modifications could be made. Second, a bypass valve will need to be installed between the heater of the steam generator and the pre-heater of the HPCP reactor to allow the operating conditions of the steam generator to reach steady-state before redirecting the flow into the HPCP. A high temperature, high pressure gate valve capable of handling steam will be needed for such an application. It will probably also be necessary to redirect some of the entrained gas flow from the steam generator directly into the HPCP at all times, or have an alternative flow into the HPCP so that when the steady-state flow from the steam generator is redirected into the HPCP, pressure and flow impulses will not occur.

Appendix B3

Steam Generator: Operating Procedure

General Operating Instructions

1) **WARNING:** The wires and connections behind the radiative tube furnace are live when the main power is on. They should not be touched, and care should be taken to keep hands or metal objects a safe distance away from them during operation of the steam generator. The voltage is 240 V.

2) Inspite of the above warning, do not attempt to make the heater safer by cutting the exposed heater elements protruding from the back of the heater. The element connections were designed to be that long and the wires connecting the power controller must be connected as they are, out on the end of the element extensions. The heater element is only one strand thick inside the insulation. The elements that protrude to provide a connection are woven into two strand thickness. Therefore, the resistance is half and less heat is generated. The length of the braided element allows it to cool before an electrical connection is made.

3) Standard thermocouple wires may be used to determine the furnace wall and steam flow heat exchanger pipe temperatures during operation. The thermocouple wires must be permanently connected to the furnace wall and stainless steam pipe at a position 1/4 to 1/3 the distance through the heater. Effort should be made to visually check that the thermocouple bead is near but not in the hot section of the heater. Thermocouples cannot be firmly attached in the heater. Therefore, they should be anchored outside the heater and loosely fastened inside the heater with ceramic tape and heating wrap. Care must be taken to avoid covering too much of the heater or especially the pipe, as this will hinder heat transfer. In the past, a two temperature hand held pyrometer (from the ME equipment room) has been used display wall and pipe temperatures during operation.

4) The heater changes resistance from run to run. Therefore, table B2.1 can only be used as a rough approximation of power output. The heater should be operated at about 100 to 200 K above the temperatures given in table B2.1 regardless of the power output.

5) Prior to operating, the water tank should be filled with distilled water from the lab in room 309. It is easily done with surgical tubing.

6) Prior to performing a steam run, the water cooling lines in the HPCP should be rerouted so that no cooling water passes through the tar filters. If not, the tar and filters will be water saturated, and water will collect in the tar lines.

7) Both the steam entrainment system and the water recovery system is designed to be taken off line during HPCP normal operation. Tubing connections are available to connect the steam generator systems.

8) The maximum allowable operating temperature of the tube furnace is 900 ^{o}C. Operation at higher temperatures may cause the furnace to melt or break.

Start Up

1) Turn on the main power switch. Then begin heating the tube furnace by placing the control on about 2. Since the heater changes resistance from run to run, the necessary controller settings will change by more than an order of magnitude. As the heater increases in temperature, the setting may be gradually increased. For all of the runs performed thus far, (18% steam, 1 atm, 30 to 50 slpm total gas flow) the control setting did not exceed four.

2) Turn on the secondary gases before the end of heat up. When the wall and tube have reached a suitable temperature, introduce the water.

3) Turn the high pressure air valves on, and pressurize the water tank. The purge valve should be completely open. Purge the water line of air through the purge valve. Set the water flow rate desired.

4) Start water flowing through the system by closing the purge valve tight.

5) As soon as water is introduced into the system, the temperature of the tube will begin to decrease. Adjust the controller accordingly to maintain the desired temperatures.

6) When the system is at steady state and at the desired conditions, start feeding the coal into the reactor. Constant attention is required to maintain specific operating conditions during a run.

Shut Down

1) Turn off the high pressure air valves and open the purge valve. This will stop water from being fed into the system.

2) Keep the furnace hot but control the power so that it doesn't get too hot!

3) Keep the HPCP hot, and leave the secondary flow into the HPCP on to dry the HPCP system of water that has condensed.

4) After an hour or so, turn off the heater.

5) While the HPCP is still under pressure, purge the condensate tanks by opening the valves located on the top of them.

Modification Needed

One important modification should be made to the steam generator before future operation. A pressure release valve needs to be installed in the air pressure line connected to the inlet of the pressurized water tank. At the moment, the only way to depressurize the tank safely is to open the air purge valve in the water line next to the mixing tee inlet, and let the water flow from the tank, through the flow meter and out the purge valve until the pressure has been reduced in the tank sufficient to remove the tubing connections. This, however, takes hours. The tank can be emptied immediately by disconnecting the gas tubing from the tank inlet. However, this could cause considerable damage to the tubing and connections. Furthermore, it is dangerous.

Appendix C

Flow Panel

Figure C.1 contains a labeled diagram of the gas flow control panel for the HPCP. Table C.1 contains a description of the labeled items in figure C.1. Finally, an explanation of how to obtain some specific flow set ups is provided.

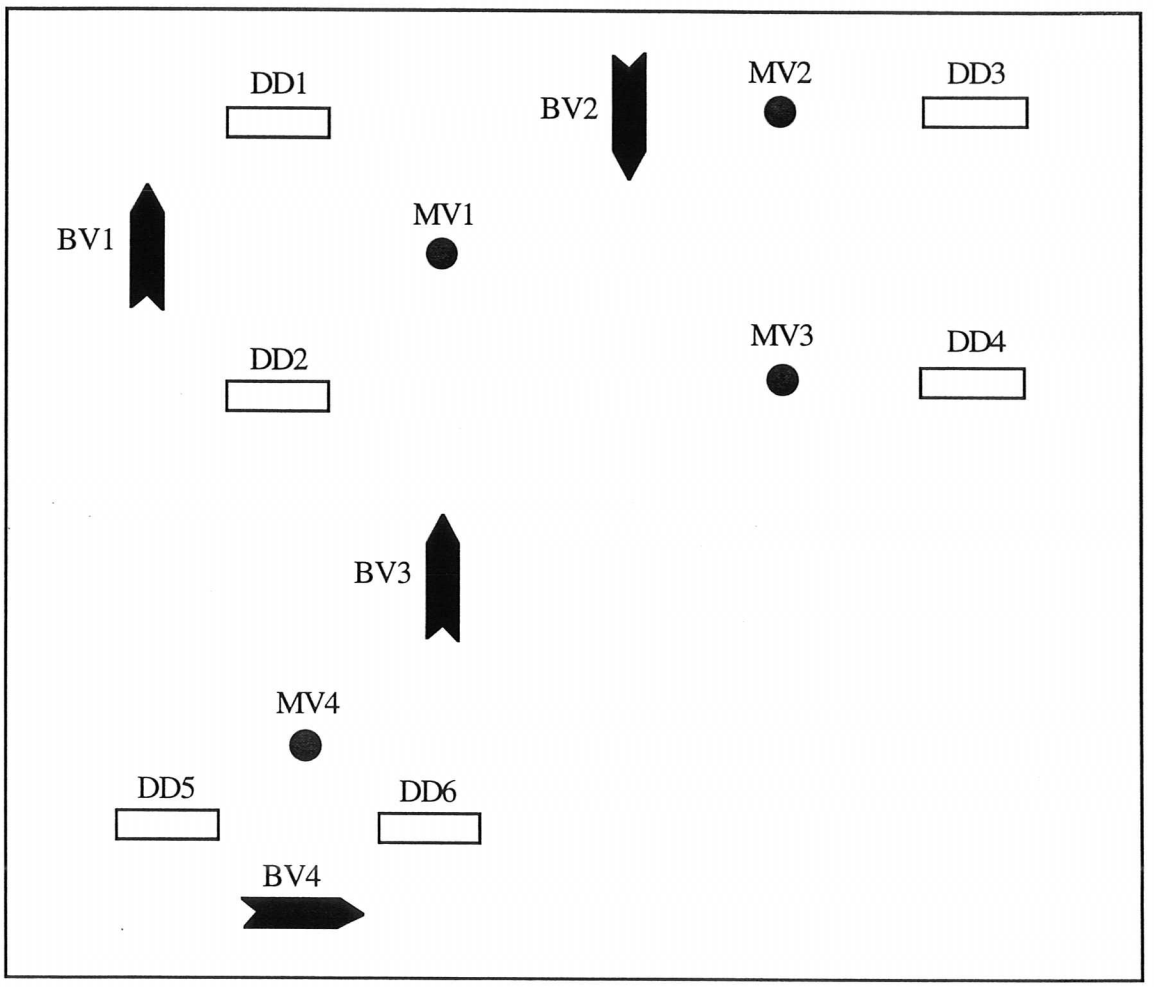

Figure C.1. HPCP gas flow panel diagram.

Combinations of the controls listed in Table C.1 must be used in order to obtain specific flow configurations. General information as well as specific combinations used for a few flow configurations are here given. The high pressure air valve outside the building must be turned on along with the high pressure air valve above the door next to the HPCP before air or steam can be used in the system. Inform Don Wallace a couple

days before you use the high pressure air. The steam and air from the high pressure tanks cannot flow through the HPCP at the same time, because the high pressure air is used to pressurize the water tank of the steam generator. If air and steam are desired at the same time, the nitrogen tanks can be replaced with air tanks. The fittings are the same.

Table C.1

Description of Gas Flow Panel Controls Labeled in Figure C.1

Control	Position	Effect on Gas Flow, or Description of Control Item
BV2	Up	Provide pressure to Steam Generator Tank
BV2	Down	Allows flow through the air flow meter (DD3) to be directed into the main flow of the HPCP.
BV1	Up	Directs He through the 50 slpm flow meter
BV1	Down	Directs He through the 250 slpm flow meter
BV3	Up	Directs part of the secondary flow (main HPCP flow) to be used as the primary (injector probe) flow.
BV3	Down	Primary flow is taken from the quench flow, which comes directly from the nitrogen gas manifolds.
BV4	Left	Directs CO_2 through the 5 slpm flow meter.
BV4	Right	Directs CO_2 through the 50 slpm flow meter.
[a]BV5	Left	Allows press. air into manifolds and air flow meter.
BV5	Right	Directs N_2 through air flow meter.
BV5	For or Back	Shuts off valve.
DD1		50 slpm He flow meter digital display
DD2		100 slpm He flow meter digital display
DD3		250 slpm Air flow meter digital display
DD4		250 slpm N_2 flow meter digital display
DD5		5 slpm CO_2 flow meter digital display
DD6		50 slpm CO_2 flow meter digital display
MV1		He metering valve
MV2		Air metering valve
MV3		N_2 metering valve
MV4		CO_2 metering valve

a. BV5 is located above the control panel, directly on the manifold assembly.

It is wise, and sometimes necessary, to completely close all metering valves that are not being used during a test. Even though check valves are installed in the system and therefore gas should not flow back through a flow meter in the opposite direction, some of the check valves leak a little. The metering valves are not needle valves and will not be damaged by complete shut off.

The CO_2 flow meters are completely integrated into the flow system. They only need to be hooked up to the manifold in place of the helium flow meters. We have adapters to allow CO_2 tanks to be connected to the manifold.

WARNING: CO_2 tanks contain oil that will deposit in the manifold. If oxygen is used sometime after CO_2 has been used, there is a possibility of an explosion. It would be best to get an entirely different manifold system for CO_2.

If air is used in the system, an oxygen analyzer must be used to determine the percentage of air in the flow gas. Furthermore, the primary gas flow must be taken from the quench. Otherwise, oxygen will be in the injection gas flow and cause premature oxidation. The flow meter on the panel next to the HPCP must be used to determine total flow, because the air flow meter on the control panel next to the computer is inaccurate. Helium is very expensive. Therefore, when operating with helium as the secondary (main) flow gas, nitrogen should be used for the quench. The nitrogen gas metering valve must be completely shut to keep it from flowing through the system with the helium. The nitrogen for the quench comes directly from the manifold and does not go though the flow meter. The primary gas, however, should be helium. This is accomplished by directing the primary flow to be taken from the secondary (main) gas flow (BV3 Up). This same configuration also applies for CO_2 gas flow.